Faculdade de Engenharia da Universidade do Porto

Low Inertia Power Grids - Role of Synchronous Condensers and Power Converters with a Grid Forming Function

Ricardo Jorge Vila Franca Gonçalves

Master in Electric and Computer Engineering Energy Major

Supervisor: Professor Doutor Carlos Coelho Leal Monteiro Moreira

July, 2025

Resumo

A transição para sistemas de energia descarbonizados tem vindo a introduzir desafios significativos à estabilidade da rede devido à integração generalizada de fontes de energia renovável (FER). Estes recursos ligados à rede através de inversores, ao contrário dos geradores síncronos tradicionais, não possuem inércia mecânica inerente, o que leva a uma redução da robustez do sistema e a uma menor estabilidade da frequência e da tensão. Esta dissertação investiga e compara o desempenho dinâmico de compensadores síncronos (CS) e inversores *grid-forming* (*GFM*) como tecnologias avançadas de suporte à estabilidade em sistemas de energia com baixa inércia.

A revisão do estado da arte explora os aspetos técnicos e regulatórios da integração de FER nas redes elétricas modernas. Para tal começa por discutir as implicações da adoção em larga escala de FER, que resulta numa redução da inércia do sistema, rápidas variações da frequência e contribuições limitadas de corrente de curto-circuito. As soluções tecnológicas para estes problemas são também discutidas, incluindo a aplicação de CS e inversores *GFM*.

Utilizando o sistema de teste IEEE de 9 barramentos modelado no *software DIgSILENT PowerFactory*, foram simulados vários cenários com diferentes níveis de penetração de FER, sendo analisadas as respostas a perturbações típicas, como perda de carga, saída de serviço de geradores e curtos-circuitos, com especial foco nesta última perturbação. O estudo destaca os efeitos adversos da redução da inércia no *nadir* da frequência, na taxa de variação da frequência (*RoCoF*) e nas questões de estabilidade devidas à operação dos conversores *(CDS)*. Este estudo demonstra que tanto os CS como os *GFM*, quando dimensionados adequadamente e posicionados estrategicamente perto das unidades de FER, podem melhorar significativamente a robustez do sistema.

Os resultados mostram que os CS oferecem uma resposta inercial e um suporte de potência reativa superiores, enquanto os *GFM* proporcionam uma melhor recuperação da frequência e amortecimento através da emulação de inércia virtual. A análise do posicionamento revela ainda que a implantação localizada destes dispositivos perto das unidades de FER é mais eficaz do que configurações centralizadas. O estudo conclui que abordagens híbridas, que combinem CS e *GFM*, podem oferecer melhor suporte à estabilidade em redes com elevada penetração de FER e baixa inércia.

Palavras-Chave: Sistemas de energia com baixa inércia, Fontes de Energia Renovável, Geração baseada em inversores, Compensadores Síncronos, Inversores eletrónicos de potência, *Grid-Following*, *Grid-Forming*

Abstract

The accelerating transition to decarbonized power systems has introduced significant challenges to grid stability due to the widespread integration of renewable energy sources (RES). These inverter-based resources, unlike traditional synchronous generators, lack inherent mechanical inertia, leading to reduced system strength and compromised frequency and voltage stability. This dissertation investigates and compares the dynamic performance of synchronous condensers (SC) and grid-forming (GFM) inverters as advanced stability support technologies for low-inertia power systems.

The state-of-the-art review explores the technical and regulatory aspects of integrating RES into modern power grids. It discusses the implications of large-scale RES adoption, which leads to reduced system inertia, faster rates of frequency change and limited fault current contributions. Technological solutions to these issues are also discussed extensively, including the application of SC and GFM inverters.

Using the IEEE 9-bus test system modelled in DIgSILENT PowerFactory, multiple scenarios with varying levels of RES penetration are simulated, analysing responses to typical disturbances such as load loss, generator trips and short circuits, with special focus on the latter. The study highlights the adverse effects of reduced inertia on frequency nadir, rate of change of frequency (RoCoF) and converter-driven stability (CDS). It demonstrates that both SCs and GFMs, when appropriately sized and strategically located near RES units, can significantly enhance system robustness.

The findings show that SCs offer superior inertial response and reactive power support, while GFMs provide better frequency recovery and damping through virtual inertia emulation. Placement analysis further reveals that localized deployment of these devices near RES units is more effective than centralized configurations. The study concludes that hybrid approaches combining SCs and GFMs may offer optimal stability support in high-RES, low-inertia grids.

Keywords: Low-inertia power systems, Renewable Energy Sources, Inverter-based generation, Synchronous Condensers, Power electronic inverters, Grid-Following, Grid-Forming

United Nations Sustainable Development Goals

The Sustainable Development Goals (SDG) are a universal call to action adopted in 2015 by all United Nations Member States as part of the 2030 Agenda for Sustainable Development. These 17 interconnected goals aim to end poverty, protect the planet and ensure prosperity and peace for all. Each goal includes specific targets designed to address the world's most pressing challenges, from hunger and education to clean energy and climate action, while balancing the economic, social and environmental dimensions of sustainable development.

The SDGs were created in response to the global need for coordinated, inclusive and long-term action that transcends national borders. They recognize that development must be sustainable and equitable if future generations are to thrive. In this context, technological innovation, access to clean energy and climate resilience are among the key priorities.

This dissertation directly contributes to SDG 7, "*Affordable and Clean Energy*" and SDG 13, "*Climate Action*". The work developed aims to enhance the stability of power grids dominated by intermittent renewable energy sources. This technological approach is crucial to enabling a sustainable energy transition, by promoting a power system that is less dependent on fossil fuels, more secure and capable of operating with high penetration of clean energy sources, even in the absence of traditional synchronous machines.

Furthermore, the adoption of advanced technologies such as grid-forming inverters aligns with SDG 9, "*Industry, Innovation and Infrastructure*". These solutions foster innovation within the electricity sector and modernize energy infrastructure by introducing technical means to support dynamic stability. Such capabilities are essential for the stable operation of future power systems.

Therefore, this dissertation not only advances technical knowledge but also contributes to global sustainability goals. It addresses the challenges of decarbonization and energy security in an integrated way, adhering to the core principles of sustainable development. A summary of the SDGs directly supported by this work is presented in the table below.

Table i - Sustainable Development Goals

SDG	Target	Indicator	Dissertation Contribution
SDG 7	**7.2** - By 2030, increase substantially the share of renewable energy in the global energy mix.	**7.2.1** - Renewable energy share in the total final energy consumption.	Enhances the viability of renewable integration by improving grid stability with high shares of intermittent sources.
	7.a - By 2030, enhance international cooperation to facilitate access to clean energy research and technology.	**7.a.1 -** International financial flows to developing countries in support of clean energy research and renewable energy production.	Promotes the development and adoption of advanced technologies (GFM inverters) that support clean energy systems.
SDG 9	**9.4** - By 2030, upgrade infrastructure and retrofit industries to make them sustainable, with increased resource-use efficiency.	**9.4.1** - CO_2 emissions per unit of value added.	Supports modernization of power infrastructure through innovative inverter-based solutions that reduce carbon dependency.
	9.5 - Enhance scientific research and upgrade the technological capabilities of industrial sectors.	**9.5.1** - Research and development expenditure as a proportion of GDP. **9.5.2**: Number of researchers per million inhabitants.	Contributes to research in advanced power electronics and control strategies, fostering innovation in the energy sector.
SDG 13	**13.1** - Strengthen resilience and adaptive capacity to climate-related hazards and natural disasters.	**13.1.1** - Number of countries with strategies for disaster risk reduction integrated into national policies.	Increases resilience of future power systems by ensuring operational stability despite climate-driven variability in renewable generation.
	13.3 - Improve education, awareness-raising and human and institutional capacity on climate change mitigation.	**13.3.1** - Extent to which (i) global citizenship education and (ii) education for sustainable development are mainstreamed.	Enhances institutional capacity through technical knowledge on inverter technologies critical for decarbonized energy transitions.

Acknowledgements

First and foremost, I would like to express my sincere gratitude to my supervisor, Professor Carlos Moreira, for his invaluable support, guidance and encouragement throughout the development of this dissertation. His expertise and dedication, not only during this project but also throughout the classes I had the pleasure to attend during my degree, have been fundamental to my academic and personal growth.

I would also like to thank Engineer Francisco Fernandes from INESC-TEC for his technical support and guidance, particularly in working with the DIgSILENT PowerFactory software. His help was essential in overcoming practical challenges and ensuring the success of the simulations.

To my colleagues and friends Bernardo Vicente and Guilherme Oliveira, thank you for being with me since the very first day of this five-year journey. Your friendship, companionship and mutual support made this experience truly special and unforgettable.

A heartfelt thank you as well to Pedro Pinto and Luís Carvalho, whom I met later during my major. Thank you for being not only great friends but also excellent group partners. I learned a great deal through our collaborations, and I truly valued every moment working together.

I am deeply grateful to my family for their unwavering support, patience and encouragement throughout this journey.

Finally, I want to thank all my colleagues and friends who are not individually mentioned here but who have been part of this chapter in one way or another. Your presence, whether in academic or informal moments, contributed immensely to this incredible journey.

Thank you all.
Ricardo Gonçalves

Contents

List of Figures

List of Tables

Abbreviations

AC	Alternating Current
AVR	Automatic Voltage Regulator
BESS	Battery energy storage systems
CDS	Converter-Driven Stability
COI	Centre of Inertia
CSCR	Composite Short-Circuit Ration
d-axis	direct-axis
DG	Distributed Generation
DSO	Distribution System operator
EPRI	Electric Power Research Institute
EU	European Union
EU CR	European Commission Regulation
exc_AC	AC excitation system
FCDS	Fast Converter-Driven Stability
FRT	Fault Ride-Through
FSM	Frequency Sensitive Mode
GENROU	Round Rotor Generator Model
GFL	Grid Following
GFM	Grid Forming
HESS	Hybrid Energy Storage Systems
HSC	Hybrid synchronous condenser
HVDC	High Voltage Direct Current
IBR	Inverter-based resources
LFSM-O	Limited Frequency Sensitive Modes- Over-frequency
LFSM-U	Limited Frequency Sensitive Modes- Under-frequency
NC	Network Codes
PGM	Power Generation Module
PI	Proportional-Integral Controller
PLL	Phase-Locked Loop
PPM	Power Park Modules
P.U.	Per unit
PV	Photovoltaic

PWM	Pulse Width Modulation
q-axis	quadrature-axis
REEC	Renewable Energy Electrical Control
REGC	Renewable Energy Generator/Converter
REPC	Renewable Energy Plant Controller
RES	Renewable Energy Source
RfG	Requirements for Generators
RoCoF	Rate of Change of Frequency
SCDS	Slow Converter-Driven Stability
SCR	Short-Circuit Ratio
SDG	Sustainable Development Goals
SDSCR	Site-Dependent Short-Circuit Ratio
SG	Synchronous Generators
SM	Synchronous Machine
SY PGM	Synchronous Power Generation Modules
TSO	Transmission System Operator
TGOV1	Turbine-Governor Model 1
UCAP	Ultra-capacitors
UFLS	Under-frequency load shedding
VSC	Voltage source converter
VSG	Virtual Synchronous Generator
VSM	Virtual Synchronous Machine
WECC	Western Electricity Coordination Council
WGO	Weak Grid Option
WSCR	Weighted Short-Circuit Ratio
WTG	Wind Turbine Generator

Chapter 1

Introduction

This chapter introduces the research topic by describing the motivation and objectives of this dissertation. It also sets the stage by highlighting the importance of the subject of the research study and the challenges it tries to address. Additionally, the chapter outlines the structure of the document, showing how the content is organized to guide the reader throughout the performed investigations and associated findings.

1.1 - Contextualization

The decarbonization of the economy is presently a matter of great importance, and renewable energy sources (RES) play an important role as European policy seeks to deliver a carbon-neutral energy system by 2050 [1]. Hence, with increasing RES shares like wind and photovoltaics power plants, conventional generation such as nuclear and thermal plants using fossil fuels are being progressively decommissioned, as illustrated in **Figure 1.1** [2]. However, the integration of large-scale RES into the electrical system brings significant technical difficulties.

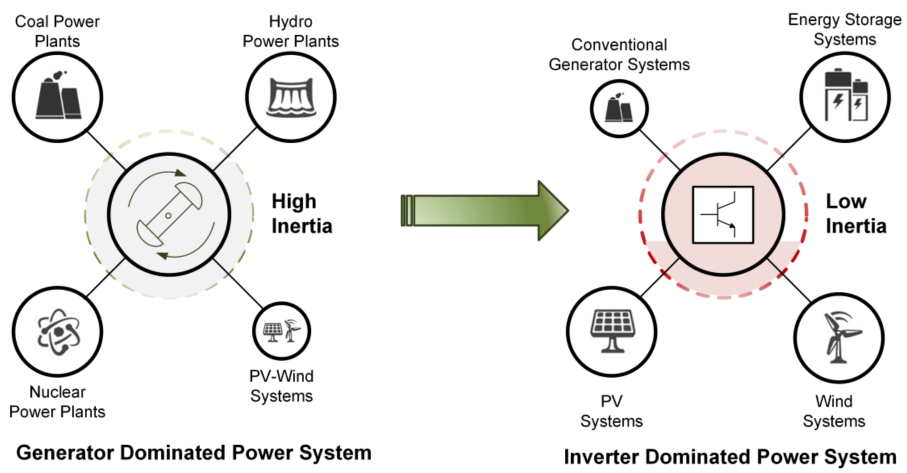

Figure 1.1- Evolution towards an inverter dominated power system. (source: [2])

The main challenges brought by the integration of RES are related to the grid's inertia, power-frequency regulation mechanisms and voltage and reactive power control. In traditional systems, frequency regulation is primarily handled by the inertial and governor response of synchronous generators [2]. When a disturbance occurs, the kinetic energy stored in the rotating masses of synchronous machines temporarily balances the generation-demand mismatch, slowing down frequency changes [2]. This response is followed by primary frequency control through turbine governors, which adjust mechanical input power, based on frequency deviations and later by secondary and tertiary controls to restore nominal frequency levels [2].

With RES integration, especially from inverter-based sources this frequency regulation chain is disrupted as inverter-based generation lacks natural inertia and traditional governor mechanisms [2]. As a result, the system becomes more susceptible to rapid frequency changes and deeper frequency dips during disturbances.

Additionally, voltage and reactive power control become more complex in RES-dominated grids. Synchronous generators inherently provide voltage support through their excitation systems by regulating reactive power [2]. In contrast, RES inverters must actively control their output to maintain voltage levels, relying on control strategies that track the existing grid voltage and adjust reactive power output in response [3].

This grid-following approach has led to stability challenges, particularly in weak grids, where voltage and frequency are less stable and more susceptible to disturbances. In such conditions, the Phase-Locked Loop (PLL), which the inverter uses to detect the grid voltage angle and synchronize its output, may struggle to track rapid fluctuations or distortions [3]. This can result in delayed or incorrect responses by the inverter, potentially leading to oscillations, loss of synchronism, or even disconnection from the grid [3]. Moreover, since grid-following inverters rely on an existing voltage waveform to operate, their performance degrades significantly when the grid is not strong enough to provide a clear and stable reference signal [3].

In order to mitigate these challenges, regulatory efforts have sought to address these stability issues through the development and enforcement of updated grid codes. These grid codes, set minimum technical requirements for generators, including frequency and voltage support capabilities, fault ride-through behaviour and reactive power provision [4]. While these measures aim to enhance the robustness of inverter-based generation and harmonize integration practices, they are largely preventive and rely on compliance rather than active physical contributions to system stability [4].

However, as RES penetration increases and the proportion of synchronous generation declines, compliance with grid codes alone has proven insufficient to maintain dynamic stability. As a result, complementary technical solutions have become necessary to support the grid's physical needs.

As a solution, synchronous condensers, which are based on synchronous machines, have been employed [5]. These devices offer capabilities similar to conventional generators, such as mechanical inertia and voltage regulation [5]. Recently, voltage source converters (VSC) operating in grid-forming mode, combined with adequate energy storage systems, have been explored to provide virtual inertia and enhance system robustness, allowing for higher RES penetration [5].

The transition to power systems with high RES penetration requires advanced control mechanisms to mitigate the impacts of reduced natural inertia. Studies show that combining technologies like synchronous condensers and grid-forming inverters can ensure stability even in systems dominated by inverter-based generation [5].

1.2 - Motivation and Goals

The research presented in this dissertation is intended to handle some of these challenges, focusing on problems arising from decreased inertia in modern power grids having high-RES penetration. Low-inertia power grids are more susceptible to frequency and voltage instabilities, which can compromise their reliability and security. The objective is to understand the new complex dynamics introduced by low-inertia systems and seek effective mitigations that will help enhance stability and reliability in the new power system.

This has particular importance as the need to meet these challenges grows more acute worldwide with decarbonization efforts. The large-scale harnessing of renewable energy sources will be possible only if the grid infrastructure and its operational methodologies are adapted to accommodate these new dynamics.

The primary motivation of this work is to understand and address the stability problems caused by low-inertia power systems, especially in grids with high levels of RES penetration. The core objective is to investigate how this transition impacts system dynamics and to evaluate viable solutions that can restore or enhance the lost inertia and grid strength.

To this end, the dissertation focuses on two specific technologies: Grid-Forming inverters and Synchronous Condensers. These solutions are selected for their potential to provide synthetic or real inertia and improve voltage stability and fault ride-through capabilities. The work aims to assess the individual and comparative contributions of these technologies to system stability through dynamic simulations under various disturbance scenarios.

Another key goal is to determine the most effective placement of these technologies within the grid. By analysing the influence of their location, whether close to RES units or in more centralized grid positions, the study seeks to identify configurations that maximize their stabilizing effects.

In summary, the dissertation aims to:

- Understand the issues arising from low system inertia due to RES integration;
- Evaluate and compare the performance of Grid-Forming inverters and Synchronous Condensers under equivalent conditions;
- Analyse the impact of these technologies on frequency and voltage stability;
- Identify optimal placement strategies within the network for effective system support.

These objectives collectively contribute to the broader aim of facilitating a stable, reliable and resilient operation of future power systems dominated by renewable energy.

1.3 - Structure of the Document

This document is organized into six main chapters, each addressing specific components of the research and its findings:

- **Chapter 1 - Introduction**: This chapter provides an overview of the research topic, outlining the context, motivation and objectives. It highlights the importance of addressing stability challenges in low-inertia power grids and the scope of this study.
- **Chapter 2 - State of the Art Review**: This chapter delves into the existing knowledge and challenges related to the integration of renewable energy sources (RES) in modern power grids. It reviews key concepts like grid inertia, frequency stability and technological solutions such as grid-following and grid-forming inverters and synchronous condensers. The chapter also includes the mathematical analysis behind the swing equation and a review of the existing European grid codes.
- **Chapter 3 - Dynamic Modelling and Simulation of Low Inertia Systems:** This chapter details the simulation platform developed in DIgSILENT PowerFactory and the test system used. It explains how synchronous machines, grid-following inverters, grid-forming converters and synchronous condensers are represented in the simulations, laying the foundation for dynamic stability analysis under different network scenarios.
- **Chapter 4 - System Response in Evolving Grid Scenarios:** Examines the system's dynamic frequency response to various disturbances, including load loss, generator tripping and short-circuits. The analysis is performed under different RES integration scenarios to evaluate the impact of low inertia. Key performance indicators such as RoCoF and frequency nadir are used to assess system stability.
- **Chapter 5 - Enhancing Stability in Low-Inertia Power Systems:** Investigates the effectiveness of advanced stabilizing solutions, namely grid-forming inverters and synchronous condensers. Their performance is analysed under identical conditions and compared in terms of dynamic response, oscillation damping, voltage support and impact of placement within the grid.
- **Chapter 6 - Conclusions and Future Work:** Summarizes the key findings of the study, highlighting the advantages and limitations of each proposed solution. It reflects on the practical implications of the results and outlines potential directions for future research.

Chapter 2

State of Art Review

This chapter provides a comprehensive review of the state of the art in the field of research. It delves into the challenges associated with the integration of renewable energy sources (RES) into power systems, exploring the complexities and limitations that arise as renewable penetration increases. The chapter also examines various solutions that have been proposed and implemented to mitigate these challenges. Additionally, it includes an in-depth review of grid codes, focusing on their role in facilitating renewable integration while maintaining grid stability.

2.1 - Large-scale integration of RES

The integration of RES, such as wind and solar energy, has brought critical challenges to the stability of modern power grids, mainly because of shifting from traditional synchronous generators toward inverter-based generation. It results in a reduction of the system´s inertia, a crucial element for maintaining stability in power systems [2]. Synchronous Generators (SG) have intrinsic physical inertia derived from their rotating masses, which helps damp sudden changes in power supply and demand [2]. In contrast, inverter-based RES do not contribute to the system´s inertia, and as a result, leads to faster and more pronounced frequency deviations during disturbances [6].

As shown in **Figure 2.1** following the path of decommissioning of synchronous machines (SM) replaced by inverter connected generation can be noted that this reduced inertia increases the Rate of Change of Frequency (RoCoF), which refers to how quickly the system frequency changes over time, thus jeopardizing system security [6]. An increased RoCoF can cause protection systems to misoperate and can prevent the operation of controls relating to frequency, therefore leading to problems of grid stability [6]. This affects the impedance viewed by generators due to reduced short-circuit power from the loss of synchronous generators [6]. This not only deepens voltage dips but also widens their influence, which may lead to commutation failures in high-voltage direct current (HVDC) systems and operational disturbances in inverter-based equipment [6].

The weaknesses in stability characteristics of RES further aggravate these challenges. In contrast to synchronous generators, inverter-based RES show limited fault current contributions and reduced voltage support during grid disturbances [7]. Their electromagnetic dynamics are influenced by power electronics controls, which are more complex during transient events [7]. As a result, large-scale RES integration can undermine both frequency and voltage stability, requiring advanced control strategies to mimic the inertial response of traditional generators [7].

The decrease in inertia in low-inertia systems makes frequency stability more volatile, as the reduced kinetic energy from synchronous machines can no longer dampen the fluctuation of frequencies [7]. In that respect, the RoCoF in high-RES penetrated grids may increase suddenly, hence compromising grid security [7].

Another important aspect in low-inertia grids is the issue of voltage stability. The rapid and large variations in power generation by RES causes fluctuations in the grid voltage [7]. Traditional synchronous generators contribute inherently to voltage stability by reactive power support, while power-electronic interfaced sources need extra control strategies for maintaining voltage levels and support reactive powers to prevent voltage instability in response to any sudden load or generation changes [7].

In low-inertia grids, rotor angle stability is affected because the conventional synchronizing torque provided by synchronous machines is not there. Thus, high shares of inverter-based RES, which inherently do not synchronize with the grid, result in a higher tendency for desynchronization or even oscillations [7].

While the decarbonization of power systems through RES is a crucial step toward sustainability, it demands significant adaptations to grid design and operation to ensure stability in a low-inertia environment. The coordinated application of technological innovations and regulatory measures will be essential to address these evolving challenges effectively.

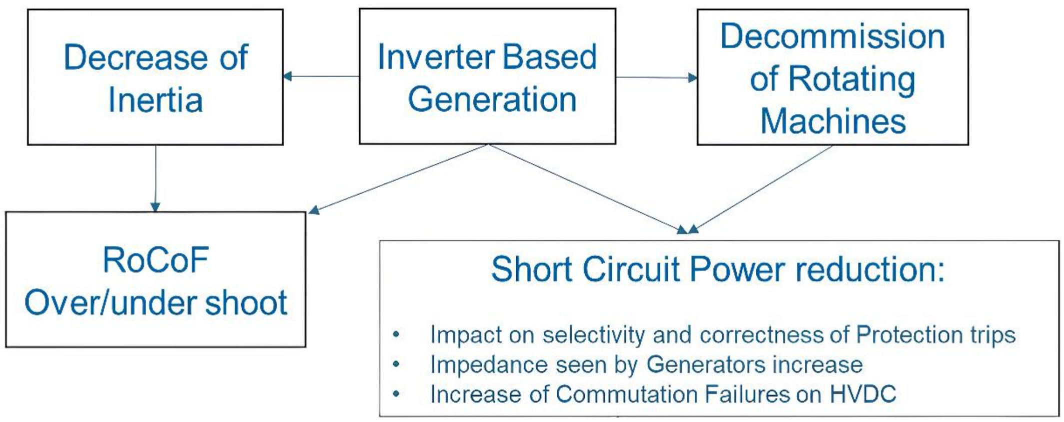

Figure 2.1 - Map of interaction (source: [6])

2.2 - Frequency Dynamics

Synchronous machines are the primary source of system's inertia, hence playing an important role in stabilizing the power grid as a response to changes in load and generation [7]. It is necessary to understand synchronous machines in more detail and the contribution of SG to system inertia. Therefore, this section introduces the swing equation of a synchronous machine as well as key frequency indicators, namely the RoCoF and frequency Nadir.

The following equations will make clear the dynamic interaction between electrical and mechanical power, torque and angular velocity, as well as demonstrate how SG affect the overall efficiency and resilience of the power grid [8].

Firstly, let us understand what inertia is in the context of rotational motion. Inertia represents the resistance of a rotating body to changes in its angular velocity. In power systems, this concept is crucial as it relates to the rotating masses of synchronous generators, which store kinetic energy and help maintain system frequency stability. Mathematically, the rotational form of Newton's second law is:

$$T = J * \alpha = J * \frac{dw}{dt} \tag{2.2.1}$$

Where:

T: Torque applied to the rotating mass.

J: Moment of inertia.

α: Angular acceleration.

w: Angular velocity.

Moving to electrical systems, the previous formulation refers to a mechanical mass rotating with a mean angular speed [6], and it can be expressed as:

$$T_m - T_e = T_a \tag{2.2.2}$$

Where:

T_a: Accelerating torque, measured in Nm.

T_m: Mechanical torque, measured in Nm.

T_e: Electromagnetic torque, measured in Nm.

The term $T_m - T_e$ represents the torque balance [Nm] between the mechanical torque applied to the rotating mass by a prime mover and the electrical torque determined by the power exchanged with the system [6].

In the given equation, T_m and T_e are considered positive for a generator and negative for a motor. The imbalance between these torques accelerates the combined inertia of the generator and the prime mover [8]. Consequently, the equation of motion is defined as follows:

$$J\frac{dw_m}{dt} = T_m - T_e = T_a \tag{2.2.3}$$

Where:

J: Combined moment of inertia of the generator and turbine, measured in kg/m^2.

w_m: Angular velocity of the rotor, measured in mechanical radians per second (rad/s).

t: Time, measured in seconds (s).

The equation can be normalized using the per-unit inertia constant H, which is defined as the kinetic energy in watt-seconds at the rated speed divided by the machine VA base. Letting w_{m0} represent the rated angular velocity in mechanical radians per second [8], the inertia constant is expressed as:

$$H = \frac{1}{2}\frac{Jw_{0m}^2}{VA_{base}} \tag{2.2.4}$$

The moment of inertia J can be expressed in terms of the inertia constant H as follows:

$$J = \frac{2H}{w_{0m}^2} VA_{base} \tag{2.2.5}$$

Substituting the above in 2.1.3 gives:

$$\frac{2H}{w_{0m}^2} VA_{base} \frac{dw_m}{dt} = T_m - T_e \tag{2.2.6}$$

Rearranging the equation gives:

$$2H \frac{d}{dt}\left(\frac{w_m}{w0_m}\right) = \frac{T_m - T_e}{VA_{base}/w0_m} \tag{2.2.7}$$

Given that $T_{base} = VA_{base}/w0_m$, the motion equation can be expressed in per-unit form as follows:

$$2H \frac{d\overline{w_r}}{dt} = \overline{T_m} - \overline{T_e} \tag{2.2.8}$$

In the above equation:

$$\overline{W_r} = \frac{w_m}{w0_m} = \frac{w_r/p_f}{w_0/p_f} = \frac{w_r}{w_0} \tag{2.2.9}$$

Where:

w_r: Angular velocity of the rotor in electrical radians per second (rad/s).

w_0: Rated angular velocity (rad/s).

p_f: Number of field poles.

If δ represents the angular position of the rotor in electrical radians relative to a synchronously rotating reference, and δ_0 denotes its value at t=0 [8] we have:

$$\frac{d^2\delta}{dt^2} = \frac{dw_r}{dt} = \frac{d(\Delta w_r)}{dt} = w_0 \frac{d(\Delta \overline{w_r})}{dt} \qquad (2.2.10)$$

Substituting from the above equation into equation 2.2.8, we obtain:

$$\frac{2H}{w_0}\frac{d^2\delta}{dt^2} = \overline{T_m} - \overline{T_e} \qquad (2.2.11)$$

For a synchronous machine and considering Torque (T) and Power (P) values expressed in per unit values, if $w_m = w_{0m}$ then $\overline{T} = \overline{P}$ [8]. Substituting in equation 2.2.11 we obtain:

$$\frac{2H}{w_0}\frac{d^2\delta}{dt^2} = \overline{P_m} - \overline{P_e} \qquad (2.2.12)$$

Where:

P_m: Mechanical power, measured in W.

P_e: Electrical power, measured in W.

Including a damping torque component is achieved by introducing an additional term proportional to the speed deviation in the existing equation [8], as shown below:

$$\frac{2H}{w_0}\frac{d^2\delta}{dt^2} = \overline{P_m} - \overline{P_e} - D\Delta\overline{w_r} \qquad (2.2.13)$$

Where:

D: Load damping constant (p.u.W/rad/s).

Equation 2.1.14 describes the motion of a synchronous machine and is commonly known as the swing equation. This name arises because it models the oscillations in the rotor angle δ that occur during disturbances [8].

$$\frac{d^2\delta}{dt^2} = \frac{w_0}{2H}(\overline{P_m} - \overline{P_e} - D\Delta\overline{w_r}) \qquad (2.2.14)$$

A critical measure of an electrical grid's resilience is the rate of change of frequency (RoCoF), which represents the time rate of change of the power system frequency (df/dt) [6]. The initial df/dt value corresponds to the instantaneous RoCoF that occurs immediately after a power imbalance in the system, such as a generator disconnection or load tripping, and before any control actions are implemented [6]. The RoCoF is determined using the formula provided in equation 2.2.15 [6].

$$ROCOF|_{t=0^+} = \frac{\Delta P_{imbalance}}{P_{LOAD}} * \frac{f_0}{2H} \tag{2.2.15}$$

Where:

$\Delta P_{imbalance}$: Corresponds to the power imbalance due to the disturbance

H: System inertia.

Because of the low inertia, there is a chance that the grid frequency and RoCoF may exceed their usual operational range, potentially leading to issues such as load shedding and system blackouts [7]. Consequently, improving the inertia of the power system and constraining the RoCoF are extremely important [7].

Nadir frequency is the lowest point of the system frequency during a disturbance before it starts recovering due to corrective actions such as the primary control mechanisms deploying frequency containment reserve margins in specific generators [9]. It indicates the severity of the frequency drop after a disturbance and helps assess whether the system frequency remains within acceptable limits to avoid under-frequency load shedding (UFLS) or other protective actions [9].

The RoCoF influences the depth of the nadir frequency, i.e. a higher RoCoF, caused by low system inertia, generally leads to a deeper frequency nadir [9]. Both metrics are critical for system stability during disturbances, with RoCoF providing an early indication of imbalance and nadir frequency reflecting the severity [9].

Low-inertia systems provide a narrower time window for corrective measures to stabilize the frequency after a disturbance. For example, traditional Primary Frequency Response (PFR), which relies on governor-driven adjustments from synchronous generators, may not activate quickly enough to mitigate the rapid frequency decline. In such systems, the frequency nadir is reached sooner, limiting the effectiveness of conventional frequency control mechanisms [10]. This urgency necessitates faster-acting support, such as Fast Frequency Response (FFR), which can inject power almost instantaneously, counteracting frequency deviations before they become critical. Without these enhancements, the risk of system instability increases, as traditional controls cannot respond swiftly enough in a low-inertia environment [10].

2.3 - System Strength

To comprehend and tackle the intricate challenges posed by the rapid technological transition already in progress, the concept of "system strength" has emerged. This term encapsulates a wide array of issues and their impacts on the operability of modern power systems with high integration of RES.

The stability of power system equipment and the system's overall ability to recover intact from significant disturbances are heavily influenced by the electrical "strength" at the connection point. Intuitively, "stronger" systems are more resilient to variations and disruptions in operating conditions, allowing them to recover more effectively from major events such as faults or the sudden loss of equipment [11]. As [12] states "The term "system strength" can be described as the ability of the power system to maintain voltage stability and quality at the RES interconnection points." In other words, system strength refers to the ability of the power system to maintain or restore voltage within the permissible range during steady-state operation and after disturbances [13].

System strength can be evaluated by the Short-Circuit Ratio (SCR) [13]. The SCR is defined as the ratio of the short-circuit capacity at a connection point to the rated capacity of connected power electronic equipment. When the SCR is high, the system is considered "strong," and when the SCR is low, it is deemed "weak." System strength plays a crucial role in grid stability during faults. In low-SCR systems, voltage changes can cause larger disturbances that propagate further across the network. If unmanaged, these disturbances may trip generation units or damage equipment [14].

In cases where the SCR is too low, protection systems designed to open circuit breakers and isolate faults may fail to detect ongoing faults, leaving the network in an unsafe and unstable state. Low SCR levels increase the likelihood of significant voltage deviations, stability issues, power oscillations, or challenges with fault ride-through following a disturbance.

SCR can be calculated as follows [13]:

$$\text{SCR} = \frac{S_{ac}}{P_N} \tag{2.3.1}$$

Where:

S_{ac}: is the short circuit capacity, that is equal to the short circuit current times the rated voltage [13].

P_N: is the rated capacity of power electronic equipment, can be expressed in MW or MVA [13].

The SCR reflects the power system's capability to handle active and reactive power injection or absorption effectively. A low SCR signifies that the system lacks sufficient strength to ensure the reliable operation of power electronic devices [13].

The presence of synchronous generators historically ensured high SCR and system strength due to their inherent ability to provide fault current and stabilize voltages. However, with the transition to inverter-based resources (IBR), maintaining system strength has become more challenging. The replacement of synchronous generators with IBRs, such as solar and wind plants, reduces the available fault current at grid connection points. This decline in short-circuit capacity compromises the grid's ability to isolate faults efficiently and maintain stability during disturbances [12].

Other methods to improve the calculation of the system strength with large integration of RES and considering the interactions among renewable generation plants have been studied and developed such as weighted short-circuit ratio (WSCR), composite short-circuit ratio (CSCR) and site-dependent short-circuit ratio (SDSCR) [12].

2.4 - Solutions and Emerging Technologies for Enhanced Dynamic Performance

Maintaining stability in modern power systems is essential, especially when increasing the penetration levels of renewable energy sources such as wind and solar. Unlike most traditional power sources, renewables are integrated using inverters, which inherently does not have the potential to contribute to the grid's stability in the way that traditional synchronous generators do. Such a change can bring about new challenges of instability in frequency and voltage, mainly in those power systems with high penetration levels of renewable energy. To work around them, mitigating measures are taken that help maintain stability in the system. Some of the solutions to mitigate these issues are the revision of the grid codes, introduction of new systems services, energy storage systems and solutions to increase grid flexibility.

2.4.1 - Revision of Grid Codes for EU Network

To mitigate some of the negative impacts of the RES integration, a set of requirements was accorded and developed by the Transmission System Operators (TSO). Based on the European Network Code on Requirements for Generators (COMMISSION REGULATION (EU) 2016/ 631) the main compliance requirements for generators integrated into the European electricity grid are highlighted below.

Power Generating modules are classified into four categories (A, B, C and D) based on their connection characteristics, generation capacity and voltage connection levels [15], [16]. Each type plays a specific role in ensuring grid stability and operational reliability:

- Type A - These modules connect at voltage levels below 110 kV and have a maximum generation capacity of 0.8 kW or more. These units are required to fulfil essential requirements for automated responses and basic control functions, focusing on minimizing production losses and supporting the grid during critical events [15].
- Type B - With connection points below 110 kV and a generation capacity that meets or exceeds a threshold determined by the relevant TSO, Type B facilities deliver enhanced dynamic responses to grid disturbances. They offer improved frequency and voltage regulation through more active interaction with grid operators [16].
- Type C - Similar to Type B, these modules connect below 110 kV but must meet higher capacity thresholds set by TSOs. They are designed to maintain grid balance and security of supply by providing stable dynamic responses. Type C facilities are

also equipped to support real-time grid operations with detailed data sharing and advanced control mechanisms [15].

- Type D - These modules are characterized by connection points at or above 110 kV, or below 110 kV if they meet a high-capacity threshold. They play a crucial role in stabilizing the interconnected European grid by offering large-scale ancillary services, stringent operational control and robust support for cross-border system stability [15].

The Network Code on Requirements for Generators (NC RfG) defines maximum capacity thresholds for generator types across Europe's synchronous areas [15]. These values reflect variations in capacity requirements and operational stability across synchronous areas, ensuring the reliability of the European power grid [15]. The thresholds set by NC RfG for the different generator types are indicated in **Table 2.1**.

These requirements have been progressively implemented by individual member states. In the case of Portugal, the transposition of the NC RfG into national legislation was established through [17], which sets out the technical requirements applicable to the connection of generating units to the public electricity network. This national implementation ensures consistency with European standards while accounting for the specific operational characteristics of the Portuguese power system.

Table 2.1- Limits for thresholds for type B, C and D power-generating modules (source: [15])

Limit for maximum capacity threshold for each type of module			
Synchronous Area	**Type B Threshold (MW)**	**Type C Threshold (MW)**	**Type D Threshold (MW)**
Continental Europe	1	50	75
Great Britain	1	50	75
Nordic	1.5	10	30
Ireland and Northern Ireland	0.1	5	10
Baltic	0.5	10	15
Portugal [17]	10	45	-

The requirements outlined in the RfG follow a technology-neutral approach, emphasizing capability differences based on generator types. These requirements are organized into four categories, considering the nature of their grid connections, i.e. the requirements for [18]:

- All Generating Modules: Applicable to all generators regardless of their generation technology or grid connection type, as defined by the NC RfG under the term PGM (Power Generating Module).
- Synchronous Generating Modules (SY PGM): These are generators connected to the grid in a synchronous manner.

- Power Park Modules (PPM): Generating units that are connected to the grid via power electronic systems.
- Offshore Farms: Includes offshore generation facilities, except those with a DC connection, which fall under the requirements of a different Network Code (HVDC NC).

A core principle of the NC RfG is to strike a balance between the overarching needs of the European power system and the unique requirements of local systems. The technical requirements outlined in the NC RfG for generating modules are applied differently at the national level, categorized as follows [16], [18]:

- Exhaustive Requirements: These establish the functional or principled capabilities of generators with clearly defined parameters. No further adjustments or specifications are needed at the national level.
- Non-exhaustive Requirements: These outline fundamental capabilities but leave the specific parameters or settings undefined. These details must be determined at the national level to reflect regional or local system characteristics, eventually making them "exhaustive."
- Optional Requirements: These may be implemented by TSOs and/or DSOs, but they must first be fully defined at the national level. At the NC RfG level, these requirements are typically left incomplete.
- Project-specific Requirements: These can either be optional or non-exhaustive but must be tailored and defined for each individual project before implementation.

The grid connection requirements specified in the NC RfG are determined by the generator type (A, B, C and D) and their classification as either synchronous or non-synchronous generating facilities. A summary of these requirements, along with the corresponding system aspects they address [16], is provided in **Table 2.2**.

Technical requirements cover several critical grid aspects. For frequency stability, all generators must withstand frequency ranges with minimum operational periods, shown in **Table 2.3** (for Continental Europe), and RoCoF withstand capabilities, shown in **Table 2.4**. Larger generators (Types C and D) can also provide synthetic inertia to help manage dynamic frequency response, which is critical in systems very highly saturated with converter systems.

In the context of overall system and frequency stability, the NC RfG mandates that generators reduce their output power when the frequency surpasses a specified threshold, known as Limited Frequency Sensitive Mode – Overfrequency (LFSM-O). The relevant national TSO or authority is responsible for defining the response characteristics, which include Frequency threshold (measured in Hz) and Power-frequency (P/f) droop setting (expressed as a percentage) [15], [16]. Additionally, the national authority may impose further requirements regarding delay times and operational characteristics. This requirement applies to all generators covered by the NC RfG, regardless of their capacity [16]. **Table 2.5** presents the proposed requirements for individual countries.

Table 2.2- Overview of system aspects and requirements addressed by the NC RfG (Source: [16])

System aspect	Requirement	A	B	C/D
Frequency stability	Operating frequency ranges	X	X	X
	RoCoF withstand capability	X	X	X
	Limited Frequency Sensitive Mode - Overfrequency	X	X	X
	Constant active power output regardless of changes in Frequency	X	X	X
	Limitation of power reduction at underfrequency	X	X	X
	Automatic connection	X	X	X
	Remote ON/OFF	X	X	X
	Active power reduction remote control		X	
	Additional requirements related to frequency control			X
	Provision of synthetic inertia			X
Robustness of power generating modules	Fault-ride-through		X	X
	Post-fault active power recovery		X	X
System restoration	Coordinated reconnection		X	X
General system management	Control schemes and settings		X	X
	Electrical protection and control schemes and settings		X	X
	Priority ranking of protection and control		X	X
	Information exchange		X	X
	Additional requirements to monitoring			X
Voltage stability	Reactive power capability		X	X
	Fast reacting reactive power injection		X	X
	Additional requirements for reactive power capability and control modes			X

Table 2.3 - Minimum operating times required for a power-generating module, in Continental Europe, including Portugal, to run at frequencies deviating from the nominal value without disconnecting from the network (source: [15]).

Frequency Range (Hz)	Time Period for Operation	Applicable Types
47.5 - 48.5	≥30 minutes	A, B, C, D
48.5 - 49.0	Unlimited	
49.0 - 51.0	Unlimited	
51.0 - 51.5	≥30 minutes	

Table 2.4- RoCoF Withstand Capability in Selected European Countries (source: [16]).

Country	ROCOF withstand capability	
	Requirement and (measurement period)	Applicable Types
Austria	2 Hz/s	A, B, C, D
Belgium	2 Hz/s	
Germany	2 Hz/s (500ms)	
Denmark	2 Hz/s (200ms)	
France	1 Hz/s (500 ms)	
UK	1 Hz/s (500 ms)	
Ireland	1 Hz/s (500 ms)	
Netherlands	2 Hz/s (500ms)	
Spain	2 Hz/s (500ms)	
Italy	2.5 Hz/s (100ms)	
Portugal[17]	2 Hz/s (500ms)	

Table 2.5 - Frequency Sensitive Mode – Overfrequency (LFSM-O) Settings in Selected European Countries (source: [16]).

Country	LFSM-O		
	Requirement Droop	**Threshold**	**Delay**
RfG definition	2% to 12%		
Austria	5%	50.2 Hz	none
Belgium	5%	50.2 Hz	none
Germany	5%	50.2 Hz	none
Denmark	CE:5%(SYPG/PPM) N:4% (SYPG/PPM)	CE:50.2Hz N: 50.2Hz	none
France	5%	50.2 Hz	<2 s
UK	10%	50.4 Hz	<2 s
Ireland	4%	50.2 Hz	none
Netherlands	5%	50.2 Hz	none
Spain	5%	50.2 Hz	none
Italy	2.6%	50.2 Hz	none
Portugal[17]	4% to 6%	50.2 Hz	<2 s

Voltage stability is ensured through reactive power capabilities, which vary by country related to voltage stability, the NC RfG defines requirements for the reactive power capabilities of generators. These capabilities must be provided by all generators of type B and above, as specified by the relevant TSO or national authority [16]. The detailed conditions and specifications vary based on generator types (B, C, D) and technologies (SY PGM and PPM) [16]. Additionally, fast reactive power injection is mandatory for Type C and D generators to stabilize voltage during disturbances.

Fault ride-through (FRT) capability is another key requirement. To enhance generator robustness during disturbances and faults, the NC RfG mandates that all type B generators provide FRT capabilities [16]. This includes the ability to supply fast fault current (both symmetrical and unsymmetrical) at the connection point during voltage deviations. Additionally, generators must ensure "post-fault active power recovery" to restore normal operation promptly [16]. Additionally for Portugal, given by [17], the national implementation requires that even smaller generation units, namely type A SY PGM above 15 kW, remain connected to the grid during voltage dips caused by both symmetrical and asymmetrical three-phase faults, including those involving ground. This requirement applies as long as the voltage at the point of connection remains above the threshold capacity curves defined for type B modules.

The specific requirements for FRT, including the voltage-time profile at the connection point, fast fault current injection and post-fault active power recovery, are determined by the relevant TSO [16]. The detailed conditions and specifications vary based on generator types (B, C, D) and technologies (SY PGM and PPM) [16]. The FRT requirement is defined as the lower limit of a voltage-time profile at the connection point, illustrated in **Figure 2.2**, where the generator must remain connected to the grid.

The profile is described using four key voltage and time parameters:

- Uret: Retained voltage during the fault.
- tclear: The moment when the fault is cleared.
- Urec1/trec1,2 and Urec2/trec3: Lower voltage limits during the recovery phase after fault clearance.

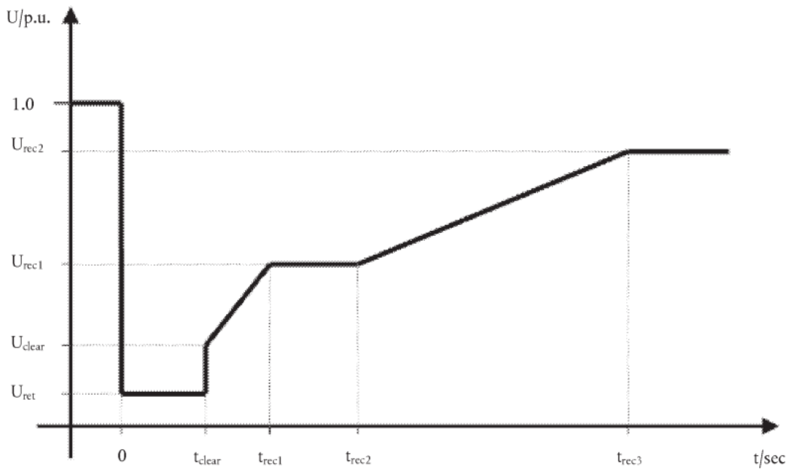

Figure 2.2 - Fault-ride-through profile of a power-generating module (source: [15]).

Portugal enforces a stricter, broader FRT policy than Spain, covering smaller units, requiring all fault types, and mandating reactive power injection [17]. Both countries follow the ENTSO-E “voltage–time” profile pattern using similar Uret, tclear, Urec1/2 parameters [16].

Table 2.6 - Fault-Ride-Through (FRT) Profile for Portugal (source: [16],[17]).

Parameter	Description	Typical Value in Portugal
Uret	Retained voltage during the fault	0.25 p.u.
tclear	Fault clearance time	0.14 to 0.25 s
Urec1	First voltage recovery level	0.5–0.7 p.u.
trec1	Time to reach Urec1 after tclear	up to 0.45 s after tclear
Urec2	Second voltage recovery level	0.85–0.9 p.u.
trec3	Final voltage recovery time after tclear	1.5 s after tclear

Regarding fast fault current injection capabilities, the NC RfG provides only a general definition, leaving the detailed implementation to be determined at the national level. Consequently, the current documents reveal significant variability, especially in the level of detail [16]. While some countries offer comprehensive specifications for implementation, others only provide a basic definition, highlighting a wide range of approaches to this requirement [15]. The detailed conditions and specifications vary based on generator types (B, C, D) and technologies (SY PGM and PPM) [16].

The NC RfG establishes a comprehensive framework for connecting PGM to EU grids, addressing a wide range of regulatory issues. By balancing strict technical requirements with regional flexibility, it promotes grid stability, facilitates the integration of RES and supports the development of a unified electricity market. Successful implementation depends on close collaboration among TSOs, DSOs, regulatory authorities and generators. This cooperation is essential to overcome technical challenges, manage cost implications and encourage innovation and sustainability within the evolving energy landscape.

2.4.2 - Minimum Inertia Thresholds

As stated before, the increasing integration RES, especially those connected via power electronic interfaces, has led to a gradual reduction in power system inertia. This trend presents a critical challenge to frequency stability, as the rotational inertia of synchronous generators plays a key role in containing the RoCoF following disturbances.

In power systems, the inertia constant H, quantifies the stored kinetic energy in rotating machines relative to their rated power. For systems with multiple synchronous generators, the overall system inertia constant H_{eq} is calculated as [19]:

$$H_{eq} = \frac{\sum_{i=1}^{N} H_n S_n}{(S_b + S_c)} \tag{2.4.1}$$

where:

H_n is the inertia constant of generator n.

S_n is the rated power of generator n.

S_b is the total base power of synchronous machines.

S_c is the power contributed by converter-based RES.

This equivalent inertia represents the system's resistance to frequency deviations immediately after a disturbance. As RES penetration increases S_c rises, while H_{eq} decreases, diminishing the system's ability to absorb disturbances [19].

To ensure frequency stability under low-inertia conditions, it is essential to define a minimum threshold of inertia below which the system becomes dynamically unstable. The research presented in [19] propose an analytical approach to determine the minimum required inertia constant H_{min} , below which system stability cannot be guaranteed.

This analysis is based on the transfer function of the dynamic frequency control model, which incorporates the effects of the governor, turbine and load damping. The characteristic equation derived from this model is subjected to the Routh-Hurwitz stability criterion, leading to a closed-form expression for H_{min} [19]:

$$H_{min} = \frac{T_g T_t (D + \frac{1}{R})}{2(T_g + T_t)} \tag{2.4.2}$$

where:

T_g is the governor time constant.

T_t is the turbine time constant.

D is the damping coefficient.

R is the governor speed regulation parameter.

This critical inertia value corresponds to the marginal stability boundary. If the system inertia falls below H_{min}, the characteristic equation exhibits right-half-plane poles, indicating unstable frequency behaviour [19].

Simulations in [19] confirm that once this threshold is crossed, conventional frequency control mechanisms cannot recover system stability.

The concept of a minimum inertia threshold emerges as a crucial technical parameter in the safe transition toward power systems dominated by renewable energy with inherently low inertia.

To deal with the reduction in inertia levels, some regions have established plans defining minimum requirements for inertia. For instance, Australia has planned to establish regional inertia floors tailored to specific power demands and generation characteristics to allow for more controlled frequency response over its sub-networks [20]. Similarly, grid codes in the UK and Ireland are being adapted in order to ease RoCoF limits and allow a wider range of frequency deviations before triggering protective actions [20]. Also, monitoring and forecasting system inertia is critical, transmission power systems developing techniques based on dynamic simulations or online tests to estimate and predict inertia levels [20]. Changes reflect adaptation for stabilizing grids with growing shares of RES having low inherent inertia.

2.4.3 - Power Electronic Interfaces

Power electronic inverters and converters play a critical role in integrating renewable energy resources (RES) into power grids. These components act as essential interfaces, enabling the smooth transfer of energy from renewable sources, such as solar and wind, to the electrical grid. As the global energy sector advances toward a fully decarbonized system, with increasing capacities of RES being connected to the grid and the gradual phase-out of conventional power generation, the power system is undergoing a significant transformation toward inverter-based dominance [21].

This shift highlights the growing importance of inverter technology in maintaining grid stability and reliability. Within the domain of inverter controllers, two primary classes have emerged as key players: grid-following (GFL) controllers and grid-forming (GFM) controllers [22]. Each of these technologies offers unique functionalities that are critical for adapting to the evolving needs of the modern power grid, paving the way for a sustainable and resilient energy future.

The grid-following (GFL) inverters are usually designed to inject power into the existing grid by following the frequency and voltage of the grid, acting as current sources [23], this control offers the benefit of being able to quickly regulate the current [22]. However, GFL inverters rely on the grid to supply voltage and frequency references, as they lack autonomous control over these parameters. This dependence limits their ability to support frequency and voltage stability independently [22][23]. GFL inverters are easier to implement and are the adopted control strategy for grid-connected PV and wind inverters [22], where the inverter's primary function is efficient power injection rather than grid stabilization [23]. A basic block diagram of the GFL inverter model is shown in **Figure 2.3**.

As illustrated a GFL inverter employs a Phase-Locked Loop (PLL) to detect the grid's frequency. Based on the frequency and voltage magnitude measured by the PLL, control functions are implemented to determine the appropriate active and reactive power reference values [22]. These references are then compared with the measured power output and the result is processed through a PI controller to produce a current reference [22]. Before reaching the current control stage, this reference may be subject to a current limitation mechanism. The current controller then compares the limited reference with the measured current and, through another PI controller, generates the corresponding voltage reference. This voltage reference is then used to produce the required PWM signals [22].

In contrast, grid-forming (GFM) inverters act as voltage sources that can set the grid's frequency and voltage on their own [23]. This capability makes GFM inverters very suitable for supporting grid stability by themselves, thus highly appropriate for systems of high renewable penetration and low inertia, where synchronous generators are scarce [23]. By emulating synchronous generators, GFM inverters provide synthetic inertia, enabling them to stabilize frequency fluctuations and enhance overall grid resilience, even if traditional generators are not present [23]. They can also support and even perform a black start of an islanded network due to its capability to supply grid voltage through its voltage-source characteristics [22].

The primary control strategies employed in GFM converters are Droop Control and the Virtual Synchronous Machine (VSM) approach. These methods define how the converter interacts with the grid, enabling it to regulate voltage and frequency autonomously, much like traditional synchronous generators.

The purpose of droop control is to replicate the behaviour of synchronous generators by adjusting the converter's output in response to changes in system conditions [24]. This method dynamically modifies the reference values for frequency and voltage magnitude, which are then passed to the internal voltage and current control loops [24]. Depending on the control mechanism used, droop control can be classified into different types, including frequency-based droop control, angle-based droop control and Power Synchronization Control [24]. A simple block diagram of GFM with droop control is shown in **Figure 2.4**.

A VSM is a control technique that emulates both the internal dynamics and external behaviours of conventional synchronous generators. It does so by applying a mathematical representation of a synchronous machine, incorporating rotor dynamics and electromagnetic transient equations into the converter's control structure [25]. This approach allows the converter to function similarly to a synchronous generator by replicating its inertia and damping properties [25]. Under VSM control, the converter can operate as an equivalent synchronous unit within an AC power system, enabling autonomous control of active power in response to frequency deviations and reactive power in response to voltage changes. Additionally, it provides virtual inertia and damping support, enhancing the system's dynamic stability [25]. As grid conditions evolve, such as changes in load or disturbances, the converter actively adjusts its output to maintain system balance and stability [25]. A simple block diagram of GFM with VSM control is shown in **Figure 2.5.**

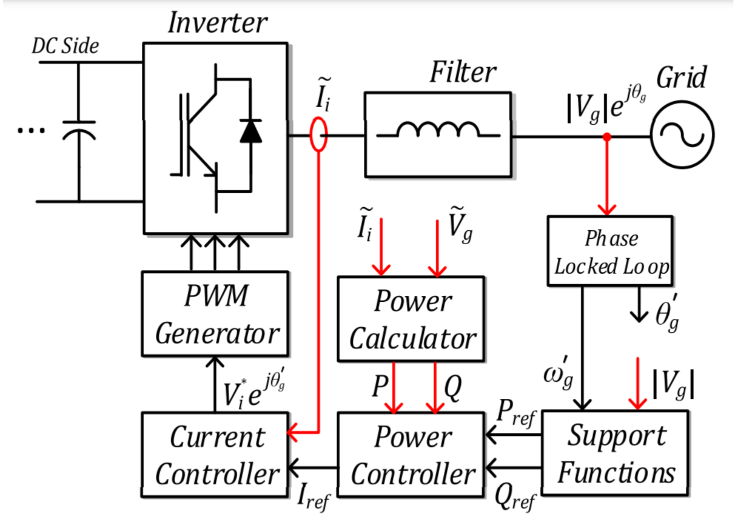

Figure 2.3 - Block diagram of a typical GFL Inverter (source: [22])

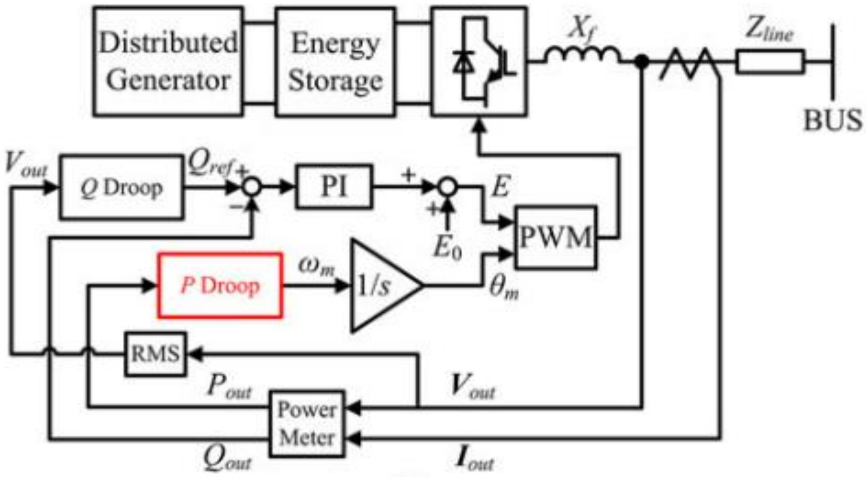

Figure 2.4 - Block diagram of GFM with droop control (source: [26])

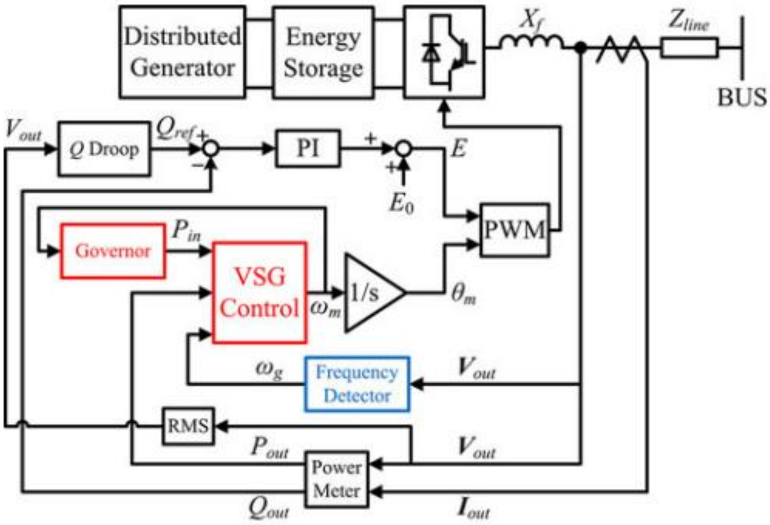

Figure 2.5 - Block diagram of GFM with VSM control (source: [26])

In summary, a GFL converter enables fast power control while a GFM converter, which emulates synchronous generators, provides frequency and voltage support [27].

There are already multi-converter system studies that show that combining GFL and GFM converters can leverage their respective strengths, resulting in a hybrid GFL/GFM multi-converter system, shown in [27]. However, the interaction between GFL and GFM controls may lead to instability issues that require thorough analysis [27].

2.4.4 - Integration of Grid-Forming Technology with Hybrid Energy Storage Systems

The combination of GFM technology with Hybrid Energy Storage Systems (HESS) represents a huge step in solving problems related to low-inertia power systems. The integration of GFM technology with hybrid storage systems, consisting of ultra-capacitors (UCAP) and battery storage, aims to emulate the performance of traditional synchronous generators, thereby stabilizing grids dominated by renewable energy sources [28]. The combination of GFM and HESS provides additional flexibility to the system [28]. The ultra-capacitors provide a fast response to transient events, such as sudden load changes, while the batteries supply long-term energy support. This decoupling of power and energy functions reduces the burden on batteries, thus lowering degradation and operating costs [28]. This hybrid configuration excels in providing critical grid services, including frequency regulation, voltage support and grid resynchronization. Very fast, UCAPs respond to high-frequency fluctuations, while batteries take care of longer-term demands. In this way, the system achieves a remarkably efficient operation under the most diverse scenarios, including island mode and transitions to grid-connected operation [28].

Simulation results, shown in [28], demonstrate the effectiveness of HESS-GFM systems in dynamic conditions. Tests show that the system can seamlessly switch between island and grid-connected modes, handle load variations and maintain stability. UCAPs consistently manage rapid power fluctuations, alleviating the burden on batteries and ensuring continuous service provision.

2.4.5 - Synchronous Condensers

Synchronous condensers (SC) provide powerful support to grid stability by supplying reactive power and inertia, which is an important action for the mitigation of stability risks in low-inertia grids.

SC are rotating machines similar to synchronous generators but without a prime mover [29]. Traditionally utilized for reactive power compensation and voltage stability, SC have become increasingly significant in the context of modern grids dominated by inverter-based resources (IBR) [29]. They emulate the properties of Synchronous generators (SG), providing instantaneous power response to grid disturbances [20]. Owing to the fact that SC have a rotating mass, it allows them to resist frequency changes during disturbances, thus providing grid inertia [20]. During a sudden drop or rise in frequency, the kinetic energy stored in the rotating mass helps to stabilize the frequency until other resources are capable of responding [20].

Other than inertia, SC contribute to grid strength by enhancing voltage stability and supporting short-circuit current requirements. SC can respond quickly to changes in reactive power demand, stabilizing voltage levels [20]. SC improve short-circuit capacity, enhancing the operation of protective relays and increasing grid resilience against faults [20].

The combination SC with electronic inverters, particularly GFL and GFM inverters, is an effective solution to improve grid stability, shown in [30]. As seen previously GFL inverters depend on a pre-defined grid voltage waveform for synchronization and, therefore, are vulnerable to instabilities in weaker grids. SC expand the functionality of GFL inverters by offering the sinusoidal voltage reference that is needed for maintaining stable inverter operation [30]. GFM inverters, however, generate voltage and frequency autonomously and emulate operating characteristics of synchronous generators [28]. In the presence of SC, GFM get additional inertial and reactive power support which mitigates frequency and voltage deviations more effectively [30]. This is a synergistic integration of SC and inverters that combines the best of both technologies to ensure better fault tolerance and dynamic response in renewable-dominated grids.

Hybrid synchronous condenser (HSC) systems, which combine SC with battery energy storage systems (BESS), have shown great potential in enhancing low-inertia grids [28]. While BESS provides rapid active power support during frequency deviations, SC provide inertia and reactive power, increasing the stability and strength of the overall system [20]. This combination allows the grid to handle both transient and steady-state matters with ease [20]. BESS integration allows for fast frequency regulation and efficient state-of-charge management, while SC support the voltage and maintain the resilience of the system during disturbances [31].

2.5 - Case studies and Applications

This section provides an examination of GFM converter technologies and their applications in regions where RES constitute a significant portion of the energy mix. This review outlines the challenges posed by the increasing reliance on IBR due to the diminishing presence of traditional SG and provides insights into the potential solutions offered by GFM converters.

GFM converters have demonstrated significant potential across a range of applications, particularly in systems with high renewable energy penetration. Among these applications, BESS have emerged as crucial components for stabilizing renewable-rich grids [32]. As examples, shown in [32], the Hornsdale Power Reserve in South Australia integrates a 150 MW/194 MWh BESS capable of providing synthetic inertia and fast frequency response. Similarly, the Dalrymple BESS project exemplifies the benefits of Virtual Synchronous Generator (VSG)-based GFM control, showcasing its effectiveness in supporting islanded operations and quickly recovering from faults [32].

Relatively to wind power, GFM converters have facilitated greater integration of renewable energy into the grid by addressing key stability challenges. The Dersalloch Wind Farm in Scotland operated in GFM mode using VSG control, effectively enhancing system stability during a six-week trial period [32]. Additionally, advanced GFM technologies have been employed in wind turbines to emulate the behaviour of synchronous generators, mitigating subsynchronous resonance and ensuring stable operation in systems with significant wind power contributions [32].

Hybrid energy systems combining multiple renewable sources, such as solar PV and wind, with BESS have proven to be particularly effective in microgrid and island scenarios [32]. Projects like the Graciosa Island hybrid system, referred in [32], illustrate the benefits of integrating PV, wind and GFM-enabled BESS to create a reliable and black-start-capable power system. This system effectively balances intermittent renewable sources while maintaining grid stability and reliability, demonstrating the synergy between GFM and diverse energy sources in hybrid configurations.

HVDC systems have also leveraged GFM capabilities to address the challenges of weak grids and variable power flows. For example, the Mackinac HVDC project in Michigan, referred in [32], employs GFM control to manage bidirectional power transfer, improve voltage stability and maintain robust operation in weak grid conditions.

The reviewed case studies underline the adaptability of GFM converters in providing essential grid-support functions such as frequency regulation, black start capabilities and seamless operation under weak grid conditions. However, challenges remain, particularly in standardizing control approaches, ensuring fault ride-through capabilities and achieving robust operation in highly dynamic and variable conditions [32].

Real-world implementations illustrate the advantages of GFM converters in renewable-dominant grids. Projects across different scales, ranging from microgrids to transmission-level HVDC systems, demonstrate their flexibility and scalability. Future research should focus on refining control strategies, developing hybrid control techniques, i.e. combining the benefits of droop control and VSG for enhanced system stability, Multi-Input Multi-Output (MIMO) control systems and enhancing the grid compatibility of GFM technologies to support a 100% renewable energy future [32].

2.6 - Final Remarks

This chapter provided an in-depth review of the state-of-the-art practices, challenges and solutions related to low-inertia power grids. It began by analysing the technical and operational impacts of large-scale Renewable Energy Sources (RES) integration, highlighting issues like reduced grid inertia, frequency instability and voltage challenges.

Next the chapter reviewed grid codes and the regulatory framework for renewable integration, with emphasis on the European Network Code's requirements for generators. These measures are aimed at mitigating instability risks while enabling greater RES penetration.

In addition, the chapter explored solutions, including synchronous condensers, grid-forming inverters and advanced energy storage technologies, which offer reactive power support and enhanced grid stability.

Finally, the case studies reviewed showcased real-world applications of emerging technologies. These applications highlight their success in improving fault ride-through capabilities, frequency regulation and voltage stability.

There is a strong focus on refining control strategies, standardizing inverter technologies and developing hybrid solutions that combine advanced tools and methodologies. These efforts aim to ensure a smooth transition to sustainable, low-inertia grids capable of supporting a 100% renewable energy future.

Chapter 3

Dynamic Modelling and Simulation of Low Inertia Systems

In this chapter, the dynamic modelling for simulation of low-inertia power systems is presented. It describes the simulation platform developed in the DIgSILENT PowerFactory software package and the IEEE 9-bus system used as the simulations test system. Models for synchronous generators, synchronous condensers, grid-following and grid-forming converters are explained. These models provide the basis for analysing the performance of different technologies in stabilizing low-inertia grids.

3.1 - Simulation Platform in DigSilent PowerFactory

To carry out the dynamic simulations of low-inertia power grids with high renewable energy sources (RES) penetration, the simulation tool DIgSILENT PowerFactory was chosen. This software is widely utilized for power system modelling, analysis and dynamic simulation due to its great flexibility, precision and large library of elements and control models [33].

DigSilent PowerFactory facilitates detailed modelling of inverter-based and conventional power systems, enabling the simulation of dynamic effects, for example, frequency deviations, voltage dips and response to faults. Its extensive library of preconfigured elements alongside user-defined models enables an accurate representation of synchronous machines, power electronic interfaces and a variety of control methods, such as grid-following and grid-forming inverters [33].

This software will be used in this project to simulate different configurations of the IEEE 9-bus system. The modifications from the base case are the replacement of conventional power generation by renewable sources and the incorporation of grid-forming converters and synchronous condensers. The configurations have been chosen to examine the extent to which each technology aids system stability, with particular emphasis on frequency regulation, voltage support and fault recovery.

The IEEE 9-bus test system, which is the primary network, will be described in detail in the following section. It will be followed by a description of the specific models and parameters that will be used to represent each technology in the simulated scenarios.

3.2 - The IEEE 9-Bus Network Test System

The IEEE 9-bus model represents a standardized test system modelled by the IEEE Group. It serves as a benchmark for analysing and simulating various power system issues [34].

The IEEE 9-bus test system was chosen in the scope of this dissertation because it offers a good balance between simplicity and realistic system behaviour for in-depth dynamic analysis. With only three generators and nine buses, its reduced size facilitates the implementation of models and the initial development of simulation studies. At the same time, it is widely used by researchers to study important dynamic phenomena such as rotor angle stability, frequency stability, short-circuit response and voltage support while remaining sufficiently simple to enable observation and interpretation of the impact caused by various technologies, such as grid-following and grid-forming converters and synchronous condensers.

In this context, the IEEE 9-bus system is taken as the base structure where different RES integration scenarios will be included. By altering the underlying test system, we can simulate disturbances such as load changes or short circuits and analyse transient and steady-state responses of the system to various configurations. Such tests are instrumental in determining the relative efficacy and impact of each technology on grid stability.

The IEEE 9-bus has nine electrical buses that are the major points at which power can be input and loads connected, three synchronous generators, each of which is connected to a bus, generator SG1 is connected to slack bus 1 while generators SG2 and SG3 are connected to PV-buses, three two winding power transformers and three different loads [34]. Finally, the network is connected by six transmission lines [34]. The single line diagram is shown in **Figure 3.1**.

The detailed data of the transmission lines, transformers and loads used in the network test system are provided in **Annex A**.

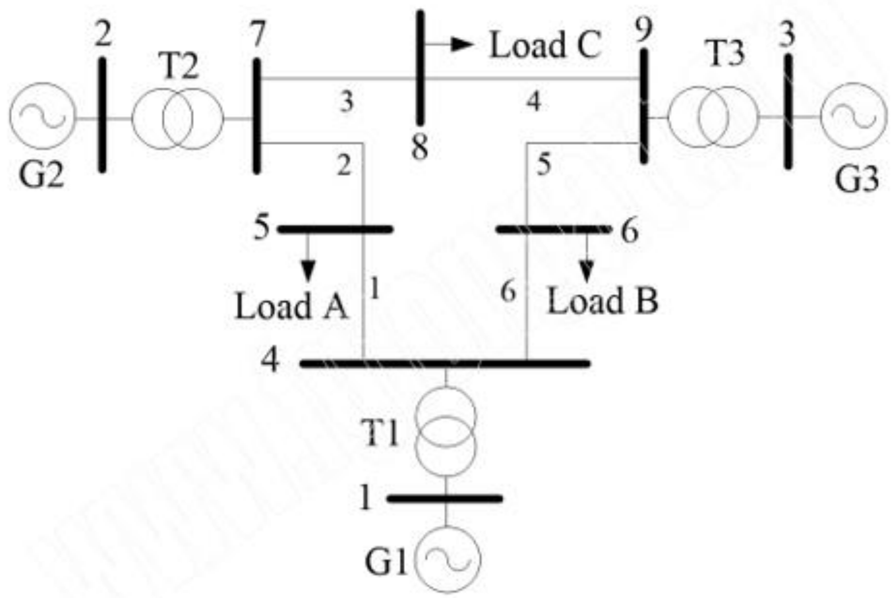

Figure 3.1 - IEEE 9-Bus System (source: [35])

3.3 - Modelling Conventional Synchronous Generation

This section presents the modelling approach adopted for the conventional synchronous generators used in the IEEE 9-bus test system.

The modelling captures both electrical and mechanical aspects of generator operation, enabling a dynamic response simulation under disturbances such as faults or sudden load changes.

By accurately reproducing the dynamic behaviour of synchronous machines through detailed parameterization and control models, the simulation framework ensures that the performance of traditional generation is realistically represented.

The subsections below describe the main components of the synchronous generation model, including the electrical machine representation, the voltage regulator and the mechanical prime mover with its governing system.

3.3.1 - Synchronous Generator and Automatic Voltage Regulator

All three generators in the IEEE 9-bus test system were modelled as round-rotor synchronous machines (*GENROU*), which are generators typically used in thermal power plants [36]. The *GENROU* model represents a detailed round-rotor synchronous machine, capturing both transient and sub-transient electromagnetic dynamics along the direct (d) and quadrature (q) axes. It includes differential equations associated with the main field winding and damper windings, enabling accurate simulation of flux and current dynamics during disturbances. The d-axis primarily handles the excitation system through the field winding, while the q-axis models torque-related interactions. Flux linkages such as Ψ' and Ψ'' are used to track the machine's dynamic states, with time constants and reactances defining their behaviour. The model outputs the stator currents (**Id** and **Iq**), which are crucial for simulating the machine's response under grid faults, switching events, and other transient conditions. The *GENROU* modelling framework used for these generators is shown in **Figure 3.2** and the key parameters are detailed in **Table 3.1**.

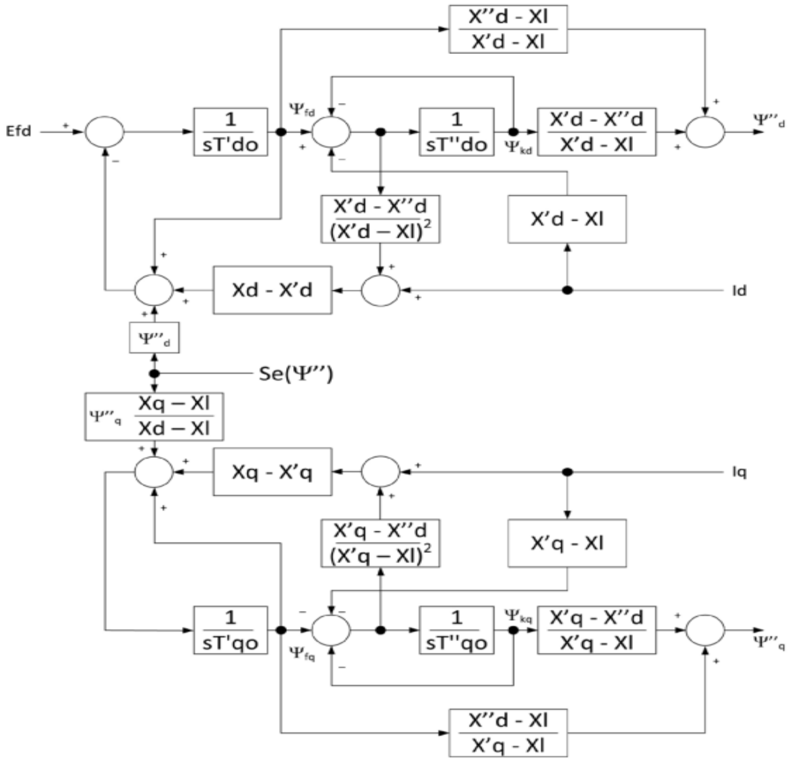

Figure 3.2 - The *GENROU* model (source: [37])

Table 3.1 - Parameters Nomenclature of the *GENROU* model (Adapted from: [36], [37])

Parameters Nomenclature of the *genrou* model		
Parameter	**Nomenclature**	**Unit**
D	Damping coefficient	p.u.
H	Inertia constant	s
Xd	d-axis synchronous reactance	p.u.
Xq	q-axis synchronous reactance	p.u.
Xd'	d-axis transient reactance	p.u.
Xq'	q-axis transient reactance	p.u.
Xd"	d-axis sub-transient reactance	p.u.
Xq"	q-axis sub-transient reactance	p.u.
Xl	Leakage reactance of the generator stator	p.u.
rstr	Stator resistance	p.u.
T'do	d-axis transient time constant	s
T'qo	q-axis transient time constant	s
T"do	d-axis sub-transient time constant	s
T"qo	q-axis sub-transient time constant	s
SG10	Saturation parameter	p.u.
SG12	Saturation parameter	p.u.

These parameters were configured in DIgSILENT PowerFactory, for each generation unit, the detailed values for each parameter are provided in **Annex B**.

Each synchronous machine is also equipped with an automatic voltage regulator (AVR), the “exc_AC” model available in the DIgSILENT library. The block diagram of this regulator is presented in **Figure 3.3**.

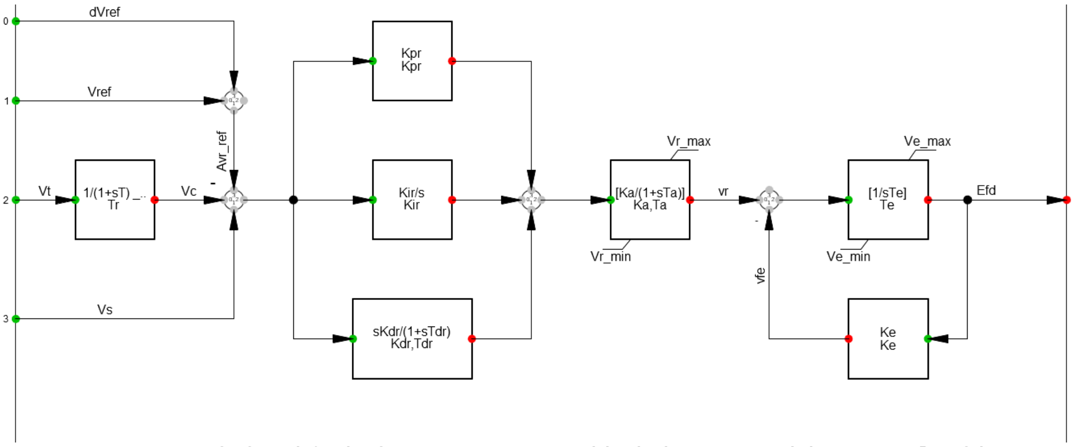

Figure 3.3 - exc_AC: Simplified AC excitation system block diagram model (source: [DigSilent Powerfactory Library])

The excitation system model comprises several control blocks, including a proportional-integral (PI) voltage regulator, dynamic compensators, and output limiters. The voltage error, calculated as the difference between the reference voltage and the measured terminal voltage, is processed through the PI regulator to generate a control signal. This signal is then modified by an optional stabilizing filter and passed through dynamic amplifiers and saturation limits to ensure system stability and safety. The final output, after applying rate and magnitude limiters, defines the field voltage (*Efd*) applied to the synchronous machine.

The numerical settings of the AVR are also detailed in **Annex B**.

3.3.1.1 - Synchronous Condensers

A synchronous condenser can be modelled as a synchronous generator without the prime mover. Essentially, this type of unit is a synchronous machine that operates without mechanical torque input. In dynamic simulations, the SC can therefore be modelled using a synchronous generator model, but without the turbine governor model.

This illustrates that a synchronous condenser does not produce active power from a prime source but still helps to keep the grid stable with its own mechanical inertia and its ability to produce or consume reactive power. The SC model retains the major electrical features of the synchronous machine, such as rotor and stator portions, damper windings and the excitation system, needed to properly model voltage support and fault current contribution.

Basically, the synchronous condenser model is based on the synchronous machine and AVR described in **Chapter 3.3.1**, with the active and reactive power injection set to 0. Is important to note that a SC consumes a small amount of energy (Wh) to keep the rotor spinning and supply auxiliary systems (such as excitation, ventilation, and lubrication). This consumption is typically in the range of 1% to 3% of the machine's rated power.

3.3.2 - Prime Mover

To represent the mechanical power input to each synchronous generator, the model used was the IEEE TGOV1 turbine governor. The model block diagram is given in **Figure 3.4**.

This model captures the essential dynamics of a steam turbine governor system, incorporating several key functional components. The governor droop characteristic, R determines how the mechanical power output adjusts in response to frequency deviations, thereby contributing to primary frequency control [38]. The model also includes a representation of the main steam control valve, whose motion is governed by a time constant, T1 and constrained by upper and lower operational limits, VMAX and VMIN, to reflect realistic mechanical behaviour and physical restrictions of the valve system [38].

To account for the energy transport delay and mechanical response within the turbine, the model integrates a single lead-lag transfer function, characterized by the time constants T2 and T3. This block simulates the time lag associated with steam flow through the reheater and turbine stages. The ratio T2/T3 denotes the fraction of the turbine's total power that is developed by the high-pressure turbine stage. T3 represents the time constant of the reheater [38].

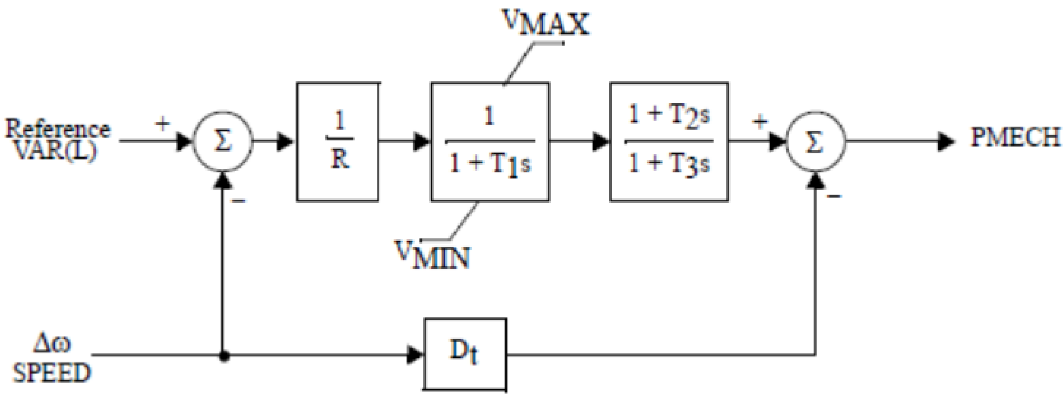

Figure 3.4 - gov_IEEE_TGOV1 Simple steam turbine-governor block diagram model (source: [38])

The numerical settings of the governor are also detailed in **Annex B**.

3.4 - General Simulation Models for Wind and Solar Generation with Grid Following Converters

The integration of the renewable energy sources, particularly photovoltaic generation, in the IEEE 9-bus system was modelled using a standardized scheme and elements available in

DIgSILENT PowerFactory. The photovoltaic power plant was modelled using the "WECC Large-scale PV Plant 110MVA 50Hz" template available in the DigSilent global library. This template ensures conformity with the second-generation generic models for renewable energy systems [39].

The second-generation models are grouped into five main categories, each representing a distinct aspect or function relevant to the overall system [39]:

- the Renewable Energy Generator/Converter (REGC_*) models represent the electrical interface between IBR and the power grid. These models are designed to mimic the behaviour of the power electronic converter, capturing how it interacts with the grid by converting control commands into current or voltage injections [39];
- the Renewable Energy Electrical Control (REEC_*) models simulate the local automatic control systems operating within each individual IBR unit. These models govern the behaviour of the generator/converter by managing key functions such as active and reactive power control, voltage regulation and response to dynamic grid conditions [39];
- the Renewable Energy Plant Controller (REPC_*) models simulate the centralized supervisory control system responsible for managing the coordinated operation of all IBR units within a renewable energy plant [39];
- the mechanical and aerodynamic models (WTG***_*) represent the physical subsystems and control mechanisms within wind turbine generators (WTG) [39];
- The auxiliary control models support specialized functions to enhance system performance under specific conditions. These include the weak grid option controller (WTGWGO_A), designed for type 4 WTGs to improve stability in low short-circuit strength networks and the inertia-based fast frequency response controller (WTGIBFFR_A) [39].

Table 3.2 presents the available models for each category included in the Second-Generation Generic RES Models.

Table 3.2 - Second-Generation Generic RES Models [source:39]

Generator/Converter Models	Electrical Controller Models	Power Plant Controller Models	WTG Mechanical and Aerodynamic Models	Auxiliary Controller Models
REGC_A	REEC_A	REPC_A	WTGA_A	WTGWGO_A
REGC_B	REEC_C	REPC_C	WTGQ_A	WTGIBFFR_A
REGC_C	REEC_D		WTGP_A	
			WTGP_B	
			WTGT_A	
			WTGT_B	

The template "WECC Large-scale PV Plant 110MVA 50Hz" used to define the PV system model is composed of the following components: the Renewable Energy Generator/Converter Model REGC_C, the Renewable Energy Electrical Control Model REEC_D, the Weak Grid Option Model WTGWGO_A and is also equipped with a protection model for over/under-voltage and over/under-frequency events.

The REGC_C model developed by EPRI in 2019/2020, as stated in [39], provides a detailed representation of the power electronic interface that connects the IBR to the grid. The developed model enables the conversion of current command signals into corresponding voltage reference signals behind a defined impedance, enhancing the numerical robustness of the IBR model, particularly when operating in low short-circuit strength grids [40]. Additionally, this model, in contrast to the REGC_A model, incorporates the influence of both the inner current control loops and the phase-locked loop (PLL) on the IBR's dynamic behaviour. By including these internal control dynamics, the model significantly improves the accuracy of positive sequence simulations, allowing them to capture oscillatory behaviour that originates from fast-reacting inner control systems [40].

The block diagram of the REGC_C model is represented in **Figure 3.5**.

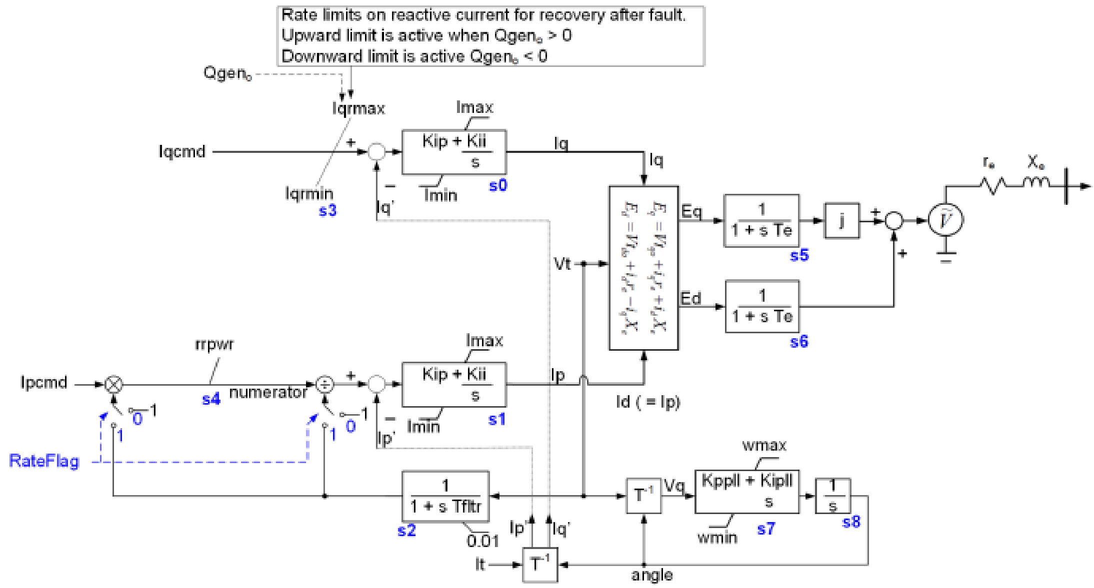

Figure 3.5 - REGC_C block diagram model (source: [39])

The REEC_D developed in 2018, manages the electrical control of the inverter, including active and reactive power control logic [39]. The model includes mechanisms for active current regulation, which generate the active current command signal (Ipcmd) and reactive current regulation, responsible for producing the reactive current command signal (Iqcmd). In addition, the model incorporates a current limiting function that ensures both active and reactive current outputs remain within the converter's specified operating limits [39].

Compared to the REEC_A model, the REEC_D model exhibits some extra characteristics. Firstly, it lacks the state-transition logic associated with the reactive current injection path found in REEC_A, meaning that this path remains continuously active unless explicitly disabled by setting the gain to zero or applying a very wide deadband [39]. Secondly, the active power control in REEC_D is not influenced by rotor speed, making it incompatible with mechanical models like WTGT_A or WTGT_B and therefore not advisable for modelling WTG [39]. Thirdly, the REEC_D model includes an additional control path that provides a basic representation of battery charge and discharge behaviour, which makes it especially suited for modelling BESS. Lastly, the model allows for bidirectional active power flow, as the minimum active current (Ipmin) is set equal to the negative of the maximum (-Ipmax) [39].

The block diagram of the REGC_C model is represented in **Figure 3.6**.

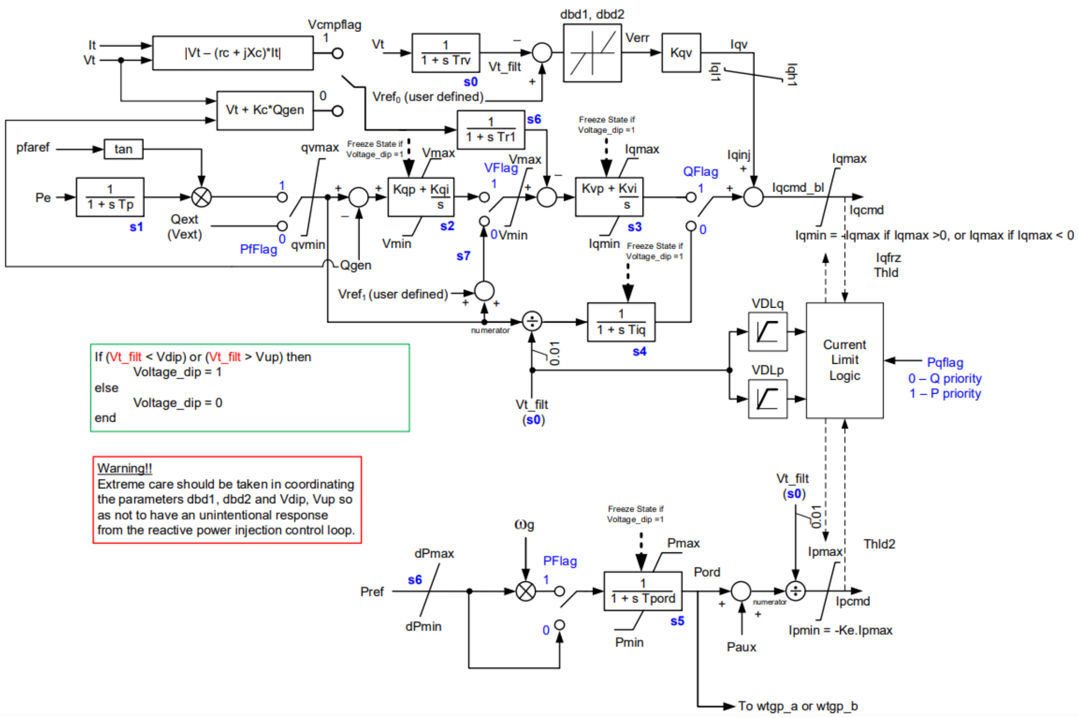

Figure 3.6 - REEC_D block diagram model (source: [39])

All the parameters associated to the PV power plant models are detailed in **Annex C**.

3.5 - General Simulation Models for Grid Forming Converters

Grid-Forming converters are modelled using the "Virtual Synchronous Machine - Storage" template available in the DIgSILENT library. This model provides essential functionalities such as voltage and frequency regulation, virtual inertia emulation and robust dynamic support during disturbances.

By analysing **Figure 3.7,** it is shown that the composite model structure used for the GFM converter, is composed of several functional modules, each responsible for a specific control task essential to grid-forming operation:

- **AC Voltage Controller**: This module regulates the converter's output voltage by adjusting it to match a reference value, ensuring voltage amplitude remains within acceptable limits during normal and disturbed operating conditions.
- **Power Calculation Module**: It continuously computes the instantaneous active and reactive power outputs based on the voltage and current at the point of connection. This information is used in other control loops, such as frequency and voltage regulation.
- **Grid-Forming Control via Virtual Synchronous Machine**: This core module emulates the dynamic behaviour of a synchronous generator by introducing virtual inertia and damping. It allows the converter to respond to frequency deviations similarly to a physical rotating machine.
- **Virtual Impedance**: This element introduces a programmable impedance in the control loop to improve current sharing among multiple inverters and to enhance system stability during disturbances
- **Output Voltage Calculation / Inner Controller**: Responsible for tracking the internal voltage reference generated by the VSM block and regulating the converter's switching actions accordingly. This inner control loop ensures fast and accurate voltage control.
- **Frequency Sensitive Mode (FSM)**: This module adjusts the power output of the converter based on frequency deviations. By modifying the power setpoint in proportion to the frequency variation, it enhances the converter's ability to support frequency containment during transients.

The DC modules shown in the GFM model have been disabled, as their dynamic behaviour is not relevant for this study. Since the analysis focuses on short-duration phenomena, the charge and discharge dynamics of the BESS have minimal impact and can be neglected. Disabling these components simplifies the model without affecting the representation of the key grid-forming functionalities.

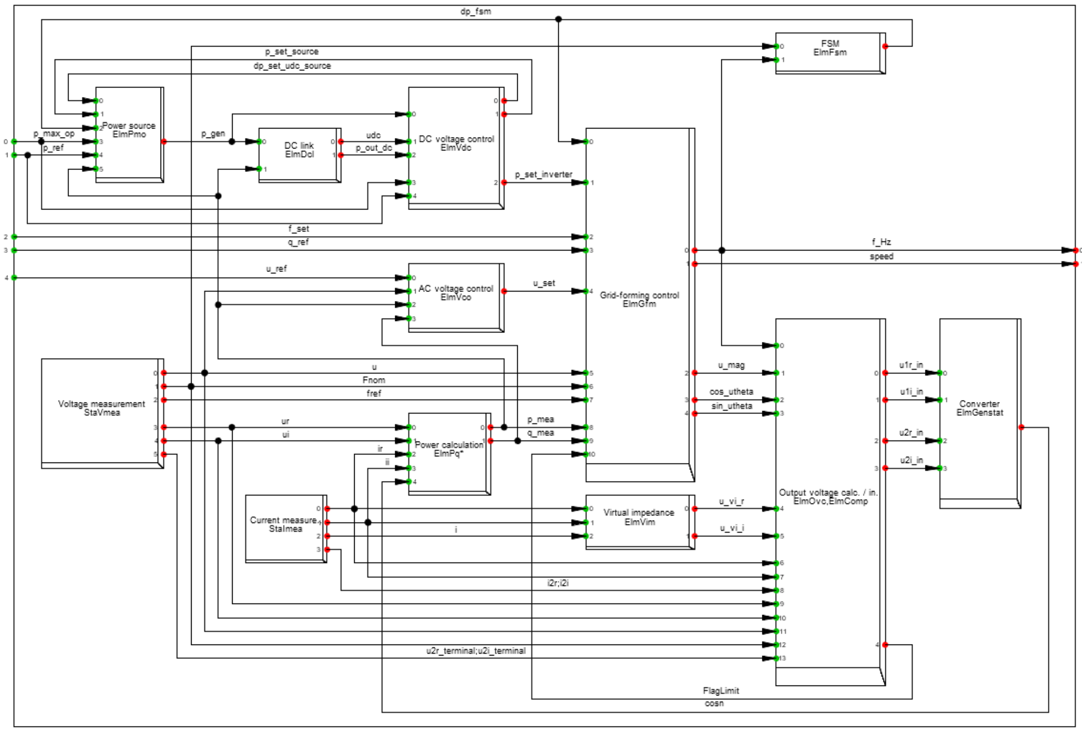

Figure 3.7 - Grid Forming Converter Frame (source: [DigSilent Powerfactory Library])

The Virtual Synchronous Machine (VSM) is the heart of the Grid-Forming (GFM) converter, responsible for controlling the voltage and frequency output to the grid. The VSM control block is shown in **figure 3.8.**

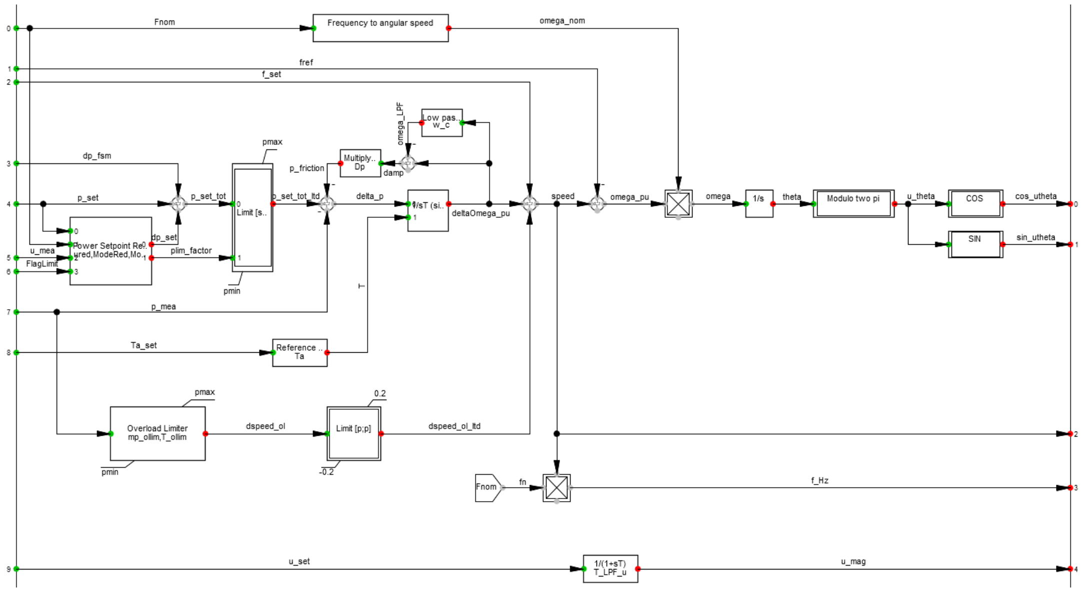

Figure 3.8 - Virtual Synchronous Machine block diagram model (source: [DigSilent Powerfactory Library])

This block diagram illustrates the control mechanism of the VSM. The process begins with a nominal frequency input (Fnom) and a power setpoint (p_set) which are fed into a power setpoint reduction and limiting subsystem that adjusts the power setpoint (p_set_tot) based on various flags and limits to ensure safe operation. The adjusted power setpoint is compared against the inverter's actual output power (p_mea) to generate a power imbalance signal

$(\mathrm{delta\_p})$. At the core of the system is the block $\frac{1}{sT}$, this inertia block models the motor's mechanical inertia reflecting the natural gradual acceleration or deceleration of the motor shaft, preventing abrupt speed changes and ensuring realistic dynamic behaviour. This block plays a critical role by converting the power imbalance into a frequency deviation $(\mathrm{deltaOmega})$. Simultaneously, torque setpoint $(\mathrm{Ta\_set})$ and overload limiting blocks process torque and speed limits to prevent motor overloading, producing a limited speed change $(\mathrm{dspeed\_ol\_ltd})$. The frequency deviation is processed through a low pass filter and a damping factor. The inclusion of the damping coefficient and is associated dynamics reduce oscillations and stabilize frequency variations by applying virtual damping torque. The total motor speed $(\mathrm{omega\_pu})$ is then calculated by combining the nominal angular speed, the change in angular velocity filtered through the inertia block and the overload limiter speed, which is then converted to actual angular speed (omega) and further to mechanical angle (theta) via the integrator $\frac{1}{s}$.

The outputs of these control blocks are combined to produce the final control signals $\mathrm{cos\_utheta}$ and $\mathrm{sin\_utheta}$, which combine with the Virtual impedance and the voltage measurements output signals, commands the inverter to inject or absorb power in a manner that replicates the inertial and damping response of a synchronous generator.

The parameters of all the GFM inverters modules are detailed in **Annex D**.

3.6 - Final Remarks

This chapter established the simulation platform and detailed the models used to represent different generation technologies in a low-inertia grid environment. The IEEE 9-bus system was adapted to include synchronous generators, grid-following PV systems based on WECC templates, grid-forming converters modelled with the "Virtual Synchronous Machine – Storage" DigSilent template and synchronous condensers.

These models set the stage for dynamic simulations under various disturbance scenarios. The goal is to compare, in the next sections, how each technology contributes to frequency stability, voltage support and fault recovery in low-inertia systems.

Chapter 4

System Response in Evolving Grid Scenarios

In this chapter, the dynamic response of the IEEE 9-bus test system is examined under various operating conditions and disturbance scenarios, with a specific focus on frequency stability. Starting from a base case with full synchronous generation, the system is progressively modified through the integration of renewable energy sources (RES), particularly photovoltaic (PV) power plants using grid-following inverters. By simulating events such as load loss, generator disconnection and short-circuit faults, this chapter aims to evaluate the impacts of reduced inertia on system behaviour. The simulations establish a performance baseline and set the foundation for subsequent analyses involving grid-forming converters and synchronous condensers as potential solutions to mitigate the adverse effects observed in low-inertia power systems.

4.1 - Theoretical foundation and Required Calculations for Dynamic Simulation

This section presents the theoretical foundation and modelling assumptions necessary for conducting dynamic simulations. The primary objective is to assess the system's frequency response under various disturbances, such as generator outages, load shedding events and short-circuit faults. To achieve this, it is essential to define specific frequency stability metrics and adopt consistent assumptions regarding system components, particularly load representation.

Since we have more than one generator in the network, the overall frequency of the system (f_{system}) can be calculated based on the frequency of centre of Inertia (COI) which is a composite metric that captures the overall dynamic behaviour of the system frequency based on the inertial characteristics of each synchronous generator. Unlike individual bus frequencies, which may vary due to local disturbances or control actions, the frequency of centre of Inertia provides a system-wide average weighted by the inertia and base power of each machine. Mathematically, the frequency of centre of Inertia can be expressed as:

$$f_{system}(t) = f_{coi}(\mathrm{t}) \; = \frac{\sum_{i=1}^{N} H_i * S_{Bi} * f_i(t)}{\sum_{i=1}^{N} H_i * S_{Bi}} \tag{4.1.1}$$

Where:

H_i: Inertia constant of SG_i, in s.

S_{Bi}: SG_i power base, in MVA.

$f_i(t)$: Instantaneous frequency of SG_i, in Hz.

N: Total number of SG.

Equation 4.1.1 shows that synchronous generators with higher inertia and greater capacity contribute more significantly to the system frequency.

The instantaneous frequency of each SG is calculated using equation 4.1.2.

$$f_i(t) = \omega_i * f_N \tag{4.1.2}$$

Where:

$w_i(t)$: Instantaneous rotor speed of SG_i, in $\mathrm{p.u.}$

f_N: System's nominal frequency, in Hz.

The frequency stability of the system will be assessed by analysing two main aspects: the frequency nadir and the RoCoF. These metrics provide a detailed understanding of the system's dynamic response to sudden disturbances. As discussed in **section 2.2**, both RoCoF and frequency nadir are recognized as critical stability parameters with operational thresholds defined by ENTSO-E under the European Network Code on RfG presented in **section 2.4.1.** The RoCoF serves as an early indicator of the severity of power imbalances, reflecting how quickly system frequency deviates from nominal following a disturbance, an aspect particularly sensitive to the system's overall inertia. The frequency nadir, on the other hand, indicates the lowest point the frequency reaches before recovery begins. It is a crucial measure used to assess whether the system stays within acceptable frequency limits. Both indicators will be computed using the frequency of centre of Inertia.

Finally, for the dynamic analysis, all loads in the system were modelled as constant impedance. This modelling assumption is adopted to reflect the more realistic behaviour of aggregate loads under dynamic conditions, particularly during voltage disturbances. Unlike constant power loads, that maintain a fixed power consumption regardless of voltage changes, which can lead to numerical instabilities or non-physical results, constant impedance loads scale naturally with voltage, as both active and reactive power consumption decrease with falling voltage levels. The constant impedance approach ensures simulation stability and is a widely accepted simplification in transient stability studies, has load dynamics are not the main subject of analysis.

It is also important to consider the dynamic behaviour of the converters to be introduced and the type of instability that these models may cause. This type of new stability phenomena is not captured by traditional metrics such as RoCoF or frequency nadir and is known as Converter-Driven Stability (CDS) and is particularly relevant in weak grids with high converter penetration [41]. These instabilities are primarily due to interactions between converters and the grid or among the converters themselves. CDS is generally divided into two categories based on frequency and dynamics, Slow Converter-Driven Stability (SCDS) and Fast Converter-Driven Stability (FCDS) [41].

Slow Converter-Driven Stability (SCDS) refers to a category of instabilities that occur at frequencies below 10 Hz and are typically associated with slow dynamic interactions between the outer control loops of power converters and the grid. These instabilities manifest as low-frequency oscillations, including subsynchronous and sideband oscillations, and are especially prevalent in systems with weak grid conditions, characterized by low short-circuit ratios and high converter penetration [41].

In grid-following (GFL) converters, the phase-locked loop (PLL) used for synchronization plays a critical role. If the PLL bandwidth is too high relative to the grid strength, it can introduce poor damping and lead to unstable behaviour. Additionally, interactions between the PLL and outer voltage or power control loops can further exacerbate the instability, particularly when these control systems are not properly tuned [41].

Grid-forming (GFM) converters are also susceptible to SCDS if the voltage or power controllers introduce adverse dynamic interactions, especially when multiple converters are connected and interacting through a weak grid. The presence of several tightly coupled converters can lead to resonance phenomena and amplify small disturbances [41].

Fast Converter-Driven Stability (FCDS) encompasses high-frequency instabilities typically occurring in the range of several hundred hertz. These instabilities are primarily driven by fast inner control loops within power electronic converters, such as current control loops, and are heavily influenced by factors like control delays, PWM (pulse-width modulation) dynamics and high-frequency switching behaviour. Unlike slow instabilities, FCDS arises from the interaction of the converter’s fast internal dynamics with the grid’s impedance, particularly when converters operate close to or beyond their stability margins [41].

4.2 - Power Flow and Initial Conditions Analysis

Before performing the dynamic simulation, it is essential to ensure that the power system is in a steady-state operating point, which serves as the initial condition for the transient studies.

This preliminary step involves a power flow analysis to determine the steady-state distribution of active and reactive power, as well as the voltage magnitudes and angles at each bus.

A load flow calculation was carried out for the IEEE 9-bus test system with only synchronous generation. The results, presented in **table 4.1**, include the active and reactive power generated by each SG, the power consumed at each load bus and the voltage profile across all network buses. These values establish the reference operating point from which the dynamic disturbances will be applied.

Tabe 4.1 – Power Flow calculation

Bus	Pgen (MW)	Qgen (Mvar)	Pcons (MW)	Qcons (Mvar)	Voltage (p.u.)	Angle (rad)
1	71,6	27	0	0	1,04	0
2	163	6,7	0	0	1,02	0,162
3	85	-10,9	0	0	1,02	0,082
4	0	0	0	0	1,03	2,580
5	0	0	125	50	1,00	2,548
6	0	0	90	30	1,01	2,553
7	0	0	0	0	1,03	2,683
8	0	0	100	35	1,02	2,630
9	0	0	0	0	1,03	2,653

To achieve numerically stable dynamic simulations, it is essential to initialize the system's state variables using the steady-state solution obtained from the power flow analysis. The dynamic simulation is configured with an integration step size of 1 millisecond and a maximum error for dynamic model equations of 0.01%. When introducing RES into the system the integration step size will be reduced to 0.1millisenconds.

To proceed with the dynamic simulation, the only remaining step is to define the disturbance events.

The dynamic simulation will consider three types of disturbance events: load loss, generation loss and a short-circuit event on a line with subsequent line tripping. Each event will be tested independently to clearly document its resulting impact on system frequency dynamics.

All disturbances are applied at 2 seconds into the simulation. In the case of the short-circuit event, a three-phase short-circuit fault is applied on the middle of a transmission line at t = 2.0s and is cleared at t = 2.2s by opening the affected line. Each simulation runs for a total duration of 15 seconds, allowing the full transient and frequency response to be observed.

In the following section, the results of the simulations performed on the network with only synchronous generation are presented and discussed.

4.3 - Simulation Results with Only Synchronous Generation

This section presents the results obtained from the dynamic simulations performed on the IEEE 9-bus test system with only synchronous generation. The main objective is to evaluate the system's frequency response to the different types of disturbances described in **section 4.2**.

For each simulation scenario, the frequency of centre of inertia was calculated and used as the reference for analysing system-wide frequency behaviour. From the frequency of centre of inertia, two key stability indicators were derived, the frequency nadir and the RoCoF.

The detailed results and corresponding analyses for each disturbance type are presented in the following subsections.

4.3.1 - Load Loss Events

To evaluate the system's dynamic response to sudden reductions in demand, simulations were conducted for three distinct load loss scenarios.

Table 4.2 - Load Power

Load	Active Power (MW)	Reactive Power (Mvar)
A	125	50
B	90	30
C	100	35

The frequency evolution for the worst-case scenario following the load loss is shown in **Figures 4.1,** where a clear frequency increase is observed immediately after each event. This response is expected, as the sudden drop in active power demand creates an excess of generation, leading to system acceleration and frequency rise. In terms of frequency analysis performed in this dissertation, both the rotor frequency of each synchronous generator (f_G1, f_G2, f_G3) and the system's Centre of Inertia (COI) frequency are presented (f_System). While individual rotor frequencies reveal local dynamic responses, the COI frequency provides a weighted average that reflects the overall frequency behaviour of the system.

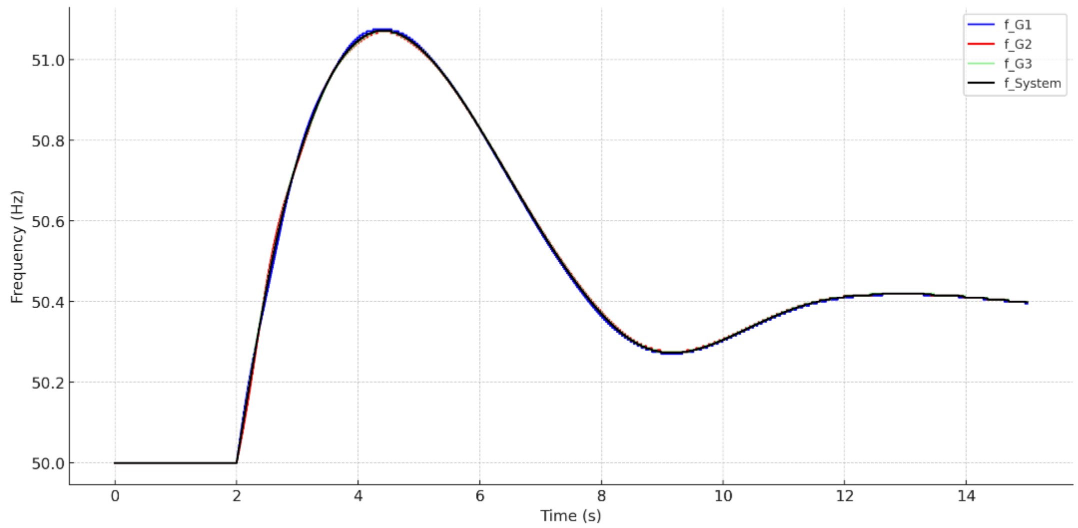

Figure 4.1 – Frequency after load A loss

The frequency nadir remained at 50.0 Hz for all three cases. This is consistent with the nature of load loss events, where the system frequency tends to increase rather than decrease. Therefore, no under-frequency excursion was recorded.

The simulation environment being explored naturally filter out high-frequency components and focus on electromechanical dynamics, therefore leading naturally to a smoothing effect in the computed values for the RoCoF. To account for this, the RoCoF is calculated using different time windows (500 ms, 250ms and 100ms) aiming to achieve a balance between capturing relevant dynamic trends and minimizing numerical artifacts. In this sense, shorter windows help identify faster system responses within the limits of RMS resolution, while longer windows provide a more stable representation of frequency trends over time. This approach improves the robustness of RoCoF analysis under the modelling assumptions inherent to RMS simulations. The results are presented in **Table 4.3**.

Table 4.3 - RoCoF and Nadir results for load loss events

	|RoCoF| (Hz/s)			
Load	**500ms**	**250ms**	**100ms**	**Nadir (Hz)**
A	0,880	0,923	0,958	50
B	0,626	0,662	0,692	50
C	0,714	0,748	0,781	50

As expected, the RoCoF values increase as the measurement window narrows. RoCoF values increase for smaller measurement windows because shorter intervals capture the most abrupt and rapid changes in frequency that occur immediately after a disturbance. These short-term transients tend to be smoothed out when using longer windows, resulting in lower average RoCoF values. All calculated RoCoF values remained below 1 Hz/s, indicating a stable inertial response.

As shown, the worst case, being Load A, results in the highest RoCoF values across all time windows. This is directly related to the higher magnitude of power imbalance caused by its disconnection. The other way around, Load B, having the lowest power, produces the smallest RoCoF. The comparison confirms the correlation between the magnitude of the disturbance, size of the load lost and the system's inertial response.

4.3.2 - Generation Loss Events

In this subsection, the system's dynamic frequency response is evaluated for generation loss events, where each of the synchronous generators (SG1, SG2 and SG3) is tripped individually at t = 2 seconds. The goal is to assess the impact of each generator's disconnection on the system frequency stability.

The generators disconnected in the respective simulations had the active and reactive power outputs under steady-state conditions as discussed in **section 4.2.**

The loss of SG2 results in the most severe frequency disturbance among the three scenarios. The results are presented in **figure 4.2** and **table 4.4**. It is observed in **figure 4.2** that from t = 2 s onward, SG2 is no longer active in the system and is therefore excluded from the frequency of centre of inertia calculation. The frequency of centre of inertia is then determined exclusively by SG1 and SG3, based on their respective inertia and power bases.

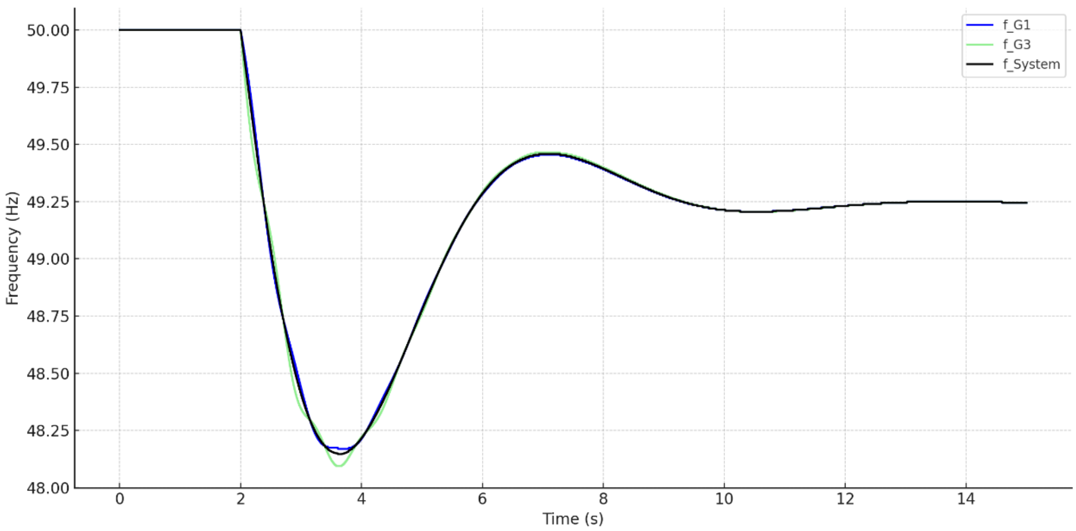

Figure 4.2 - Frequency after SG2 disconnection

Table 4.4 - RoCoF and Nadir results for generation loss events

	|RoCoF| (Hz/s)			
SG	500ms	250ms	100ms	Nadir (Hz)
1	0,476	0,502	0,555	49,25
2	1,918	2,015	2,046	48,15
3	0,821	0,867	0,895	49,24

Although all SGs have a similar kinetic energy contribution to the system the fact that SG2 is the generator with the highest active power output, supplying 163 MW at the time of the event, its loss instantly creates the largest power imbalance forcing the remaining generators to compensate for the sudden deficit. In contrast, SG1 and SG3 contribute 71.6 MW and 85 MW respectively, and their disconnection events result in proportionally smaller disturbances.

This is reflected in the simulation results, where the RoCoF following SG2 disconnection reaches 1.918 Hz/s in the 500 ms window, which is very close to the typical RoCoF withstand limit of 2 Hz/s imposed by most European transmission system operators, as outlined in ENTSO-E grid code requirements.

It is also observed that the system experienced a sharp frequency drop, with the system´s frequency reaching a nadir of 48.15 Hz. Since this is a test network without predefined operational constraints or frequency protection schemes, no automatic actions such as under-frequency load-shedding (UFLS) were triggered in the simulation. However, in real-world systems such a frequency dip would be unacceptable. According to the ENTSO-E grid code requirements, in regions such as Continental Europe, Limited Frequency Sensitive Modes - Underfrequency (LFSM-U) mechanisms are typically activated at frequencies below 49.2 Hz, with progressive stages of load disconnection implemented to prevent further frequency collapse. Therefore, while the simulation results remain valid for comparative analysis in this context, they clearly indicate that the system, under this worst condition scenario, would not meet operational security standards in an actual grid environment.

4.3.3 - Short-Circuit Fault Events

This section analyses the system's dynamic frequency response to three-phase short-circuit faults occurring on each of the six transmission lines of the test system. The results are presented below.

Table 4.5 - RoCoF and Nadir results for short-circuit faults

	|RoCoF| (Hz/s)			
Line	**500ms**	**250ms**	**100ms**	**Nadir (Hz)**
4-5 (1)	0,833	1,342	1,589	49,89
5-7 (2)	0,723	1,141	1,380	49,83
7-8 (3)	0,819	1,331	1,565	49,79
8-9 (4)	0,732	1,236	1,463	49,84
6-9 (5)	0,601	0,934	1,140	49,88
4-6 (6)	0,674	1,134	1,351	49,87

Despite the slight variations in RoCoF and nadir values, all short-circuit fault cases produced very similar frequency responses, indicating a consistent and robust inertial behaviour across the network.

Importantly, all cases showed RoCoF values below 1 Hz/s (500 ms window) and frequency nadirs above 49.7 Hz, meaning the system remained well outside any critical instability thresholds. This includes the underfrequency limit for LFSM-U activation and the RoCoF withstand limits defined in European grid codes.

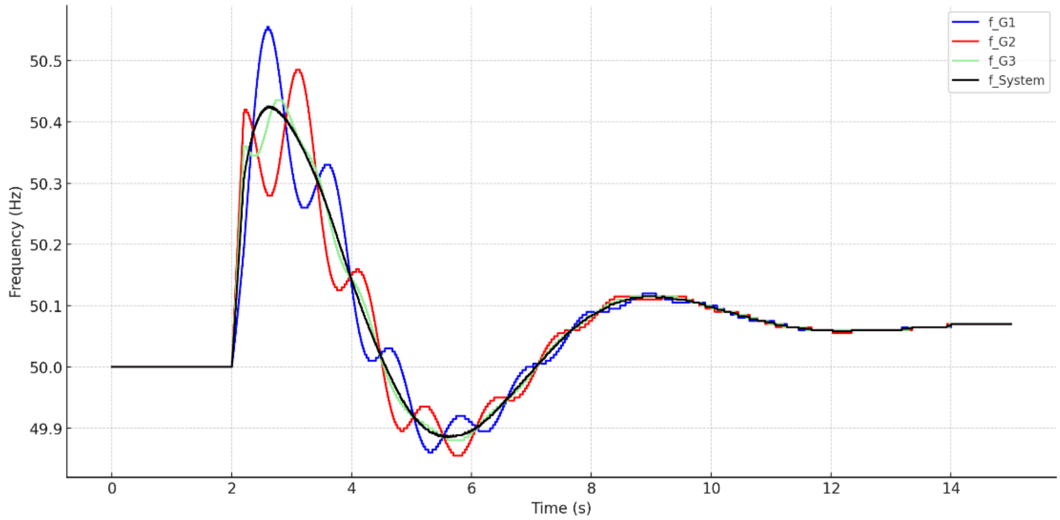

Figure 4.3 - Frequency after fault on line 1

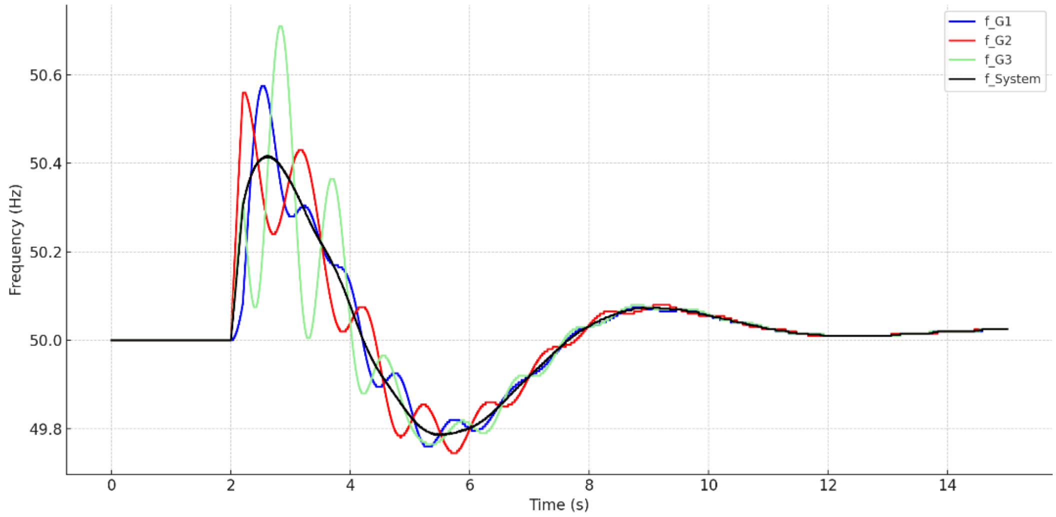

Figure 4.4 - Frequency after fault on line 3

The simulation results reveal that Line 1 and Line 3 faults lead to the most critical frequency responses in the system. Among all tested scenarios, the fault on Line 1 produced the highest RoCoF measured over a 500 ms window, reaching 0.833 Hz/s, with a corresponding nadir of 49.89 Hz. Meanwhile, the fault on Line 3, although associated with a slightly lower RoCoF of 0.819 Hz/s, resulted in the lowest frequency nadir across all simulations, at 49.79 Hz. This indicates that while Line 1 causes the fastest initial frequency change, Line 3 leads to a deeper frequency drop, which could pose a higher risk for triggering underfrequency protection mechanisms if the disturbance were slightly more severe.

The more severe frequency responses observed for faults on Lines 1 and 3 can be explained by examining the pre-fault power flow patterns and network topology. Line 1, which connects Bus 4 to Bus 5, is responsible for the transfer of power from SG1 towards the load A, the largest load in the system. A fault on this line not only interrupts this path but also forces a sudden redistribution of SG1's output across less direct routes, resulting in transient power mismatches and a rapid acceleration of generator rotors, thus explaining the elevated RoCoF.

Line 3 links Bus 7 to Bus 8 which directly feeds a major part of load C, almost 75% of the load capacity, with the power provided by SG2. Disconnecting this line disrupts the active power delivery from SG2, creating a localized power imbalance and weakening SG2's coupling to the load centre. Although this does not induce the highest RoCoF, the more sustained power deficit in that region leads to the lowest nadir observed, as the generators require more time to re-establish frequency balance.

In all cases, the severity of the frequency deviation is directly linked to the level of power flow interrupted by the fault and the topological importance of the affected line. Faults that occur on major transmission paths carrying significant power before the event cause the largest disturbances.

4.4 - Renewable Energy Sources Integration

This section investigates the impact of integrating PV power plants into the IEEE 9-bus test system, with a focus on system frequency stability during fault conditions. The analysis examines how replacing conventional synchronous generators with inverter-based PV generation affects the system's dynamic response.

Initially, the synchronous generator SG2 is replaced by a PV power plant, while SG1 and SG3 remain unchanged. The PV system used in this study is the model described in **Section 3.4**, and it is implemented as a grid-following inverter, meaning it does not contribute with inertia or frequency support to the system. No synthetic inertia or fast frequency response control is applied at this stage, in order to evaluate the baseline behaviour of standard RES integration.

After the initial configuration is set, the same series of three-phase short-circuit events previously defined in **Section 4.3.3** are applied. That is, each fault occurs at t = 2.0 seconds on the middle of the transmission line and is cleared at t = 2.2 seconds by disconnecting the affected transmission line and the total simulation time is 15 seconds.

In the following phase, the system is further modified by replacing SG3 with a second PV power plant, identical in modelling and control characteristics to the one replacing SG2. This results in a scenario where only SG1 remains unchanged, while the remaining generation is fully inverter-based. The same fault scenarios are applied once again to this new configuration in order to observe the cumulative impact of increased RES penetration on system stability.

4.4.1 - Synchronous Generator SG2 Replacement

In this scenario, the synchronous generator SG2 is replaced by a PV power plant, as described above while SG1 and SG3 remain unchanged. The objective is to assess the impact of this partial RES integration on system stability under the same short-circuit events. By removing SG2 from the system, its associated inertia constant, H = 4.1296 s, is also eliminated. This significantly reduces the total system inertia, which is critical for resisting rapid changes in frequency following disturbances.

Lower inertia means that the system has less stored kinetic energy to buffer sudden imbalances between generation and load, possibly leading to higher RoCoF values and deeper frequency nadirs during faults.

To determine a safe and operational PV capacity, a sensitivity study was performed by incrementally increasing the apparent power rating of the PV plant.

4.4.1.1 - Integration of 75 MVA PV Power Plant

The simulations began with a PV power plant rated at 75 MVA, which corresponds to a Short-Circuit Ratio (SCR) of 6.2 at the point of connection of the PV plant, indicating a strong grid, where the voltage remains more stable during disturbances and inverter-based generation can operate more reliably. So, for this scenario SG2 was replaced by a 75 MVA PV power plant, injecting 70 MW and 6.7 Mvar. The remaining active power that was previously supplied by SG2 is now provided by SG1.

Given the proximity of lines 2 and 3 to the point of common coupling of the PV power plant, these lines were selected for the analysis. Faults on these lines result in the most severe voltage dips at the PV plant terminals, which is a critical factor in the dynamic performance of grid-following inverters. Since these types of inverters rely on the grid voltage to synchronize and control their power injection, sudden and deep voltage drops can challenge their ability to maintain operation. By focusing on lines 2 and 3, the analysis captures the most stressed scenarios from the perspective of the PV system, allowing for a more accurate assessment of the system’s resilience to disturbances near inverter-based generation. The results for this scenario are presented below.

Table 4.6 - RoCoF and Nadir results for short-circuit faults with 75MVA PV1 integrated

	|RoCoF| (Hz/s)			
Line	**500ms**	**250ms**	**100ms**	**Nadir (Hz)**
5-7 (2)	0,794	1,585	1,977	49,77
7-8 (3)	0,761	1,505	1,873	49,78

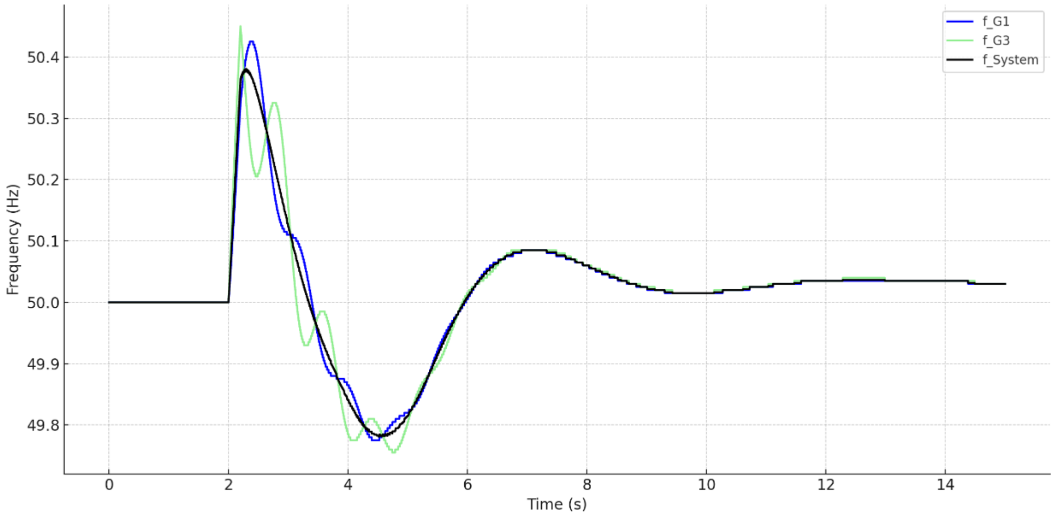

Figure 4.5 - Frequency after fault on line 3 with 75MVA PV1 integrated

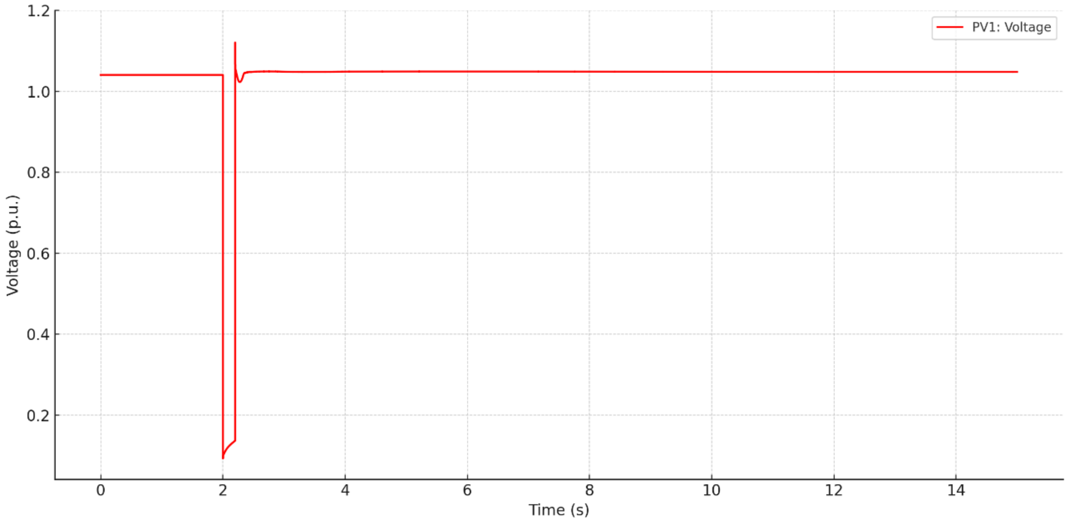

Figure 4.6 - 75MVA PV1 voltage magnitude after fault on line 3

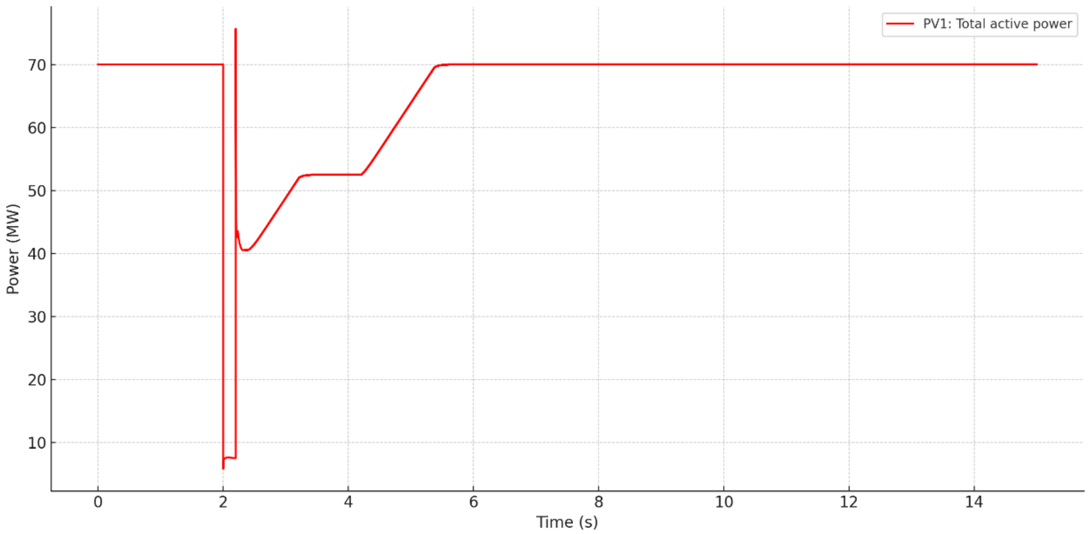

Figure 4.7 - 75MVA PV1 total active power after fault on line 3

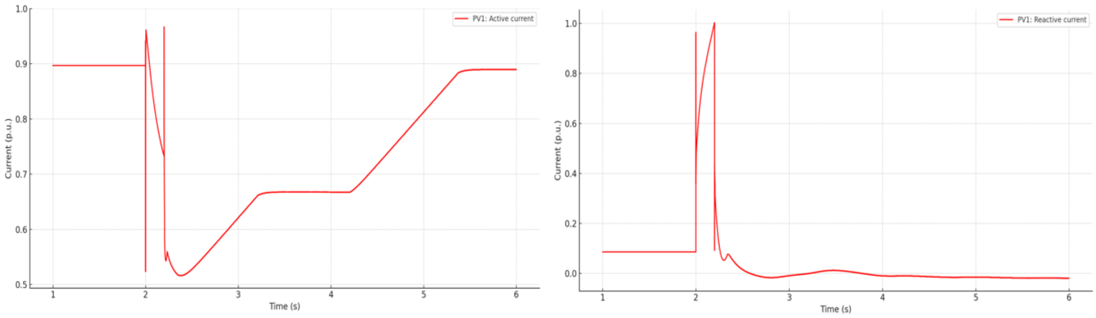

(A) (B)

Figure 4.8 - 75MVA PV1 total active (A) and reactive (B) current injection after fault on line 3

When SG2 was replaced by a 75 MVA PV plant, injecting 70 MW and 6.7 Mvar, the system remained stable during the short-circuit disturbances on the transmission lines. For all simulated fault cases under this scenario, both the RoCoF and nadir values remained within the operational thresholds established by ENTSO-E for Continental Europe. The system's ability to recover is reflected in **Figure 4.5**, where the frequency of centre of inertia stabilizes after the initial disturbance.

The response of the PV unit is illustrated in **Figures 4.6, 4.7** and **4.8**, showing the total active power, voltage magnitude and current injection during and after the fault. At the time the fault occurs (t = 2.0 s), there is an abrupt voltage drop at the PV's point of connection, which leads to an immediate reduction in the inverter’s active power output. Since the PV system is modelled as a grid-following inverter, its ability to inject active power depends directly on the availability of a stable voltage reference. During the low-voltage period, the inverter prioritizes reactive current injection to support voltage recovery, as shown in **Figure 4.8,** where the reactive current increases during the voltage dip to support grid voltage, while the active current is temporarily reduced, resulting in a temporary curtailment of active power delivery. Once the fault is cleared (t = 2.2 s) and the voltage begins to recover, the active power also increases progressively, returning to the nominal value.

It is important to note that some sharp spikes and irregularities observed in the waveforms are artifacts of the mathematical model used in the simulation environment. These are not representative of physical instabilities and should be disregarded in the interpretation of system behaviour. They typically occur at transition points due to the internal dynamics of control blocks or numerical discretization methods.

The results for line 3 confirm that the system, with a 75 MVA PV plant replacing SG2, maintains frequency and voltage stability under short-circuit conditions, without violating operational criteria.

4.4.1.2 - Integration of 170MVA PV Power Plant

In this scenario, the PV power plant replacing synchronous generator SG2 is scaled up to 170 MVA. At this capacity, the PV plant injects 163 MW and 6.7 Mvar into the grid, matching the previous active and reactive power contributions of SG2. However, this configuration results in a SCR of 2.75 at the point of connection of the PV, which characterizes a weaker grid.

Same as the 75 MVA case, the fault scenarios are applied on lines 2 and 3, given their proximity to the PV connection point and the significant voltage dips observed at the inverter terminals during these disturbances. These cases are expected to stress the inverter's control system due to the lower SCR and provide insight into the system's stability margins under more challenging operating conditions. The results for this scenario are presented below.

Table 4.7 - RoCoF and Nadir results for short-circuit faults with 170MVA PV1 integrated

	|RoCoF| (Hz/s)			
Line	**500ms**	**250ms**	**100ms**	**Nadir**
5-7 (2)	0,695	0,807	1,049	49,58
7-8 (3)	0,630	0,697	0,853	49,58

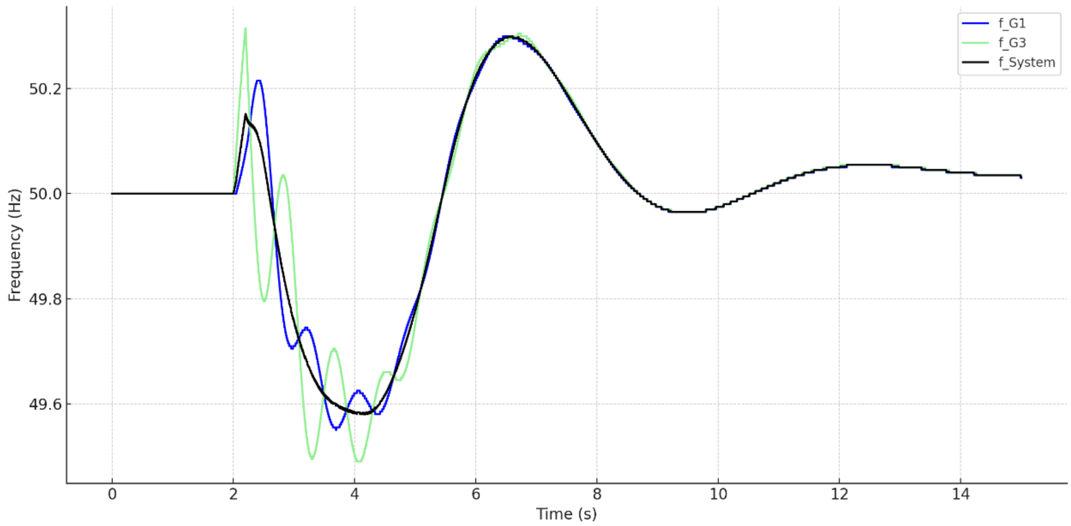

Figure 4.9 - Frequency after fault on line 3 with 170MVA PV1 integrated

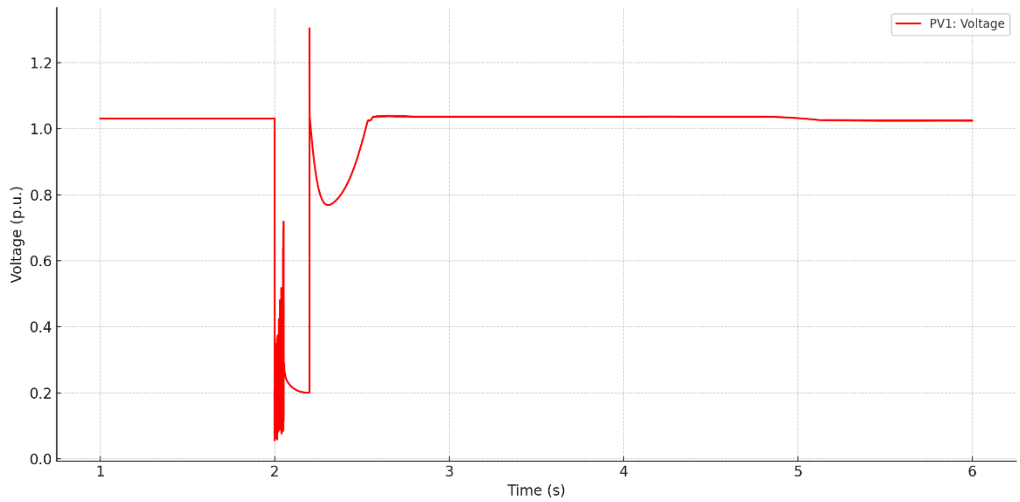

Figure 4.10 - 170MVA PV1 voltage magnitude after fault on line 3

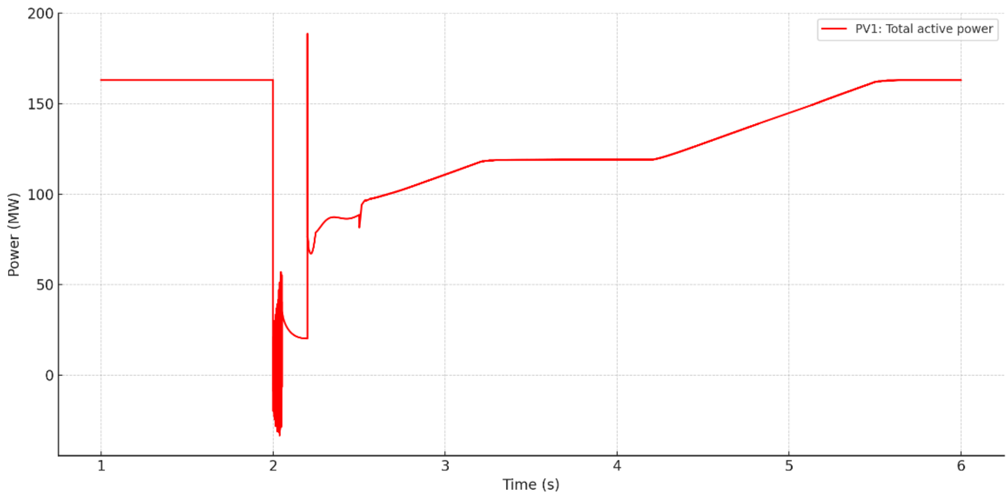

Figure 4.11 - 170MVA PV1 total active power after fault on line 3

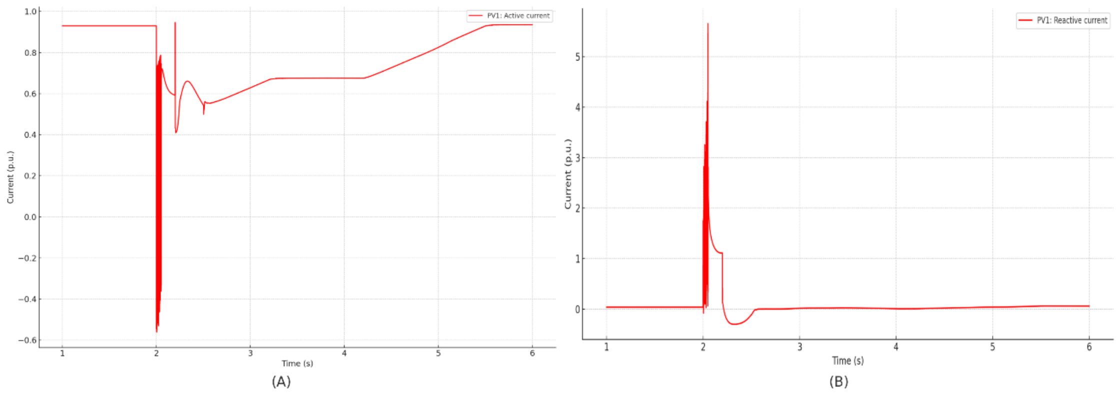

Figure 4.12 - 170MVA PV1 total active (A) and reactive (B) current injection after fault on line 3

The frequency response shown in **Figure 4.9** reveals a more pronounced nadir compared to the previous scenario, however this value stayed above the 49,2Hz threshold which indicates that no underfrequency events would occur. The RoCoF values remained within the acceptable range, not exceeding 1Hz thus staying below the 2 Hz/s operational limit set by ENTSO-E. This confirms that the system, while under stress, did not violate protection thresholds.

Aside from the oscillations observed during the fault period, the system is able to recover and reach a stable operating point once the fault is cleared. After the disturbance, all key variables including frequency, voltage, power and current injected gradually return to normal levels without signs of divergence or loss of synchronism. The behaviour of these variables is consistent with the dynamics observed in the previous section (75 MVA PV case), following the same characteristic pattern: a dip in voltage magnitude and power injection during the fault, followed by a progressive rise until stabilizing near nominal values. It is also worth noting that some of the sharp peaks observed in the graphics are caused by limitations in the mathematical modelling and simulation resolution.

In all plots during the fault period, between t = 2.0s and t = 2.2s, is noticeable the presence of repeated oscillations in the voltage, active power and current signals. These oscillations reflect the dynamic interaction between the weak grid, represented by a lower SCR compared to the previous 75MVA case, and the fast control loops of the grid-following inverter. In systems with reduced SCR and inertia, the inverter control may struggle to maintain stable tracking of the grid voltage reference during severe disturbances, especially when the voltage fluctuates rapidly. As a result, the inverter output exhibits transient oscillatory behaviour, proving the SCDS phenomena originating from the GFL inverter model.

The oscillations observed during the fault period reflect a reduction in system damping and narrower stability margins, effects that become increasingly relevant as the share of inverter-based renewable generation grows and synchronous machines are phased out. To explore this further, the next section investigates a more stressed scenario in which a second PV power plant is integrated, replacing the synchronous generator SG3, further reducing system inertia and increasing inverter-based generation. The goal is to evaluate whether the system can still maintain stability under short-circuit disturbances in this more challenging configuration.

Subsequently, in the following Chapter, the focus will shift to assessing potential stability support strategies, namely the integration of a grid-forming inverters and synchronous condensers, in order to enhance system resilience and frequency response under high RES penetration conditions.

4.4.2 - Synchronous Generators SG2 and SG3 Replacement

In this scenario, the synchronous generators SG2 and SG3 are replaced by two independent PV power plants, marking a significant step toward high renewable energy penetration in the system. This configuration is intended to assess the system's ability to maintain dynamic stability during fault conditions with only one synchronous generator, SG1, remaining online. With the removal of SG2 and SG3, their respective inertia constants, 4.1296 s and 4.768 s, are also eliminated from the system. This results in a substantial reduction of the total system inertia, leaving SG1, with an inertia constant of just 2.6312 s, as the sole remaining source of rotational inertia.

Since only one synchronous generator remains in operation, SG1´s frequency directly represents the overall system frequency.

The generator SG2 is replaced by PV1, rated at 75 MVA, injecting 70 MW of active power and 6.7 Mvar of reactive power. The SCR at PV1's point of connection is calculated to be 4.48, indicating a moderately strong electrical connection to the grid. Similarly, SG3 is replaced by PV2, also rated at 75 MVA, injecting 70 MW of active power and –10.9 Mvar of reactive power. The corresponding SCR at the connection point of PV2 is 3.6, which reflects a weaker grid condition compared to PV1.

This configuration significantly reduces the system's overall rotational inertia and short-circuit strength, increasing its dependence on inverter-based generation for frequency and voltage support. To test the system’s transient stability under this reduced-inertia configuration, short-circuit events will be applied on Lines 2, 3, 4 and 5. These lines were selected based on their electrical proximity to the PV units: lines 2 and 3 are the closest connection to PV1, while lines 4 and 5 are adjacent to PV2. These fault locations are expected to cause the most significant voltage disturbances at the inverter terminals. The results for this scenario are presented below.

Table 4.8 - RoCoF and Nadir results for short-circuit faults with 75MVA PV1 and PV2 integrated

	|RoCoF| (Hz/s)			
Line	**500ms**	**250ms**	**100ms**	**Nadir**
5-7 (2)	1,720	1,960	2,550	48,43
7-8 (3)	2,000	2,060	2,250	48,69
8-9 (4)	1,700	1,880	2,150	49,32
6-9 (5)	1,400	1,680	2,150	49,49

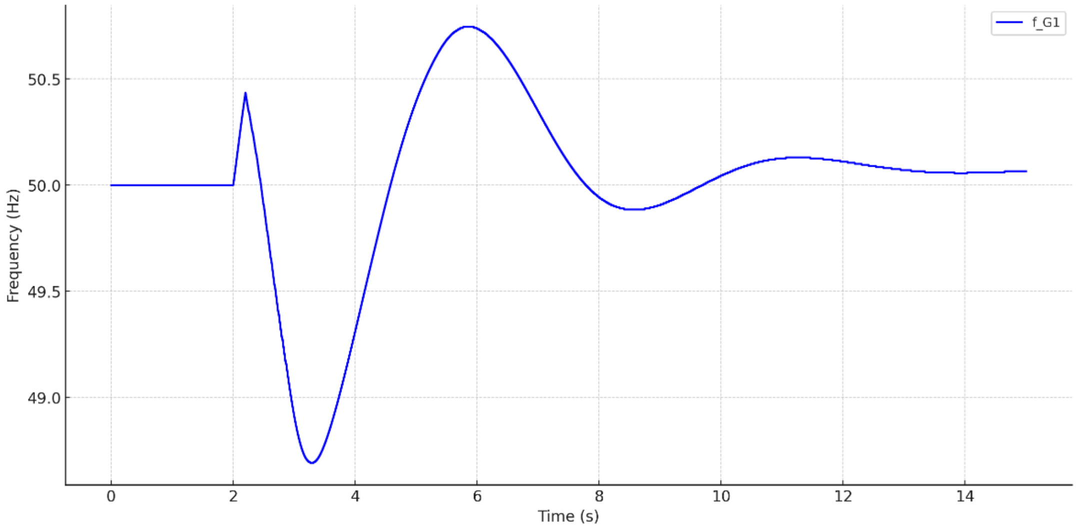

Figure 4.13 - Frequency after fault on line 3 with 75MVA PV1 and PV2 integrated

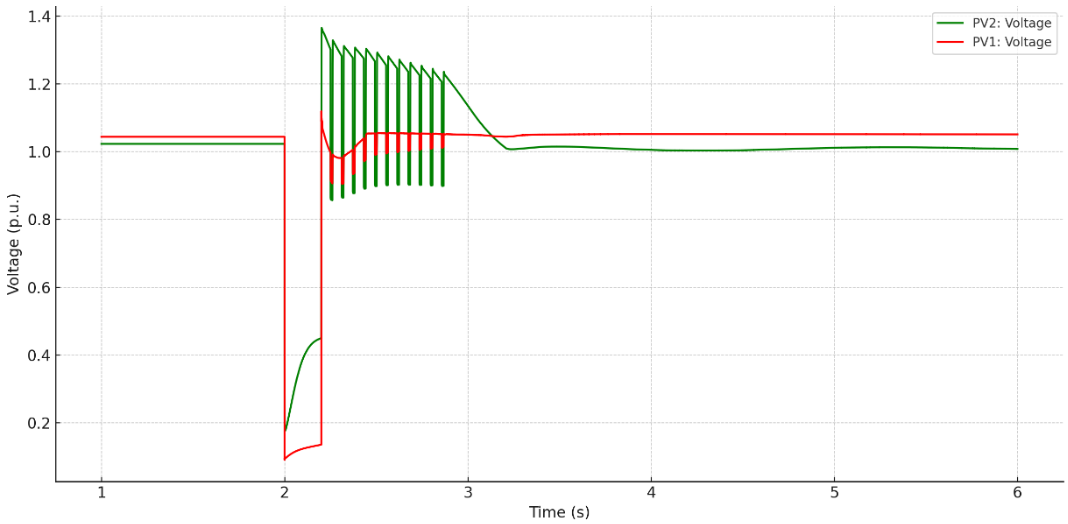

Figure 4.14 - 75MVA PV1 and PV2 voltage magnitude after fault on line 3

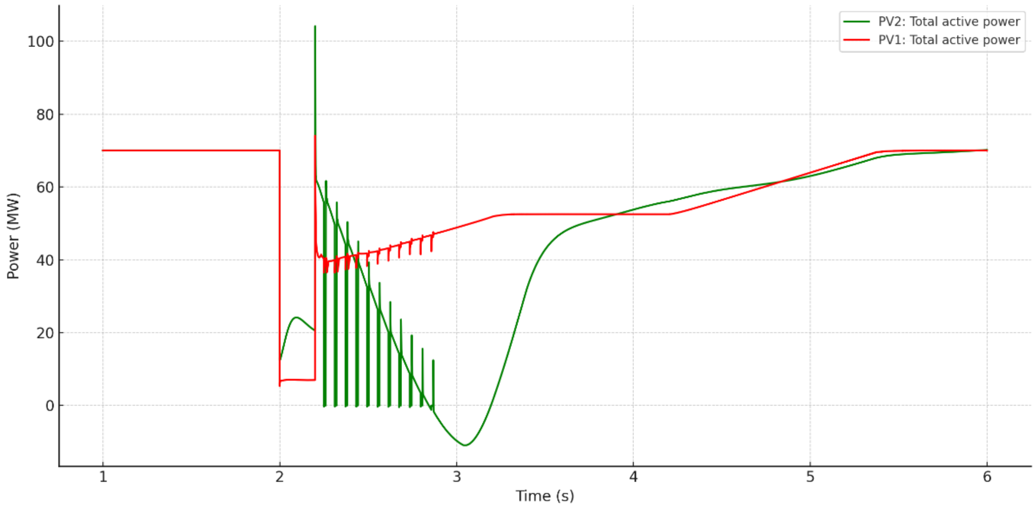

Figure 4.15 - 76MVA PV1 and PV2 total active power after fault on line 3

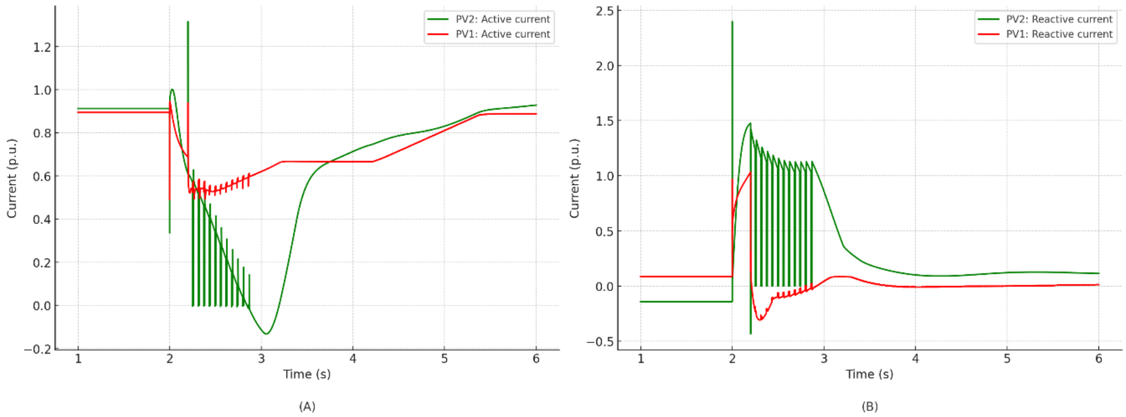

Figure 4.16 - 75MVA PV1 and PV2 total Active (A) and reactive (B) current injection after fault on line 3

Following the simulation, the results reveal a notably stressed frequency response, particularly in terms of RoCoF and frequency nadir. The RoCoF values are critically high across all tested fault scenarios, with the most severe case occurring during the fault on line 3, where the RoCoF reaches 2.00 Hz/s in the 500 ms window. This value is equal to the limit defined by ENTSO-E for Continental Europe and represents the maximum rate that most grid protection and control systems are designed to tolerate.

The nadir frequency values observed are also concerning. For faults on lines 2 and 3, the nadir falls below 49.2 Hz, breaching the threshold set by ENTSO-E. In real-world grid operation, such a frequency dip would trigger LFSM-U mechanisms. These control strategies are designed to initiate progressive load disconnection when frequency drops below 49.2 Hz, with the aim of halting further frequency collapse and protecting system integrity. While the activation of LFSM-U mechanisms is not inherently problematic, as they are part of the system's primary frequency response and exist precisely for such events, the fact that these thresholds are reached highlights a lack of dynamic robustness. What is more problematic is the combination of a low nadir and elevated RoCoF, as it reduces the available response time for corrective actions and increases the risk of triggering widespread protection responses.

This outcome underscores the critical role of synchronous inertia in stabilizing frequency and highlights the inherent limitations of grid-following PV inverters, which lack the capability to effectively counteract rapid frequency declines during severe disturbances.

In the analysis of the PV system responses during the fault on line 3 the voltage dip at PV1 is noticeably more severe than at PV2, as shown in **Figure 4.14**. This is expected since line 3 is electrically closer to PV1, meaning the disturbance has a more direct and pronounced effect on its terminal voltage. As a result of the voltage depression, both PVs exhibit a sharp reduction in active power output, shown in **Figure 4.15**, which is characteristic of grid-following inverters that scale down power injection when voltage support weakens. Once the fault is cleared, the PVs gradually restore their output, although with noticeable transient deviations. Both PV units respond with an increase in reactive current during the voltage sag, as part of their fault ride-through strategy.

However, the waveforms exhibit significant oscillations, particularly during the fault period and immediately after clearance. These oscillations suggest a level of instability or poor damping in the inverter control systems, likely exacerbated by the weak grid conditions, the SCDS phenomena originating from the GFL inverter models and the absence of synchronous machines to buffer and stabilize fast transients, as these oscillations were not present in the previous case, analysed in **section 4.4.1.1,** with only 1 75MVA PV plant integrated. Such behaviour highlights the operational stress imposed on inverter-based generation under low-inertia disturbance-prone conditions.

A more critical scenario where the PV plants would be sized to match the full power output of the synchronous generators they replaced was not tested at this stage. As increasing the capacity of PV1 and PV2 to inject the same active power levels as SG2 and SG3 would lead to a further reduction in the SCR at their connection points, resulting in an even weaker grid condition. In such a case, the negative effects on frequency stability, including sharper RoCoF values, deeper nadir dips and more pronounced oscillations, would likely be intensified.

In the next chapter, the integration of grid-forming inverters and synchronous condensers will be explored to assess their ability to support frequency stability and mitigate the oscillatory behaviour observed in the current configuration. These technologies are expected to enhance system strength, improve voltage recovery, and contribute to the damping of fast transients in low-inertia, inverter-dominated power systems.

4.5 - Final Remarks

This chapter presented the dynamic simulation of the IEEE 9-bus test system under various fault scenarios, with a focus on system frequency response. It began by establishing the theoretical framework and required calculations, followed by the load flow analysis and initial condition setup. Simulations were then conducted for different types of disturbances, including load loss, generator disconnection and short-circuit faults.

As synchronous generators were progressively replaced by PV power plants, the system's frequency stability degraded. Initially, with the replacement of SG2 by a 75 MVA PV plant, the system retained overall frequency stability, maintaining RoCoF and nadir values within acceptable operational limits. As the PV capacity was increased to 170 MVA, matching the original power injection of SG2, the system still remained technically stable, though the results revealed a reduction in frequency nadir and a higher prevalence of oscillatory behaviour.

The integration of two PV plants (PV1 and PV2), each rated at 75 MVA and replacing both SG2 and SG3, exacerbated these effects. With only SG1 remaining as a synchronous generator, the system’s inertial response was substantially weakened. Simulations of short-circuit events near the PVs demonstrated that the RoCoF reached 2 Hz/s—matching the upper operational threshold set by ENTSO-E—and that the frequency nadir fell below 49.2 Hz in some scenarios. In real systems, such nadir values would trigger underfrequency protection mechanisms like LFSM-U and initiate load shedding. Furthermore, significant oscillations were observed across voltage, power and current signals, reflecting reduced damping and compromised dynamic stability originating from SCDS phenomena.

The analyses presented in this chapter clearly demonstrate the adverse impacts of progressively replacing synchronous generation with renewable sources connected via grid-following type inverters. A significant increase in the RoCoF and a lower frequency nadir were observed in all fault scenarios, particularly as more synchronous units were replaced by photovoltaic plants. These results highlight the vulnerability of low-inertia grids to dynamic disturbances and emphasize the limitations of conventional inverter-based resources in providing effective frequency support. The findings reinforce the need for complementary technologies such as grid-forming inverters and synchronous condensers, which can offer real or synthetic inertia and enhance system robustness. As such, the results of this chapter provide a strong technical basis for the advanced stability support strategies explored in Chapter 5.

Chapter 5

Enhancing Stability in Low-Inertia Power Systems

In this chapter, the focus is on evaluating advanced stability support solutions for low-inertia power systems, particularly in scenarios with high integration of inverter-based renewable energy sources. Building upon the limitations identified in previous chapter, such as high Rate of Change of Frequency (RoCoF), low frequency nadirs, poor voltage performance and Converter-Driven Stability [CDS] phenomena, this chapter investigates the effectiveness of two key technologies: grid-forming (GFM) inverters and synchronous condensers (SC) to restore system robustness in high-RES, low-inertia scenarios. Various configurations are tested, including different levels of renewable penetration, device capacities and placements within the grid, allowing for a comprehensive comparison of their performance and practical implications.

5.1 - Briefly Recap

As demonstrated in **Chapter 4.4**, the integration of renewable energy sources (RES) through grid-following inverters introduces some frequency stability challenges. These include high values of Rate of Change of Frequency (RoCoF), frequency nadirs falling below operational thresholds and oscillatory behaviours under fault conditions as a result of converter driven instabilities. It is shown that the reduction of system inertia and short-circuit strength, due to the replacement of synchronous generators with inverter-based resources, compromises the ability of the system to maintain frequency and voltage stability during disturbances.

This chapter aims to assess the effectiveness of Grid-Forming (GFM) inverters and Synchronous Condensers (SC) as advanced stability support technologies for low-inertia power systems. The goal is to determine whether these devices can restore dynamic stability and ensure compliance with critical operational limits.

The analysis is structured around the system scenarios tested in **Chapter 4.4**, a moderate RES penetration case, where synchronous generator SG2 is replaced by a photovoltaic (PV) power plant and a high-RES penetration case, where both synchronous generators SG2 and SG3 are replaced by PV units. While the previous analysis focused on the system's performance under grid-following operation alone the present study evaluates the impact of integrating stability support mechanisms in an attempt to mitigate the issues previously identified in the system. The scenarios recap is demonstrated in **Table 5.1**.

Table 5.1 - Chapter 4.4 scenarios recap

Scenario	Nº of PVs introduced (Capacity)	SG Replaced	Description
1	1 (75 MW)	SG2	High SCR at the point of connection; RoCof and Nadir values didn't violate the thresholds imposed by ENTSO-E; Stability in the system during and after the fault.
2	1 (170 MW)	SG2	Low SCR at the point of connection; RoCof and Nadir values didn't violate the thresholds imposed by ENTSO-E; Unstable oscillations following the fault.
3	2 (75 MW each)	SG2 and SG3	Low SCR at the point of connection of PV1; Moderate SCR at the point of connection of PV2; Nadir value thresholds, set by ENTSO-E, are violated for faults closest to PV1 and the RoCof values are relatively high; Unstable oscillations following the fault.

Each scenario approached will be tested independently using both GFM inverters and SC as support solutions. In the first set of tests, the support devices are placed close to the PV systems. To further explore their effectiveness, a subsequent analysis will assess the impact of device placement, comparing performance when these devices are relocated toward more centralized positions in the network.

5.2 - System with 1 PV Plant Integrated

This section revisits the scenario previously analysed in **Section 4.4.1.2**, in which the synchronous generator SG2 is replaced by a 170 MVA PV power plant, injecting 163 MW and 6.7 Mvar, resulting in an SCR of approximately 2.75 at the point of connection. SG1 and SG3 remain as synchronous generators. The same simulation procedure is adopted here, where the same three-phase short-circuit faults are applied to Lines 2 and 3 to keep the coherence between results. In both cases, the support devices are installed near the PV plant, aiming to reinforce the local grid strength and mitigate the instabilities observed in the original configuration.

5.2.1 - Integration of Grid-Forming Inverter Near RES

In this configuration, the GFM inverter operating under VSM control was parameterized with an acceleration time constant of Ta = 5 s and a damping coefficient of D = 100 p.u., in order to achieve adequate damping and emulate the inertial response of a typical synchronous machine. The GFM was connected at the same bus as the PV plant.

After several simulation iterations with varying capacities, it was determined that a minimum size threshold was necessary to eliminate the oscillatory behaviour previously observed in **Section 4.4.1.2** under grid-following operation. The minimum GFM rating identified to suppress these oscillations was 35 MVA. The results presented below correspond to this minimum effective configuration.

Table 5.2 - RoCof and Nadir results for short-circuit faults with 170MVA PV1 with 35MVA GFM integrated

	|RoCof| (Hz/s)			
Line	**500ms**	**250ms**	**100ms**	**Nadir**
5-7 (2)	0,698	0,862	1,072	49,60
7-8 (3)	0,676	0,745	0,845	49,59

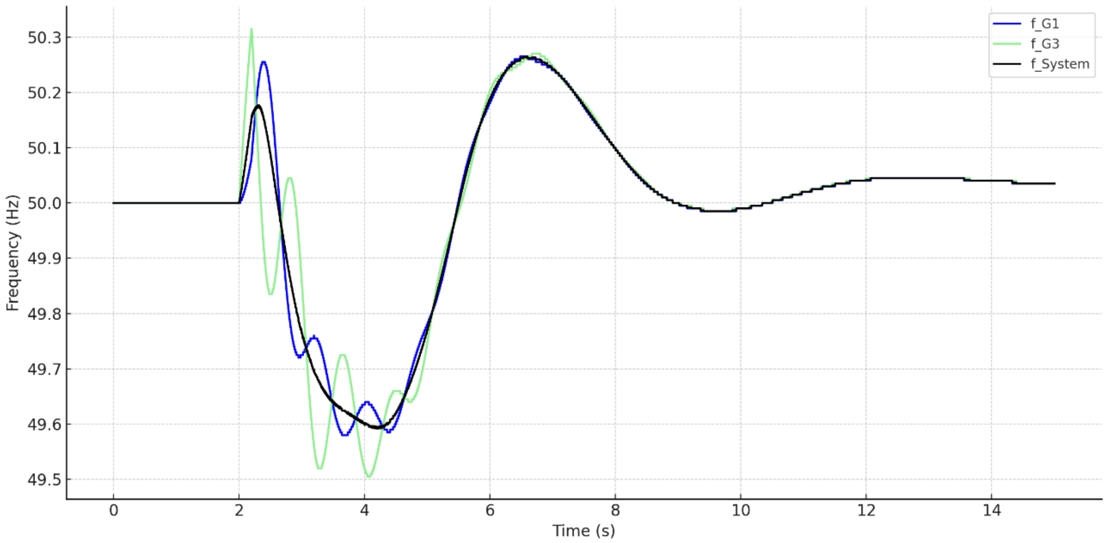

Figure 5.1 - Frequency after fault on line 3 with 170MVA PV1 and 35MVA GFM integrated

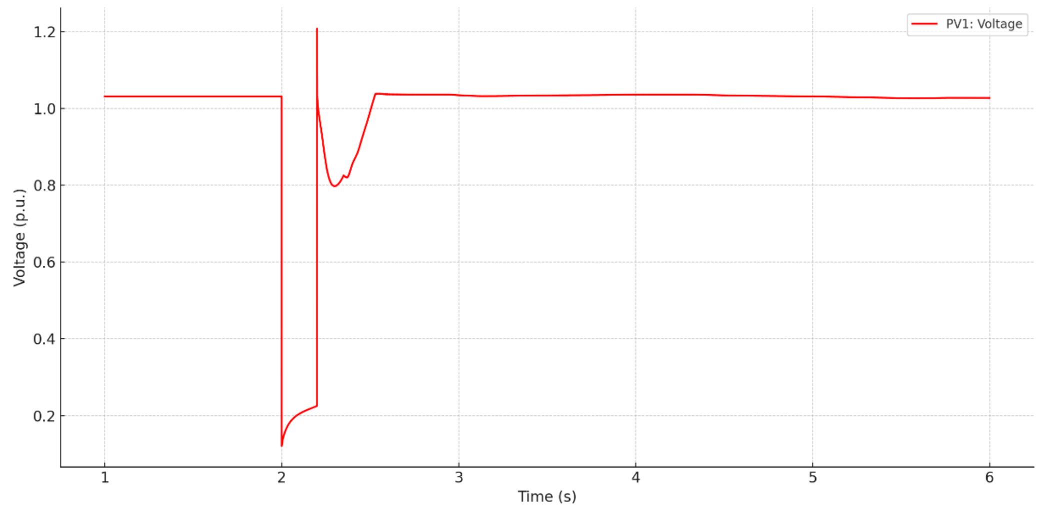

Figure 5.2 - 170MVA PV1 voltage magnitude after fault on line 3 with 35MVA GFM integrated

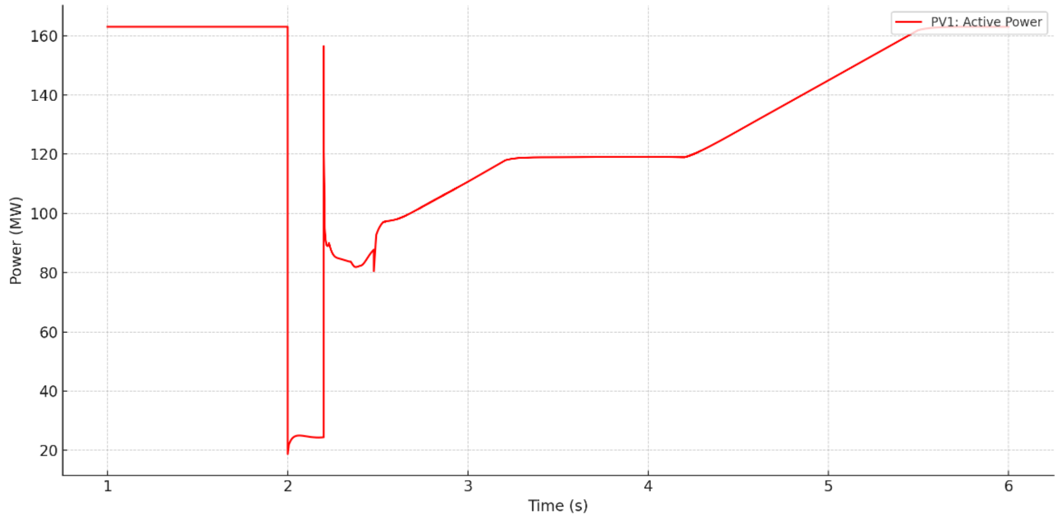

Figure 5.3 - 170MVA PV1 active power after fault on line 3 with 35MVA GFM integrated

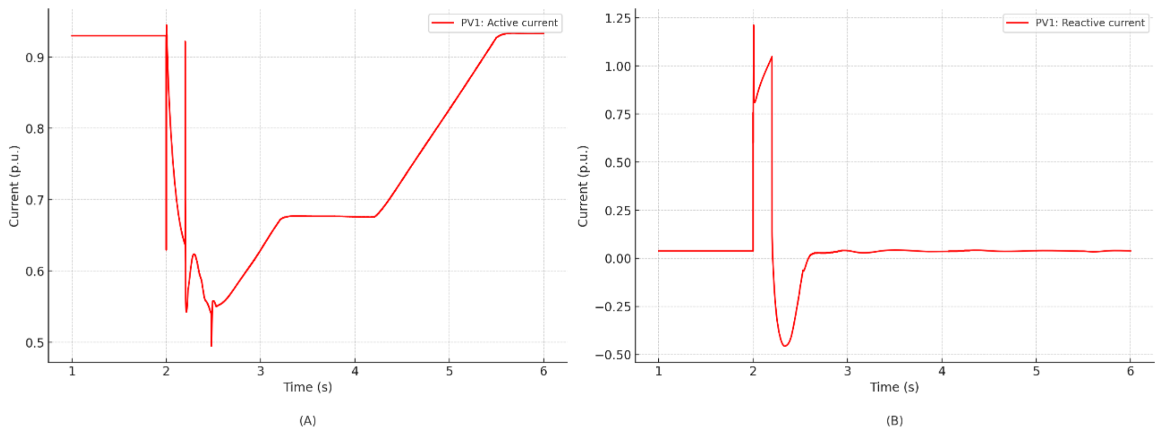

Figure 5.4 - 170MVA PV1 total active (A) and reactive (B) current injection after fault on line 3 with 35MVA GFM integrated

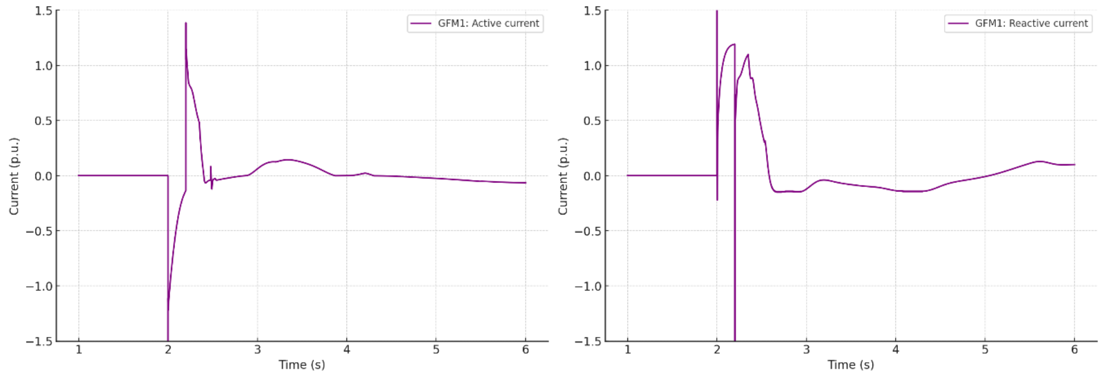

(A) (B)

Figure 5.5 - 35MVA GFM total active (A) and reactive (B) current injection after fault on line 3 with 170MVA PV1 integrated

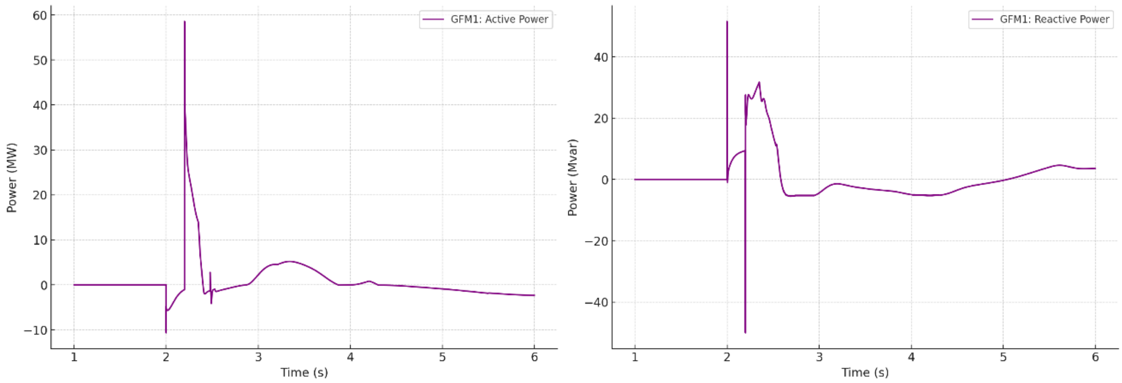

(A) (B)

Figure 5.6 - 35MVA GFM total active (A) and reactive (B) power injection after fault on line 3 with 170MVA PV1 integrated

The integration of a 35 MVA GFM inverter at the same bus as the PV plant brought noticeable improvements in the system's dynamic behaviour, even though the RoCoF and frequency nadir values remained relatively close to those obtained in the grid-following scenario of **Section 4.4.1.2**. As shown in **Table 5.2**, the observed RoCoF values were slightly higher than in the grid-following-only case, though, the frequency nadir also increased, indicating that the system performed somewhat better in maintaining frequency stability.

Nevertheless, the most relevant improvement lies in the damping of oscillations during the fault period, between t=2 s and t=2.2 s. In the grid-following-only case (**Figures 4.10 to 4.12**), the PV´s voltage, active power and current responses exhibited persistent oscillations and instability during the fault. In contrast, with the GFM (**Figures 5.2 to 5.4**), these oscillations completely disappear indicating a more stable and steadily operation during the fault period.

It is once again important to note that the instantaneous spikes observed in the figures result from the mathematical modelling and numerical resolution used in the simulation and therefore should not be interpreted as physical instability.

To further assess the effectiveness of GFM inverters in supporting system stability, the same scenario is now tested with a GFM rated at 100 MVA, also connected at the same bus as the PV plant. The objective is to evaluate whether increasing the GFM capacity enhances its ability to support voltage recovery and maintain frequency stability during and after the fault. By comparing this higher-rated configuration with the previously tested 35 MVA GFM, it is possible to determine how the size of the grid-forming device influences the system's dynamic performance. The results are presented below.

Table 5.3 - RoCof and Nadir results for short-circuit faults with 170MVA PV1 with 100MVA GFM integrated

	|RoCof| (Hz/s)			
Line	**500ms**	**250ms**	**100ms**	**Nadir**
5-7 (2)	0,672	0,894	1,072	49,64
7-8 (3)	0,699	0,811	0,927	49,62

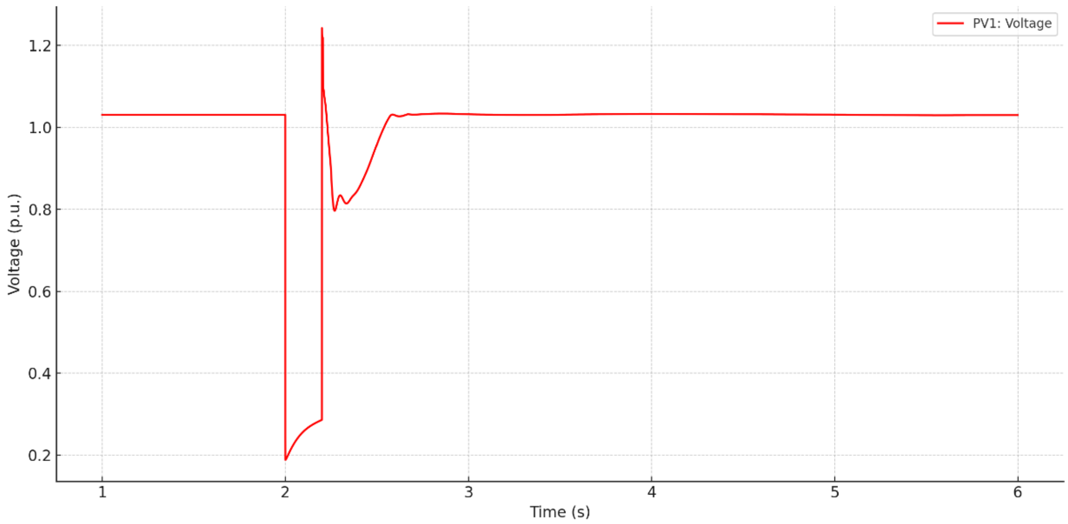

Figure 5.7 - 170MVA PV1 voltage magnitude after fault on line 3 with 100MVA GFM integrated

By increasing the capacity of the grid-forming inverter from 35 MVA to 100 MVA, a clear improvement is observed in the system's dynamic response, particularly in terms of frequency nadir and voltage stability. As shown in **Table 5.2**, the frequency nadir slightly improved for both fault scenarios compared to the previous configuration, rising from 49.59 Hz to 49.62 Hz for the line 3 fault.

This effect is also visible in the voltage response shown in **Figure 5.7**, where the voltage dip is noticeably smaller than in the 35 MVA case (**Figure 5.2**). The stronger GFM offers greater short-circuit strength, which improves the local grid stiffness and reduces the depth of voltage sag at the PV connection point during the fault. As a result, since the PV inverter depends on local voltage to control its active power injection, the smaller voltage drop allows it to maintain a higher level of active power delivery, mitigating the total power imbalance during the fault. This also contributes directly to the improved frequency behaviour.

The key to this improvement lies in the GFM's ability to inject more reactive current during the disturbance. With a higher MVA rating, the GFM can provide a larger reactive power boost, which is essential for supporting voltage recovery immediately after the fault. Additionally, the increased fault current contribution enhances the electromagnetic support to the surrounding buses, helping stabilize both the voltage waveform and frequency response.

Increasing the GFM capacity leads to a stronger and more resilient dynamic performance, reducing the severity of voltage dips, limiting the loss of PV active power and supporting frequency stability more effectively. While the RoCoF values remain similar, the improvements in nadir and voltage behaviour clearly demonstrate the advantage of deploying larger GFM units in weak grid conditions.

5.2.2 - Integration of Synchronous Condenser Near RES

In this section, the same test scenario previously analysed in **Sections 4.4.1.2** and **5.2.1** is revisited, but this time with the integration of a SC instead of a GFM inverter. The objective is to assess the SC’s ability to enhance system stability, particularly in mitigating the oscillatory behaviour observed under grid-following PV operation. The SC, referred to as SC1, is modelled based on the original SG2, but with the governor control removed, allowing it to operate as a synchronous condenser. This ensures that the device retains the same electromechanical characteristics, including the inertia constant of 4.1296 s.

It was determined that a minimum capacity of 15 MVA, giving an overall kinetic energy to the system of 61,944 MJ, was required for the SC to effectively suppress the oscillations identified in **Chapter 4.4.1.2**. The results presented in the following figures correspond to this minimum effective configuration.

Table 5.4 - RoCoF and Nadir results for short-circuit faults with 170MVA PV1 with 15MVA SC integrated

	|RoCoF| (Hz/s)			
Line	**500ms**	**250ms**	**100ms**	**Nadir**
5-7 (2)	0,675	0,818	1,057	49,58
7-8 (3)	0,661	0,724	0,847	49,57

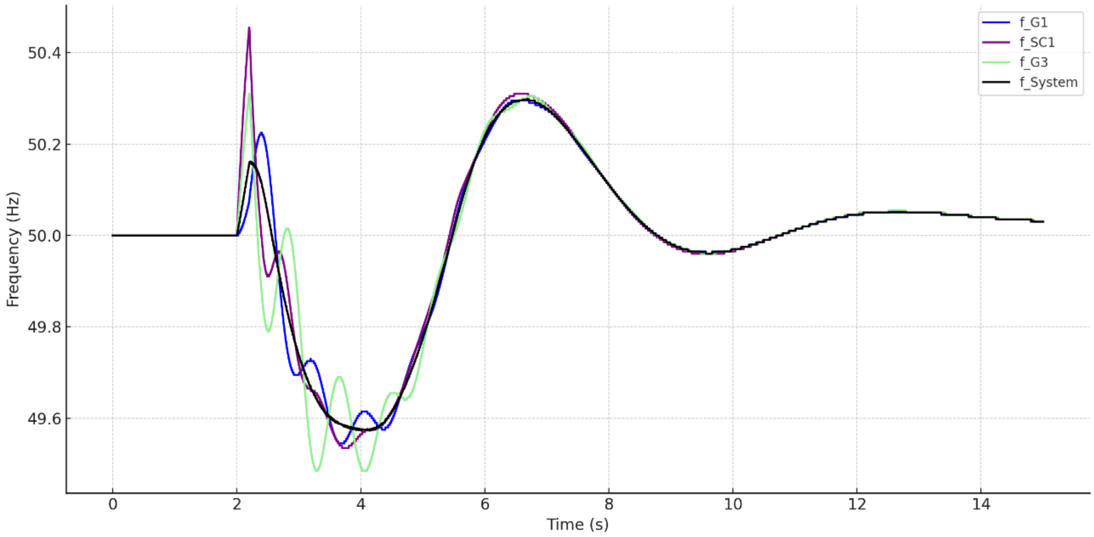

Figure 5.8 - Frequency after fault on line 3 with 170MVA PV1 and 15MVA SC integrated

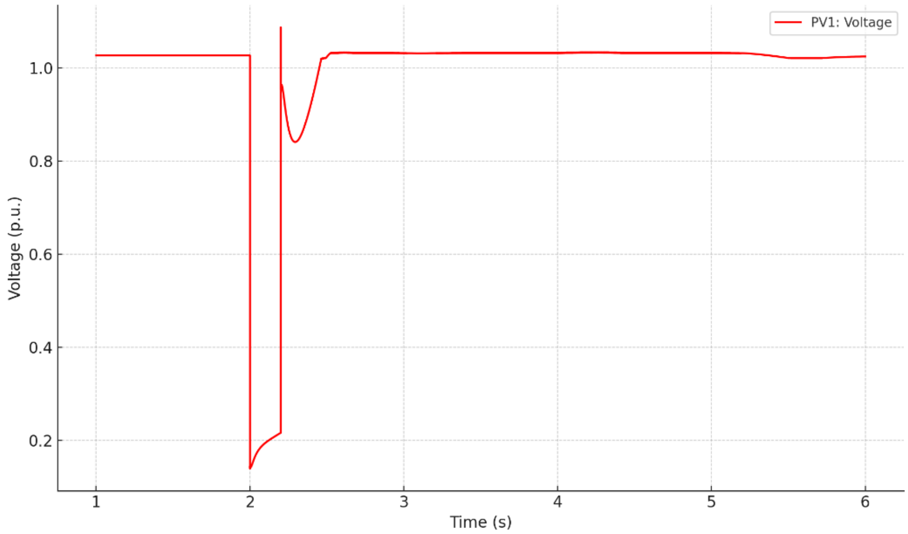

Figure 5.9 - 170MVA PV1 voltage magnitude after fault on line 3 with 15MVA SC integrated

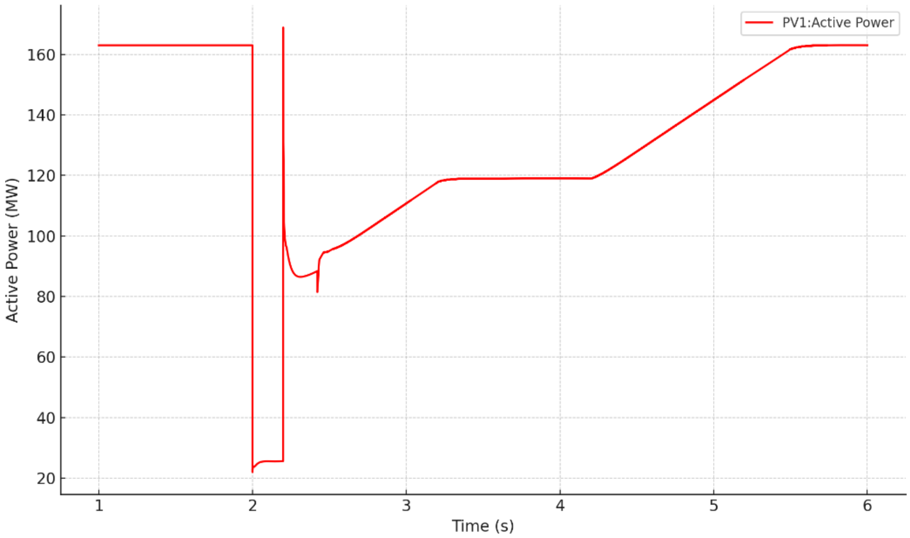

Figure 5.10 - 170MVA PV1 active power after fault on line 3 with 15MVA SC integrated

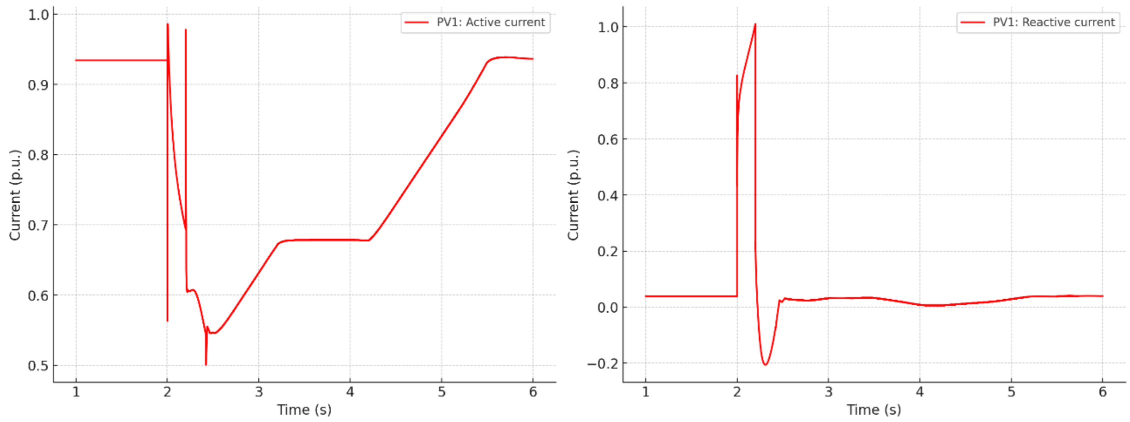

(A) (B)

Figure 5.11 - 170MVA PV1 total active (A) and reactive (B) current injection after fault on line 3 with 15MVA SC integrated

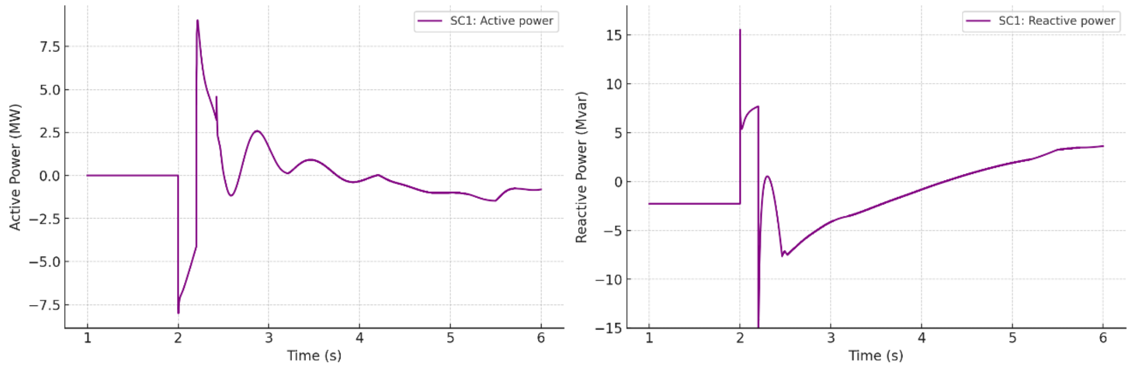

(A) (B)

Figure 5.12 - 15MVA SC total active (A) and reactive (B) power injection after fault on line 3 with 170MVA PV1 integrated

The integration of a 15 MVA SC provided notable improvements in the system's transient behaviour, even though the RoCoF and nadir values remained nearly identical to those observed in the grid-following-only case. The main benefit lies in the improved overall stability and the mitigation of the oscillatory behaviour previously identified.

The SC's role in this improvement is evident in **Figure 5.12**, which shows its contribution of reactive power support and damping torque during and after the fault. Despite its lower capacity compared to the GFM previously tested, the SC leverages its rotational inertia to provide a natural stabilizing effect, reducing transient oscillations and improving the voltage profile across the affected buses. While it does not provide frequency regulation through active power control, its electromagnetic coupling and reactive support are sufficient to enhance system damping and suppress instability.

Same as in the previous section, to further evaluate the impact of the tested solution on system stability, the same scenario is now tested with a 100 MVA SC, maintaining the same connection point as in the previous configuration. The goal is to determine whether increasing the SC capacity enhances its ability to support voltage recovery and improve frequency response during and after fault events. By comparing this higher-rated SC with the previous 15

MVA case, it becomes possible to assess how the size of the synchronous condenser influences its effectiveness in providing inertial support and reactive power injection. The results are presented below.

Table 5.5 - RoCoF and Nadir results for short-circuit faults with 170MVA PV1 with 100MVA SC integrated

	|RoCoF| (Hz/s)			
Line	**500ms**	**250ms**	**100ms**	**Nadir**
5-7 (2)	0,567	0,785	1,013	49,60
7-8 (3)	0,583	0,703	0,903	49,59

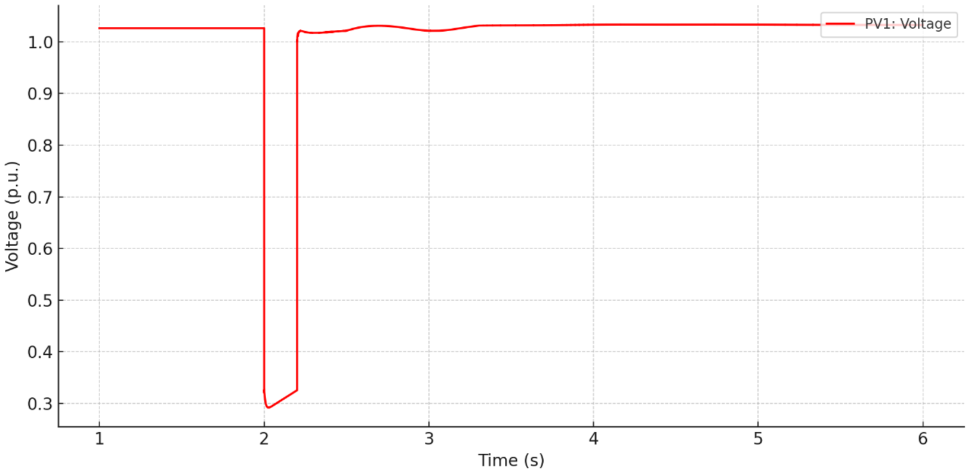

Figure 5.13 - 170MVA PV1 voltage magnitude after fault on line 3 with 100MVA SC integrated

Increasing the capacity of the SC from 15 MVA to 100 MVA led to improvements in both frequency and voltage stability. As shown in **Table 5.5**, the RoCoF is smaller compared to the lower-rated SC configuration (**Table 5.4**), and the frequency nadir increased slightly with values rising from 49.57 Hz to 49.59 Hz for the line 3 fault. This improvement is primarily due to the higher inertia contribution of the larger SC, which enhances the system's ability to resist sudden frequency deviations.

The impact on voltage support is even more evident. Comparing **Figure 5.13** to **Figure 5.9** the voltage dip at the PV terminal is reduced (from 0,2 to 0,3 p.u.) and the recovery is faster and smoother. This improvement results from the increased reactive power injection capacity of the higher-rated SC, which plays a crucial role in supporting voltage during faults.

Synchronous condensers support the grid by acting as electrically coupled rotating machines that provide inertia, reactive power and voltage regulation, without injecting active power from an external source. Their rotating mass helps buffer frequency fluctuations, while their excitation system dynamically adjusts reactive power to sustain voltage levels during disturbances. So, it is expected that a SC with higher capacity enhances both these roles: higher inertial response improves frequency containment and higher reactive capability strengthens grid voltage.

5.2.3 - Results Comparison Analysis of 100MVA Device Solutions

In this section, the results obtained with a 100 MVA GFM are compared with those from a 100 MVA SC, under the same fault scenario where SG2 is replaced by a 170 MVA PV plant.

Although both support devices have the same rated capacity and are connected to the same bus, the system's dynamic response differs in key aspects, particularly in terms of RoCoF, frequency nadir, and voltage dip and recovery.

Table 5.6 – RoCoF and Nadir variation between GFM1 and SC1

	|RoCoF| variation GFM Vs SC (Hz/s)			Nadir variation GFM Vs SC (Hz)
Fault	**500ms**	**250ms**	**100ms**	**Nadir**
line 2	+0,105	+0,109	+0,059	+0,040
line 3	+0,116	+0,108	+0,024	+0,025

Table 5.6 presents a comparative analysis of the system's dynamic performance using Grid-Forming inverters versus Synchronous Condensers, focusing on RoCoF and frequency nadir variations. The values represent the difference between the GFM-based and SC-based scenarios under identical fault conditions (GFM – SC). A positive RoCoF variation indicates that the GFM scenario resulted in higher RoCoF values, which is less favourable from a stability perspective. Indeed, the data confirms that the GFM configuration led to slightly higher RoCoF values for both faults on lines 2 and 3, suggesting a weaker initial frequency containment response compared to the SC-based setup.

On the other hand, the frequency nadir values were higher in the GFM case, which is beneficial, as it means the system frequency did not dip as low after the fault. This reflects the GFM's ability to provide virtual inertia and damping, aiding frequency recovery even if the initial response is less robust.

However, the main difference between the scenarios with GFM and those with SC lies in how the system frequency is determined. In the GFM case, since only SG1 and SG3 remains as synchronous machines, the system frequency, represented by the frequency of the centre of inertia, is derived from the rotor speed and inertial capabilities of SG1 and SG3. In contrast, in the SC scenario, the synchronous condenser contributes real electromechanical inertia, just like a conventional synchronous generator, and is therefore included in the frequency calculation. As a result, the system frequency becomes a weighted average of SG1, SG3 and SC1, providing a more distributed and representative measure of the system's inertia.

Voltage behaviour also differs between the two configurations, as illustrated in **Figures 5.7** and **5.13**. In the GFM scenario (**Figure 5.7**), the voltage at the point of connection of PV1 drops to approximately 0.2 p.u., whereas in the SC scenario (**Figure 5.13**), the voltage dip is less severe, reaching a minimum of around 0.3 p.u. This difference is relevant because deeper voltage dips increase the power imbalance at the inverter's point of connection, leading to stronger dynamic stress.

5.3 - System with 2 PV Plants Integrated

In this section, the analysis is extended to a more critical scenario, where both synchronous generators SG2 and SG3 are replaced by PV power plants, as in **Section 4.4.2**. However, to further increase the system's complexity and stress level, the PV plants are now configured to inject the same levels of active and reactive power that the original synchronous machines were delivering prior to their replacement. Specifically, PV1 (170 MVA) replaces SG2, injecting 163 MW and 6.7 Mvar and PV2 (100 MVA) replaces SG3, injecting 85 MW and –10.9 Mvar, fully matching the operational setpoints of the generators they substitute. This configuration represents a highly inverter-dominated system, with minimal synchronous support, and poses significant challenges in terms of frequency stability, voltage control and dynamic response. The following sections evaluate whether the integration of grid-forming inverters or synchronous condensers can restore system stability and maintain operation within acceptable dynamic limits under such demanding conditions.

5.3.1 - Integration of 2 Grid-Forming Inverters Near RES

In this configuration, two Grid-Forming (GFM) inverters are integrated into the system previously described in **Section 5.3**, where the synchronous generators SG2 and SG3 have been fully replaced by PV1 and PV2, respectively, operating at their original generation setpoints. GFM1, already evaluated in the earlier scenarios, is retained with a capacity of 100 MVA and remains connected at the PV1 bus. A second GFM inverter (GFM2), with a capacity of 150 MVA and the same control structure as GFM1, is introduced and connected at the PV2 bus. This setup aims to evaluate whether local placement of both GFM inverters at the respective RES buses is effective in maintaining system frequency and voltage stability under high RES penetration and increased power injection. The simulation results are presented below.

Table 5.7 - RoCoF and Nadir results for short-circuit faults with 2 GFM integrated near RES

	|RoCoF| (Hz/s)			
Line	**500ms**	**250ms**	**100ms**	**Nadir**
5-7 (2)	1,080	1,360	1,500	49,60
7-8 (3)	1,080	1,360	1,450	49,59
8-9 (4)	1,660	2,020	2,100	49,40
6-9 (5)	0,760	1,280	1,550	50,00

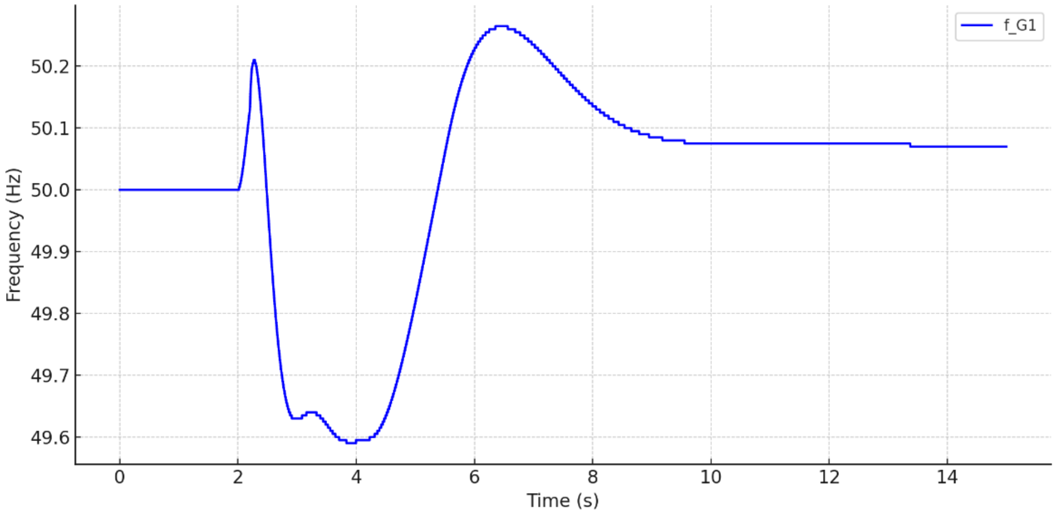

Figure 5.14 - Frequency after fault on line 3 with 2 GFM integrated near RES

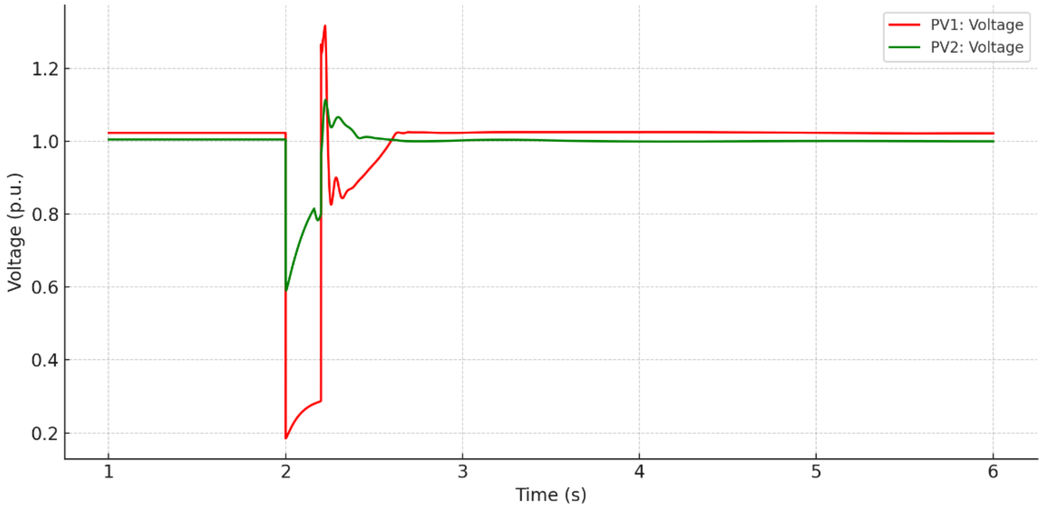

Figure 5.15 - PV1 and PV2 voltage magnitude after fault on line 3 with 2 GFM integrated near RES

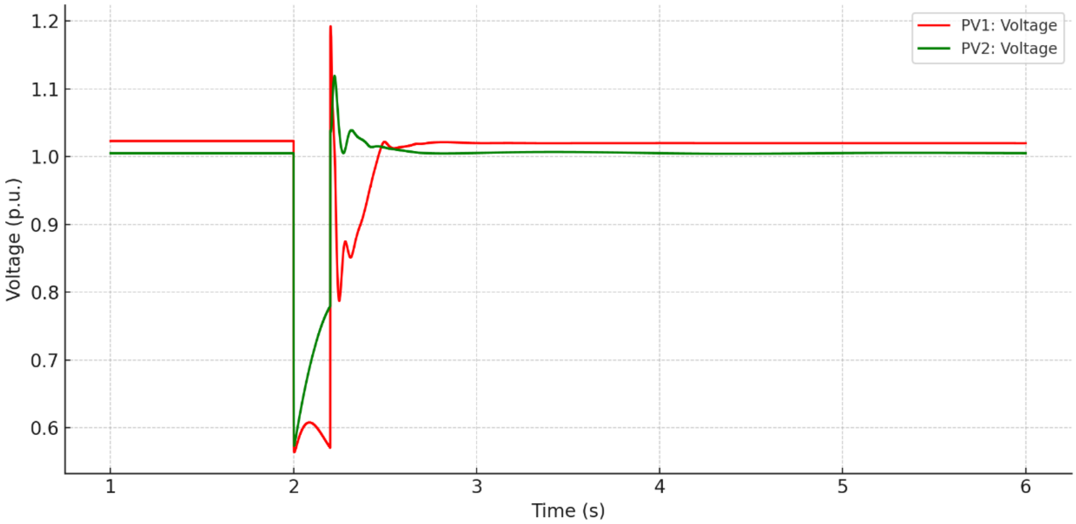

Figure 5.16 - PV1 and PV2 voltage magnitude after fault on line 4 with 2 GFM integrated near RES

The results shown in **Table 5.7** confirm that the system operates securely and stably under all tested fault scenarios with the integration of two Grid-Forming inverters. Both the RoCoF values in all windows and the frequency nadir values remain within the operational thresholds defined for Continental Europe, staying below the 2 Hz/s RoCoF limit for the 500ms window and above the 49.2 Hz nadir minimum. This demonstrates that, despite the full replacement of SG2 and SG3 with PV plants operating at their original dispatch points, the system maintains sufficient frequency support and stability due to the presence of GFM control. Compared to the results observed in **Section 4.4.2**, where only grid-following inverters were used, leading to clear instability and large oscillation's post-fault, the integration of GFM inverters completely mitigates these issues.

Additionally, the voltage waveforms of PV1 and PV2 exhibit the expected behaviour in response to fault location. As shown in **Figure 5.15**, the fault on line 3 is electrically closer to PV1, resulting in a more pronounced and oscillatory voltage dip at its terminals compared to PV2. In contrast, **Figure 5.16** shows the scenario where the fault occurs on line 4, which is closer to PV2. In this case, PV1 experiences a much less severe voltage drop. It is also noticeable that PV2's voltage profile remains relatively consistent between both fault scenarios. This can be attributed to its lower installed capacity compared to PV1, which results in a smaller overall influence on system dynamics and the presence of a higher-capacity GFM converter positioned near it. The greater inertial and voltage support from this GFM unit helps mitigate the voltage disturbance locally. Consequently, the severity of the voltage disturbance at PV2 does not vary significantly with fault location.

This localized impact is consistent with the network topology and confirms that the proximity of the fault affects voltage stability more significantly at nearby sources. Nevertheless, both voltages recover smoothly, further validating the stabilizing role of the GFM inverters.

5.3.2 - Integration of 2 Synchronous Condensers Near RES

In this section, the same test scenario previously analysed in **Section 5.3.1** is revisited, but this time with the integration of SCs instead of GFM inverters. To this end, SC1 (100 MVA) is connected at the same bus as PV1. SC2 (150 MVA) is connected at the bus of PV2 and is derived from SG3's parameters with an inertia constant of 4.768 s, ensuring the equivalent dynamic behaviour and response. The results for this scenario are presented below.

Table 5.8 - RoCoF and Nadir results for short-circuit faults with 2 SC integrated near RES

	|RoCoF| (Hz/s)			
Line	**500ms**	**250ms**	**100ms**	**Nadir**
5-7 (2)	0,670	0,744	0,856	49,55
7-8 (3)	0,660	0,726	0,783	49,52
8-9 (4)	0,918	1,083	1,156	49,47
6-9 (5)	0,399	0,784	0,997	50,00

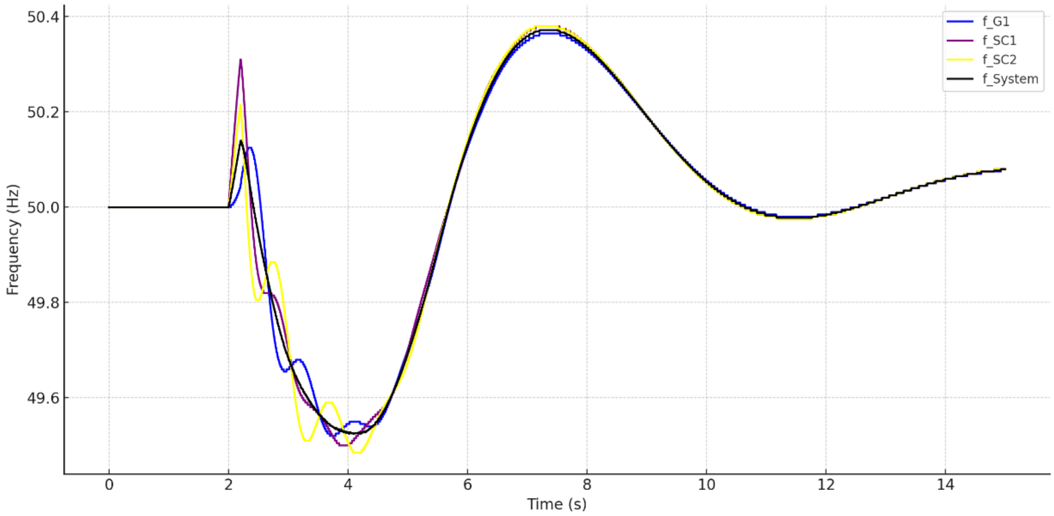

Figure 5.17 - Frequency after fault on line 3 with 2 SC integrated near RES

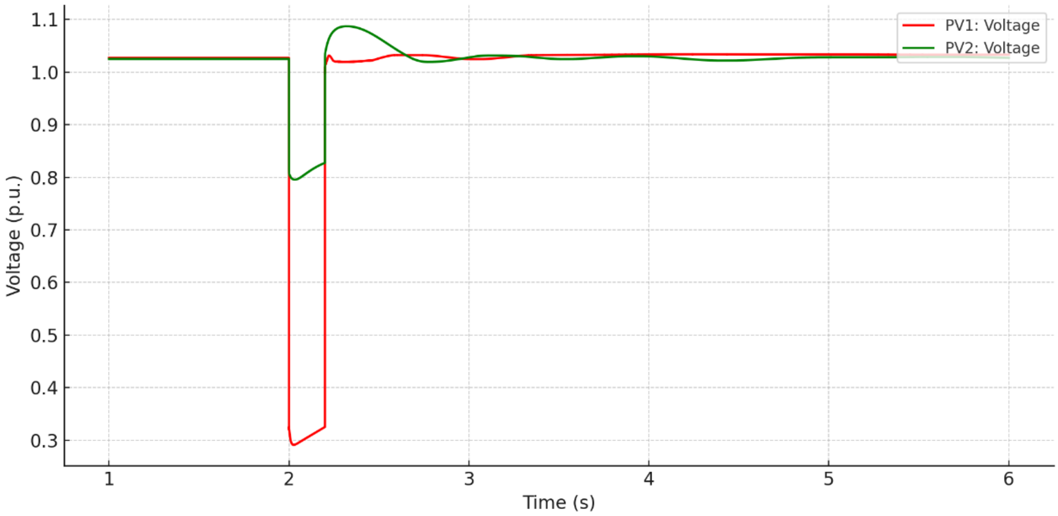

Figure 5.18 - PV1 and PV2 voltage magnitude after fault on line 3 with 2 SC integrated near RES

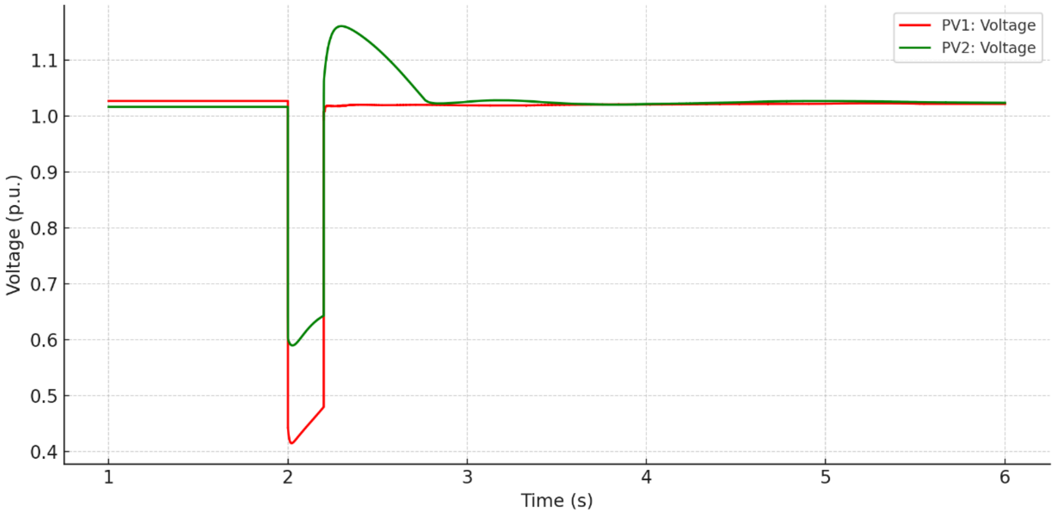

Figure 5.19 - PV1 and PV2 voltage magnitude after fault on line 4 with 2 SC integrated near RES

The simulation results for the scenario with two PV plants and two SCs integrated indicate that the system operates in a stable and secure manner under the tested fault conditions. As shown in **Table 5.8**, RoCoF remains below 1 Hz/s, for the 500ms window, across all fault locations, and the frequency nadir stays well above the 49.2 Hz threshold defined by ENTSO-E. These results confirm that the system is operating safely within dynamic performance limits, even under high inverter penetration. In contrast to the results from **Section 4.4.2**, where both PVs operated solely in grid-following (GFL) mode, the current configuration avoids critical frequency violations and eliminates the post-fault oscillations and instability that were previously observed.

Regarding the voltage behaviour, it is also observed that the voltage dip at PV1 is more pronounced than at PV2 during the fault, as shown in **Figure 5.18**. This difference can be explained the same way it was for the previous case with GFM control. The fault location, line 3, is electrically closer to PV1, making its terminal voltage more directly impacted by the disturbance. Secondly, although both PVs are supported by synchronous condensers, SC1 (connected to PV1) has a lower rated capacity (100 MVA) and a slightly smaller inertia constant compared to SC2 (150 MVA), which supports PV2. As a result, PV2 benefits from a stronger and more inertial local voltage source, allowing its terminal voltage to remain more stable. This highlights the importance not only of SC integration but also of device sizing and location, as they directly influence the voltage profile and transient performance across different parts of the network.

5.4 - Impact of Solutions Placement

In this section, the impact of the geographical placement of stability support solutions on system performance is evaluated. While previous analyses focused on configurations where these devices were installed close to the PV units they support, this section investigates whether their effectiveness is influenced by being positioned in more centralized locations of the network. The GFM and SC devices are relocated to Buses 5 and 6, which are topologically closer to the centre of the 9-bus system. The objective is to determine whether centralized placement enhances or diminishes their ability to provide frequency and voltage support and to assess whether their contribution becomes more effective when stabilizing the system as a whole rather than locally. The following simulations will compare these new configurations with previous results to identify optimal deployment strategies.

5.4.1 - Integration of Grid-Forming Inverters in Central Grid Locations

This section explores the impact of relocating GFM inverters from locations near the PV units to more centralized positions within the network. The GFM devices are moved to Buses 5 and 6, which are electrically closer to the centre of the 9-bus system. By shifting the GFM away from the immediate vicinity of the PV plants, the analysis seeks to understand whether a more centralized deployment can provide broader system-wide benefits or if proximity to the renewable sources remains a key factor in maximizing effectiveness. The results for this scenario are presented below.

Table 5.9 - RoCoF and Nadir results for short-circuit faults with 2 GFM integrated in a centralized location

	|RoCoF| (Hz/s)			
Line	**500ms**	**250ms**	**100ms**	**Nadir (Hz)**
5-7 (2)	0,760	0,880	1,000	49,31
7-8 (3)	1,060	1,120	1,150	48,71
8-9 (4)	0,950	1,020	1,050	49,30
6-9 (5)	1,100	1,380	1,750	48,52

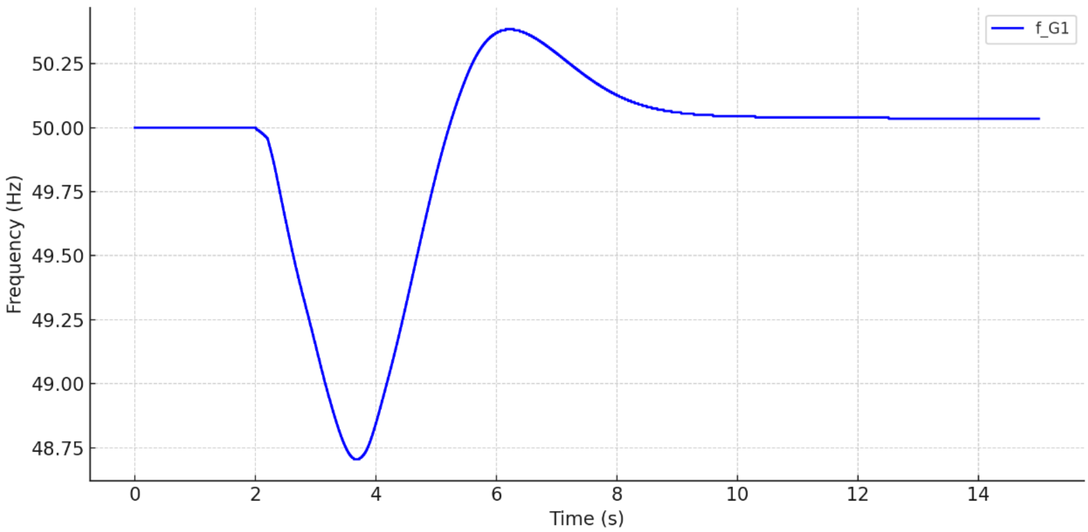

Figure 5.20 - Frequency after fault on line 3 with 2 GFM integrated in a centralized location

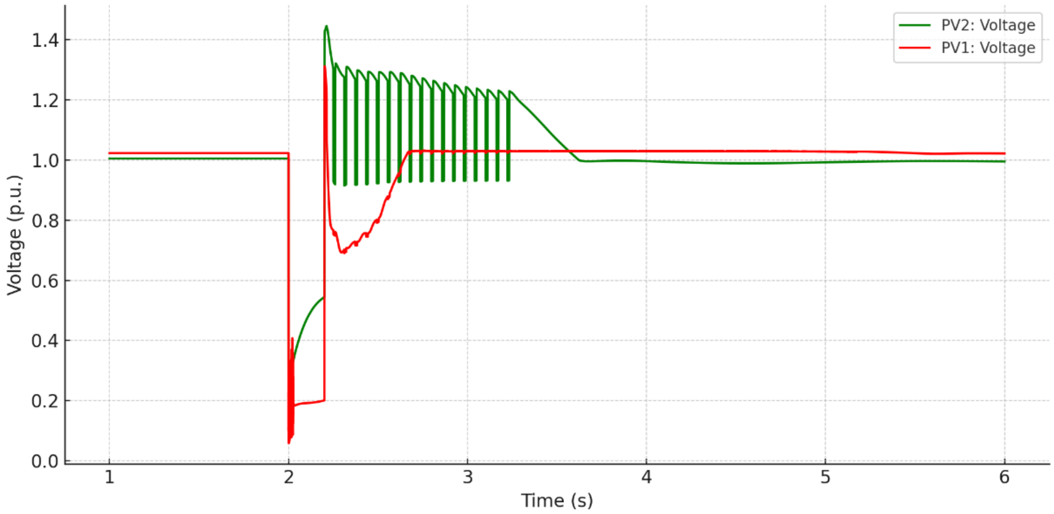

Figure 5.21 - PV1 and PV2 voltage magnitude after fault on line 3 with 2 GFM integrated in a centralized location

The results presented in **Figure 5.20** and **Table 5.9** reveal that relocating the GFM inverter to a more central location within the grid leads to a noticeable deterioration in frequency stability as the frequency nadir is much lower in this scenario going beyond the limits established by ENTSO-E in some of the fault cases.

Figure 5.21 further illustrates voltage dynamics at the points of connection of PV1 and PV2. The voltage response shows pronounced oscillations, during and after the fault suggesting instability in the control loop and weak damping due to the increased electrical distance between the GFMs and the PV plants. This contrasts with previous cases where local placement provided more effective voltage support with smoother recovery.

Increasing the capacity of the GFMs proves to be effective in improving frequency stability, as it enhances the system's ability to contain frequency deviations and results in a higher nadir, **shown in table 5.10**. However, this increase in capacity does not completely eliminate voltage-related instabilities. Voltage oscillations still occur at the terminals of inverter-based generators.

Table 5.10 - RoCoF and Nadir results for fault on line 3 with different GFM capacities

	|RoCoF| (Hz/s)			
GFM1/2 capacity (MVA)	**500ms**	**250ms**	**100ms**	**Nadir (Hz)**
100/150	1,060	1,120	1,150	48,71
300/350	0,550	0,580	0,650	49,53
1000/1000	0,240	0,300	0,400	49,79

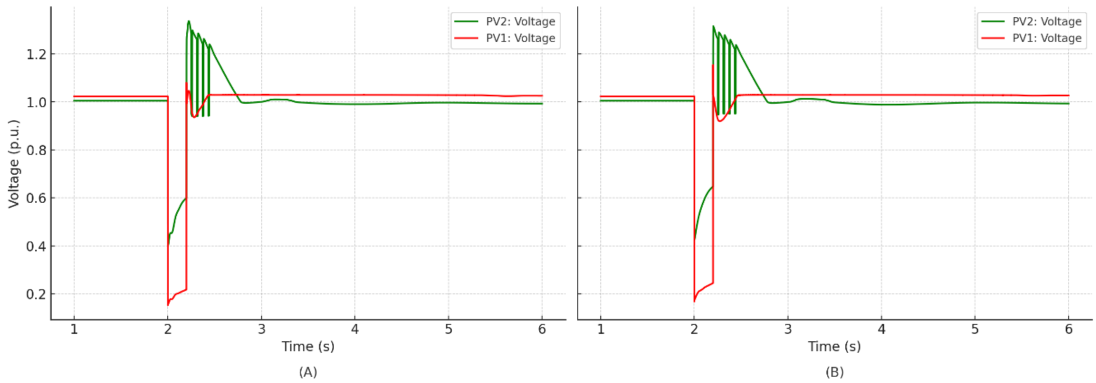

Figure 5.22 - PV1 and PV2 voltage magnitude after fault on line 3 with 2 different GFM capacities, (A) 300/350 MVA and (B) 1000MVA, in a centralized location

5.4.2 - Integration of Synchronous Condensers in Central Grid Locations

In this section, the same synchronous condensers (SC1 and SC2) used in the **Section 5.3.2** are reallocated to more centralized locations within the network, SC1 is connected to Bus 5 and SC2 to Bus 6. The results for this scenario are presented below.

Table 5.11 - RoCoF and Nadir results for short-circuit faults with 2 SC integrated in a centralized location

	|RoCoF| (Hz/s)			
Line	**500ms**	**250ms**	**100ms**	**Nadir (Hz)**
5-7 (2)	1,129	1,255	1,315	49,18
7-8 (3)	1,376	1,405	1,451	48,10
8-9 (4)	1,309	1,360	1,392	48,97
6-9 (5)	0,900	0,917	0,995	48,65

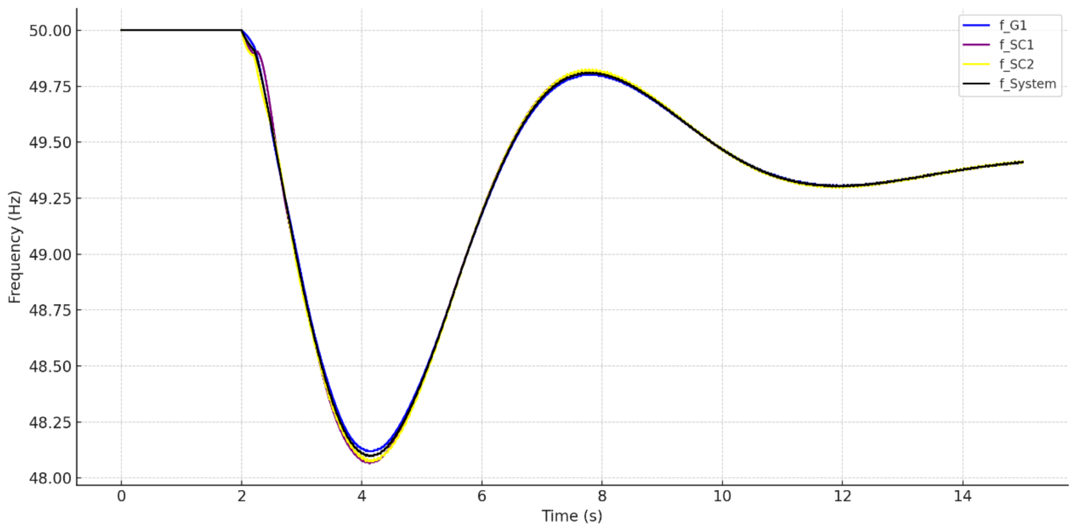

Figure 5.23 - Frequency after fault on line 3 with 2 SC in a centralized location

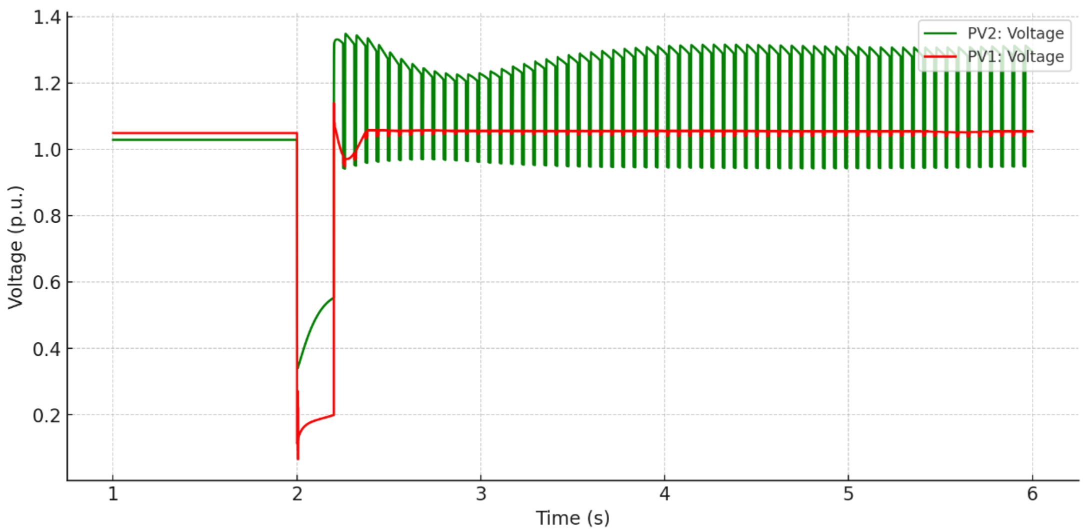

Figure 5.24 - PV1 and PV2 voltage magnitude after fault on line 3 with 2 SC in a centralized location

The results clearly indicate that relocating the synchronous condensers (SC1 and SC2) to more centralized buses in the network (Buses 5 and 6) significantly degraded system performance. As seen in **Table 5.11**, the nadir frequency dropped well below the 49.2 Hz threshold imposed by ENTSO-E for operational security, reaching as low as 48.10 Hz. This reflects the SC's diminished effectiveness in providing adequate frequency support when not positioned near the RES units.

Additionally, the voltage response shown in **Figure 5.24** confirms instability following the fault, with noticeable oscillations in both PVs, especially PV2 voltages. These oscillations indicate a loss of synchronism from the PLLs (Phase-Locked Loops) of the PV inverters, which failed to maintain proper voltage tracking. This behaviour reveals a collapse in coordination and control, ultimately leading to system instability. If this test system had implemented protections schemes like under frequency load shedding (UFLS) and other type of protections, they would've been activated and the system would've completely collapsed.

Same as the GFM case, increasing the capacity of the SC also proves to be effective in improving frequency stability, shown in **table 5.12**. The same way, this increase in capacity does not completely eliminate voltage-related instabilities. Voltage oscillations still occur at the terminals of inverter-based generators.

Table 5.12 - RoCoF and Nadir results for fault on line 3 with different SC capacities

	|RoCoF| (Hz/s)			
SC1/2 capacity (MVA)	**500ms**	**250ms**	**100ms**	**Nadir (Hz)**
100/150	1,376	1,405	1,451	48,10
300/350	0,797	0,836	0,870	49,23
1000/1000	0,080	0,099	0,147	49,91

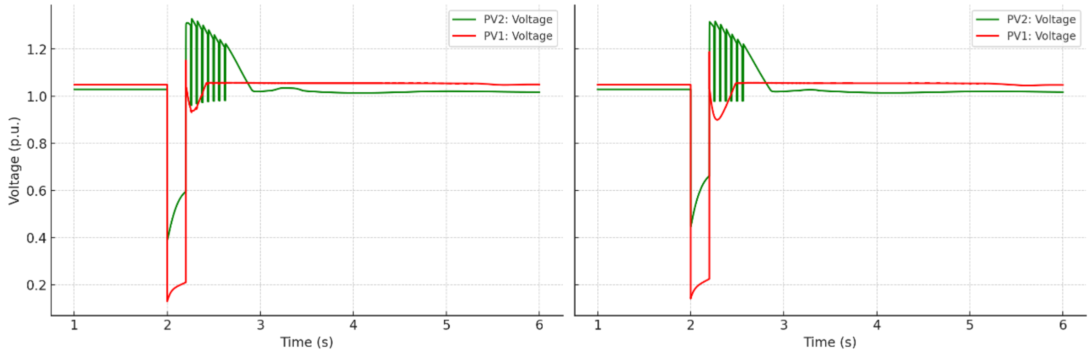

Figure 5.25 - PV1 and PV2 voltage magnitude after fault on line 3 with 2 different SC capacities, (A) 300/350 MVA and (B) 1000MVA, in a centralized location

5.5 - Final Remarks

The results presented in this chapter demonstrate that both grid-forming inverters, based on virtual synchronous machine control and synchronous condensers, when installed locally near RES, in low-inertia power systems, significantly enhance frequency stability, but they do so through distinct mechanisms.

GFM inverters offer fast and flexible frequency regulation through synthetic inertia and voltage control, while SCs provide real rotational inertia and robust reactive power support. Quantitative comparisons show that GFM devices yield faster frequency recovery and improved damping, particularly when placed near RES injection points, whereas SCs contribute more effectively to fault ride-through and system strength due to their short-circuit current capability.

In the most demanding scenario, where synchronous generators SG2 and SG3 were entirely replaced by PV units operating at full capacity, the system exhibited severe instability in the absence of additional support, with frequency nadirs and RoCoF values breaching ENTSO-E operational limits. However, the integration of two support devices, either GFMs or SCs, at the respective PV buses restored system stability, eliminated oscillations and maintained all dynamic metrics within acceptable thresholds.

Conversely, relocating the GFM and SC devices to more centralized grid locations resulted in significantly degraded performance. Frequency nadirs dropped below permissible levels, voltage oscillations reappeared and the PV inverters' PLLs lost synchronism. Even when the capacity of these devices was increased, the centralized placement could not fully compensate for the lack of proximity to the renewable generation.

The analysis revealed that optimal placement plays a key role in maximizing the effectiveness of both solutions, with decentralized configurations offering better local support and centralized placements showing stronger global frequency impacts.

Despite the promising results, trade-offs remain: GFM inverters require sophisticated control schemes and energy storage, while SCs involve higher mechanical complexity and inertia sizing challenges. These findings highlight the potential of combining both technologies in hybrid configurations for resilient, high-renewables grids.

Chapter 6

Conclusions and Future Work

6.1 - Conclusions

This dissertation addressed the dynamic stability challenges arising from the increasing penetration of renewable energy sources (RES) in low-inertia power systems. The work is framed within the broader context of the global energy transition, where maintaining grid reliability is increasingly complex due to the displacement of conventional synchronous generation. Throughout this dissertation, a comprehensive dynamic analysis of a low-inertia power system was carried out, focusing on the system's stability challenges under high penetration of RES.

Through extensive dynamic simulations using the IEEE 9-bus test system in DIgSILENT PowerFactory, the study evaluated and compared the performance of synchronous condensers (SCs) and grid-forming (GFM) inverters as advanced support technologies for improving system stability under increased shares of inverter-based resources. By replicating future but realistic operational scenarios, mainly short circuits, the study provides a robust and systematic analysis of how these technologies perform under typical grid disturbances. This comparative investigation, with particular attention to device sizing and placement, offers practical insights into how to improve system strength in a converter-dominated grid.

The loss of inertia due to the replacement of synchronous generators with inverter-based photovoltaic (PV) units operating in grid-following mode resulted in a degradation of the system's dynamic response. The results obtained in **Chapter 4** clearly demonstrate this adverse impact of reduced system inertia on frequency and converter related stability issues. As synchronous generators were progressively replaced with inverter-based RES, the system exhibited significantly higher Rate of Change of Frequency (RoCoF) and deeper frequency nadirs following disturbances. The obtained results clearly highlight the reduce ability of the system to respond to power imbalances in the absence of rotating inertia. Moreover, the analysis revealed emerging Converter-Driven Stability (CDS) issues, where grid-following inverters not only failed to support frequency dynamics but also contributed to instability due to their dependence on weak and distorted grid conditions for synchronization. In scenarios with high RES share, the reduced short-circuit strength and weakened voltage profiles further compromised inverter performance. These findings reinforce the urgent need for advanced control strategies and supportive technologies, to mitigate the dynamic challenges posed by CDS in future power systems.

Building on the challenges identified in **Chapter 4**, **Chapter 5** evaluated the ability of synchronous condensers (SCs) and grid-forming (GFM) inverters to mitigate instability in low-inertia systems, with particular attention to Converter-Driven Stability (CDS) issues. The results showed that both technologies significantly improve dynamic performance, but with distinct characteristics. The same RES scenarios tested in **Chapter 4** were revisited, including both moderate and high renewable penetration cases, allowing a direct comparison of the effectiveness of each solution. Additionally, the influence of device placement, near the PV units versus more centralized positions in the network, was studied, as well as a sensitivity analysis with respect to the installed capacity of each technological solution.

The integration of both GFM inverters and SCs near RES proved effective in mitigating the stability issues identified in **Chapter 4**. Both technologies significantly improved system behaviour by reducing RoCoF values, raising frequency nadirs and eliminating post-fault oscillations. However, important differences in performance were observed between the two solutions.

The results demonstrated that both SCs and GFMs can significantly enhance system robustness when appropriately sized and strategically placed. In one hand, SCs exhibited better initial frequency containment, with lower RoCoF values, due to their real mechanical inertia. They also provided superior voltage support during fault conditions, thanks to their robust reactive power capabilities and high short-circuit current contribution. On the other hand, GFM Inverters, while showing slightly higher RoCoF values, offered better frequency recovery (higher nadirs), as a result of their virtual inertia and damping control, implemented through the Virtual Synchronous Machine (VSM) model. However, their ability to support voltage recovery was more limited.

These differences lie in the characteristics of each solution. A SC inherently capable of providing instantaneous inertial response and dynamic voltage regulation. Its mechanical inertia resists frequency deviations naturally, without the need for control algorithms or sensors. Additionally, its ability to supply short-circuit current strengthens the local short-circuit ratio (SCR), which improves the operating environment for nearby Grid Following (GFL) inverters. A GFM Inverter provides synthetic inertia and frequency support by modulating its output using advanced control algorithms. While highly flexible and scalable, its performance depends on tuning parameters, control loop dynamics and accurate grid voltage detection and its reactive current injection is constrained by current-limiting mechanisms.

Furthermore, the study highlighted that the physical placement of these technologies plays a crucial role. Localized deployment near RES units outperformed centralized configurations in mitigating frequency and voltage deviations. However, when both Grid-Forming inverters and Synchronous Condensers were placed in central grid nodes, their effectiveness in stabilizing the system significantly declined. Despite operating with the same or even increased rated capacities, the simulations showed lower frequency nadirs, persistent voltage oscillations and, in some cases, loss of synchronism from the PV inverters' Phase-Locked Loops (PLLs). This contrast proves that electrical proximity to the RES units is essential. In central locations their impact was diluted by the electrical distance and network impedance, making them less effective in mitigating fast transients or stabilizing weak voltage references.

Both technologies offer valuable contributions to the stability of low-inertia grids. However, they do so in fundamentally different ways, and their effectiveness is closely tied to location, capacity and interaction with the rest of the system. These findings underline the importance of deploying advanced technologies not only based on their capabilities but also in accordance with grid topology and RES distribution. As power systems evolve toward decarbonization, such insights will be critical to enabling a stable and resilient energy transition.

6.2 - Future Work

While the present dissertation provided valuable insights into the dynamic behaviour of low-inertia power systems and the comparative performance of GFM inverters and SCs, several aspects remain open for further investigation and enhancement.

One key direction for future work is the extension of simulations to larger and more complex power systems, such as the IEEE 39-bus. A larger test network would allow for a more realistic assessment of how GFM and SC devices perform under diverse topological conditions. This would also help evaluate the scalability of the proposed solutions and their interactions across multiple voltage levels and geographic areas.

Another important area is the detailed tuning and sensitivity analysis of control parameters, particularly for PV inverters and GFM units. In this study, fixed parameters were used to isolate structural impacts, but in practice, the performance of GFMs is highly dependent on parameters such as virtual inertia, damping, current limits and voltage controller gains. Future studies could investigate the impact of different parameter combinations, possibly supported by optimization algorithms to identify robust tuning strategies under varying grid conditions.

Another relevant direction is the coordinated operation of multiple GFM and SC units. In this work, these devices were deployed independently. However, future research could explore hybrid topologies, where GFMs and SCs operate in parallel and interactively, each leveraging its strengths. Additionally, future work should consider the integration of Battery Energy Storage Systems (BESS), either as standalone units or in hybrid configurations with GFM or SC devices.

In summary, future research should aim to validate the current findings on a larger scale, enhance the control and coordination of support devices, and introduce additional technologies like BESS, ultimately contributing to the design of stable, flexible and resilient renewable-dominated grids.

References

[1] International Energy Agency (IEA), Net Zero by 2050: A Roadmap for the Global Energy Sector. Paris, France: IEA, May 2021. Available: https://iea.blob.core.windows.net/assets/deebef5d-0c34-4539-9d0c-10b13d840027/NetZeroby2050-ARoadmapfortheGlobalEnergySector_CORR.pdf.

[2] U. Tamrakar, D. Shrestha, M. Maharjan, B. P. Bhattarai, T. M. Hansen, and R. Tonkoski, "Virtual Inertia: Current Trends and Future Directions," Applied Sciences, vol. 7, no. 654, pp. 1-29, 2017. Available: https://doi.org/10.3390/app7070654

[3] A. Tarraso, N. B. Lai and P. Rodriguez, "Synchronous Fault Compensator for Voltage Sensorless Grid-Following Power Converters," 2021 IEEE 12th International Symposium on Power Electronics for Distributed Generation Systems (PEDG), Chicago, IL, USA, 2021, pp. 1-5, doi: 10.1109/PEDG51384.2021.9494205.

[4] C. Roberts, "Review of international grid codes," 2018.

[5] D. Lepour, M. Paolone, G. Denis, C. Cardozo, T. Prevost and E. Guiu, "Performance assessment of Synchronous Condensers vs Voltage Source Converters providing grid-forming functions," 2021 IEEE Madrid PowerTech, Madrid, Spain, 2021, pp. 1-6, doi: 10.1109/PowerTech46648.2021.9494883.

[6] ENTSO-E AISBL, Inertia and Rate of Change of Frequency (RoCoF), version 17, Brussels, Belgium, Dec. 16, 2020. Available: www.entsoe.eu

[7] C. Yongning, L. Yan, W. Zhen, L. Zhen, L. Hongzhi and Z. Zhankui, "The Characteristics and Challenge on Large-Scale Renewable Energy Grid Integration," 2019 IEEE Innovative Smart Grid Technologies - Asia (ISGT Asia), Chengdu, China, 2019, pp. 1393-1398, doi: 10.1109/ISGT-Asia.2019.8881344

[8] Kundur Prahba. Power System Stability and Control. 1994

[9] S. Yang, Q. Meng, Y. Zhang, Z. Hao and B. Zhang, "Simplified Prediction Model of Frequency Nadir for Power Systems Penetrated With Renewable Energy," 2022 IEEE Power & Energy Society General Meeting (PESGM), Denver, CO, USA, 2022, pp. 1-5, doi: 10.1109/PESGM48719.2022.9917200

[10] Mancarella P, Puschel S, Wang H, Brear M, Jones T, Jeppesen M,Batterham R, Evans R, Mareels I (2017) Power system security assessment of the future National Electricity Market. Technical report June, Melbourne Energy Institute, Melbourne

[11] CIGRÉ, "System Strength: Reference Paper," Electra, vol. 315, Apr. 2021. Available: https://electra.cigre.org/315-april-2021/reference-paper/system-strength.html [Accessed: Jan. 10, 2025].

[12] D. Wu, G. Li, M. Javadi, A. M. Malyscheff, M. Hong and J. N. Jiang, "Assessing Impact of Renewable Energy Integration on System Strength Using Site-Dependent Short Circuit

Ratio," in IEEE Transactions on Sustainable Energy, vol. 9, no. 3, pp. 1072-1080, July 2018, doi: 10.1109/TSTE.2017.2764871.

[13] L. Yu, H. Sun, S. Xu, B. Zhao and J. Zhang, "A Critical System Strength Evaluation of a Power System with High Penetration of Renewable Energy Generations," in CSEE Journal of Power and Energy Systems, vol. 8, no. 3, pp. 710-720, May 2022, doi: 10.17775/CSEEJPES.2021.03020.

[14] SSS Clutch, "Short-Circuit Level and Electricity System Strength," SSS Clutch, [Online]. Available: https://www.sssclutch.com/en/articles/short-circuit-level-and-electricity-system-strength/. [Accessed: Jan. 10, 2025].

[15] European Commission, Commission Regulation (EU) 2016/631 of 14 April 2016 establishing a network code on requirements for grid connection of generators, Official Journal of the European Union, 2016. https://eur-lex.europa.eu/eli/reg/2016/631

[16] R. Bründlinger, T. Schaupp, G. Arnold, N. Schäfer, G. Graditi, and G. Adinolfi, “Implementation of the European Network Code on Requirements for Generators on the European national level Implementation of the European Network Code on Requirements for Generators on the European national level Current Status-Trends and Challenges”. 2018. [Online]. Available: https://www.researchgate.net/publication/329124454

[17] República Portuguesa, "Portaria n.º 73/2020 de 16 de março," *Diário da República*, 1.ª série, n.º 53, pp. 3-5, Mar. 16, 2020. Available: https://diariodarepublica.pt/dr/detalhe/portaria/73-2020-130273580

[18] J. Rychlak, "National-Level Implementation of the Commission Regulation (EU) 2016/631 of 14/04/2016 Establishing a Network Code on Requirements for Grid Connection of Generators," Acta Energetica, vol. 2, no. 35, pp. 4–13, 2018. Available: https://doi.org/10.12736/issn.2300-3022.2018201

[19] A. Hadavi, M. Tarafdar Hagh, and S. Ghassem Zadeh, "Critical inertia thresholds for frequency stability in renewable energy-integrated power systems," *Int. J. Electr. Power Energy Syst.*, vol. 169, Art. no. 110733, May 2025. Available: https://doi.org/10.1016/j.ijepes.2025.110733

[20] Soleimani, H.; Habibi, D.; Ghahramani, M.; Aziz, A. Strengthening Power Systems for Net Zero: A Review of the Role of Synchronous Condensers and Emerging Challenges. Energies 2024, 17, 3291. https://doi.org/10.3390/ en17133291

[21] Y. Gu and T. C. Green, "Power System Stability With a High Penetration of Inverter-Based Resources," in Proceedings of the IEEE, vol. 111, no. 7, pp. 832-853, July 2023, doi: 10.1109/JPROC.2022.3179826

[22] S. Bhatta, B. Alattas, A. Olumide, T. E. Field, M. Peterson and P. Rastgoufard, "Comparative Analysis of Grid-Following (GFL) and Grid-Forming (GFM) Inverter Models for Studying Low Inertia Power Systems," 2024 IEEE Kansas Power and Energy Conference (KPEC), Manhattan, KS, USA, 2024, pp. 1-5, doi: 10.1109/KPEC61529.2024.10676094

[23] Bikdeli, E.; Islam, M.R.;Rahman, M.M.; Muttaqi, K.M. State of the Art of the Techniques for Grid Forming Inverters to Solve the Challenges of Renewable Rich Power Grids. Energies 2022, 15, 1879. https://doi.org/10.3390/en15051879

[24] D. B. Rathnayake et al., "Grid Forming Inverter Modeling, Control, and Applications," in IEEE Access, vol. 9, pp. 114781-114807, 2021, doi: 10.1109/ACCESS.2021.3104617

[25] Y. Teng, W. Deng, W. Pei, Y. Li, L. Ding, and H. Ye, "Review on grid-forming converter control methods in high-proportion renewable energy power systems," Global Energy Interconnection, vol. 5, no. 3, pp. 328–342, Jun. 2022. Available: https://doi.org/10.1016/j.gloei.2022.06.010

[26] J. Liu, Y. Miura and T. Ise, "Comparison of Dynamic Characteristics Between Virtual Synchronous Generator and Droop Control in Inverter-Based Distributed Generators," in IEEE Transactions on Power Electronics, vol. 31, no. 5, pp. 3600-3611, May 2016, doi: 10.1109/TPEL.2015.2465852

[27] K. Zheng, C. Luo, Z. Sun, Y. Zhu and J. Yu, "Impedance Network Modeling of GFL and GFM Converters System Considering AC/DC Couplings," 2024 The 9th International Conference on Power and Renewable Energy (ICPRE), Guangzhou, China, 2024, pp. 185-190, doi: 10.1109/ICPRE62586.2024.10768311

[28] E. Rakhshani, J. M. Ruiz, X. Benavides and E. Dominguez, "Enhancing Low-Inertia Power Systems with Grid Forming Based Hybrid Energy Storage Technology," 2024 12th International Conference on Smart Grid (icSmartGrid), Setubal, Portugal, 2024, pp. 464-468, doi: 10.1109/icSmartGrid61824.2024.10578086.

[29] L. Ding, X. Lu and J. Tan, "Small-Signal Stability Analysis of Low-Inertia Power Grids with Inverter-Based Resources and Synchronous Condensers," 2022 IEEE Power & Energy Society Innovative Smart Grid Technologies Conference (ISGT), New Orleans, LA, USA, 2022, pp. 1-5, doi: 10.1109/ISGT50606.2022.9817556.

[30] R. W. Kenyon, A. Hoke, J. Tan and B. -M. Hodge, "Grid-Following Inverters and Synchronous Condensers: A Grid-Forming Pair?," 2020 Clemson University Power Systems Conference (PSC), Clemson, SC, USA, 2020, pp. 1-7, doi: 10.1109/PSC50246.2020.9131310.

[31] Nuhic, M., Kkuni, K. V., Yang, G., & Ramachandran, J. (2020). Comparative study of hybrid synchronous condenser incorporating battery energy storage system for ancillary service provision. In Proceedings of 19th Wind Integration Workshop Energynautics GmbH.

[32] M. Tozak, S. Taskin, I. Sengor and B. P. Hayes, "Modeling and Control of Grid Forming Converters: A Systematic Review," in IEEE Access, vol. 12, pp. 107818-107843, 2024, doi: 10.1109/ACCESS.2024.3437236.

[33] https://www.digsilent.de/en/powerfactory.html [Accessed: May. 20, 2025].

[34] N. U. Putri, F. Rossi, A. Jayadi, J. P. Sembiring and H. Maulana, "Analysis of Frequency Stability with SCES's type of Virtual Inertia Control for The IEEE 9 Bus System," 2021 International Conference on Computer Science, Information Technology, and Electrical Engineering (ICOMITEE), Banyuwangi, Indonesia, 2021, pp. 191-196, doi: 10.1109/ICOMITEE53461.2021.9650178.

[35] Francisco M. Gonzalez-Longatt, "Test Case P.M. Anderson Power System," Power Systems Test Cases, [Accessed May. 20, 2025]. [Online]. Available: http://fglongatt.org/OLD/Test_Case_Anderson.html

[36] S. Talpur, "Testing and model validation of round rotor synchronous generator (GENROU)," Renewable and Sustainable Energy Reviews, vol. 80, pp. 880–887, Dec. 2017. Available: https://doi.org/10.1016/j.rser.2017.05.244

[37] P. Pourbeik, B. Agrawal, S. Patterson, and R. Rhinier, "Modeling of synchronous generators in power system studies," CIGRE Science & Engineering, no. 6, pp. 21–31, Oct. 2016. Available: https://www.researchgate.net/publication/309632209

[38] IEEE PES Power System Dynamic Performance Committee, "Dynamic Models for Turbine-Governors in Power System Studies", IEEE PES Technical Report PES-TR1, Jan. 2013. Available: https://site.ieee.org/fw-pes/files/2013/01/PES_TR1.pdf

[39] Electric Power Research Institute (EPRI), "Model User Guide for Generic Renewable Energy System Models" Technical Update, ID: 3002027129, October 2023. Available: https://www.epri.com/research/products/000000003002027129

[40] G. Misyris, D. Ramasubramanian, M. Val Escudero, T. Kërçi, and S. Murray, "Weak Grid Analysis for Interconnecting Inverter-Based Generation – Ireland Case Study," CIGRE Science & Engineering, no. 29, pp. 1–19, Jun. 2023. Available: https://cse.cigre.org/cse-n029/weak-grid-analysis-for-interconnecting-inverter-based-generation-ireland-case-study/

[41] C. Eckel, D. Babazadeh, and C. Becker, "Classification of Converter-Driven Stability and Suitable Modeling and Analysis Methods," IEEE Access, vol. 12, pp. 1–1, 2024, doi: 10.1109/ACCESS.2024.3388098.

Annex A

IEEE 9-Bus System Data

This annex provides the detailed data of the transmission lines, transformers, generators and loads used in the IEEE 9-bus test system.

A.1 – Generator Data

Generator	Connected to Bus	Un (KV)	Sn (MVA)	Power Factor
SG1	1	16,5	512	0,9
SG2	2	18	270	0,85
SG3	3	13,8	125	0,85

A.2 – Transformer Data

Transformer	From Bus	To Bus	V1 (KV)	V2(KV)
T1	1	4	16,5	230
T2	2	7	18	230
T3	3	9	13,8	230

A.3 - Line Data

Line	From Bus	To Bus	Lenght(Km)	R1(Ohm)	X1(Ohm)	Susceptance B' (µS)
1	4	5	1	5,29	44,965	332,7
2	5	7	1	16,928	85,169	578,45
3	7	8	1	4,4965	38,088	281,66
4	8	9	1	6,2951	53,3232	395,08
5	6	9	1	20,631	89,93	676,75
6	4	6	1	8,993	48,668	298,69

A.4 - Load Data

Bus	Voltage (KV)	Pload (MW)	Qload(Mvar)
1	16,5	0	0
2	18	0	0
3	13,8	0	0
4	230	0	0
5	230	125	50
6	230	90	30
7	230	0	0
8	230	100	35
9	230	0	0

Annex B

Synchronous Machines Dynamic Models Parameters

This annex presents the dynamic model parameters used for the synchronous machines in the IEEE 9-bus test system.

B.1 – GENROU parameters of Synchronous Generators

Parameters Values of Synchronous Generators				
Parameter	**Unit**	**SG1**	**SG2**	**SG3**
D	p.u.	0	0	0
H	s	2,6312	4,1296	4,768
Xd	p.u.	1,7	1,7	1,22
Xq	p.u.	1,65	1,62	1,16
Xd'	p.u.	0,27	0,256	0,174
Xq'	p.u.	0,47	0,245	0,25
Xd"	p.u.	0,2	0,185	0,134
Xq"	p.u.	0,2	0,185	0,134
Xl	p.u.	0,16	0,155	0,078
rstr	p.u.	0,004	0,0016	0,004
T'do	s	3,8	4,8	8,97
T'qo	s	0,48	0,5	0,5
T"do	s	0,01	0,01	0,033
T"qo	s	0,0007	0,0007	0,07
SG10	p.u.	0,09	0,125	0,1026
SG12	p.u.	0,4	0,45	0,432

B.2 – Excitation System (exc_AC) parameters of Synchronous Generators

Parameter	Unit	SG1	SG2	SG3
Tr	s	0,02	0,02	0,02
Kpr	p.u.	20	20	20
Kir	p.u./s	5	5	5
Kdr	p.u.	10	10	10
Tdr	s	0,1	0,1	0,1
Ka	p.u.	2	1	1
Ta	s	0,1	0,1	0,1
Ke	p.u.	1	1	1
Te	s	1,2	1,2	1,2
Vr min	p.u.	0	0	0
Ve min	p.u.	0	0	0
Vr max	p.u.	6	6	6
Ve max	p.u.	6	6	6

B.3 – Turbine Governor (TGOV1) parameters of Synchronous Generators

Parameter	Unit	SG1	SG2	SG3
Trate	MW	460,8	229,5	106,25
R	p.u.	0,05	0,05	0,05
T1	s	0,5	0,5	0,5
T2	s	1	1	1
T3	s	3	3	3
Dt	p.u.	0	0	0
Vmin	p.u.	0	0	0
Vmax	p.u.	1	1	1

Annex C

Renewable Energy Sources Dynamic Models Parameters

This annex presents the dynamic model parameters used for the renewable energy sources operating in grid-following mode implemented in the IEEE 9-bus test system.

C.1 – REGC_C Generator-Converter model parameters

Parameter	Unit	Description	Value
Tq	s	Converter time constant	0,0001
Tfltr	s	Voltage filter time constant	0,02
RateFlag	-	Rate limit: 0 =active current, 1 = active power	1
re	p.u.	Source resistance	0
xe	p.u.	Source reactance	0,1
te	s	Emulated delay in converter controls	1,00E-05
Kip	-	Proportional gain of the inner current loop	1
Kii	1/s	Integral gain of the inner current loop	30
Kppll	rad/s/p.u.	Proportional gain of the PLL	10
Kipll	rad/s/p.u./s	Integral gain of the PLL	300
Vpllfrz	p.u.	Lower voltage level to freeze PLL	0,5
Iqrmin	p.u./s	Min. Reactive current rate limit	-2,5
Wmin	rad/s	Lower limit on the PLL	-10
Iqrmax	p.u./s	Max. Reactive current rate limit	2,5
rrpwr	p.u./s	Active current rate limit	10
wmax	rad/s	Upper limit on the PLL	20

C.2 - REEC_D Electrical control model parameters

Parameter	Unit	Description	Value
PfFlag	-	Power factor flag: 1= pf control, 0 = Q control	0
Vflag	-	Voltage control flag: 1 = Q ctrl., 0 = voltage ctrl.	1
Tp	s	Filter time constant for power measurement	0,001
Kqp	p.u.	Proportional gain	2
Kqi	p.u.	Integral gain	1
QFlag	-	Q control flag: 1 = voltage/Q, 0 = const. Pf or Q ctrl.	0,00E+00
Kvp	p.u.	Proportional gain	3
Kvi	p.u.	Integral gain	3
Trv	s	Filter time constant for voltage measurement	1,00E-05
dbd1	p.u.	Voltage deadband for overvoltage iq injection	-0,005
dbd2	p.u.	Voltage deadband for undervoltage iq injection	0,005
Kqv	p.u.	Gain for reactive current injectionduring fault	30
Vdip	p.u.	Undervoltage condition trigger voltage	0,95
Vup	p.u.	Overvoltage condition trigger voltage	1,1
Tiq	s	Time constant on lag delay	1,00E-05
Tpord	s	Time constant	0
PqFlag	-	Priority flag on current limit 1 = P, 0 = Q priority	0
Imax	p.u.	Maximum converter current limit	2,5
Thld2	s	Ipcm max delayafter fault	0
Ke	p.u.	Ipmin scalling factor	0
Pflag	-	Power control flag: 0= P reference, 1 = speed reference	1
Vref0	p.u.	Reference voltage, 0 = terminal voltage	0
Vref1	p.u.	User-defined ref./bias on inner loop control	0
Rc	p.u.	Current-compensation resiltance	0
Xc	p.u.	Current-compensation reactance	0,1
VcmpFlag	-	0 = reactive droop, 1 = current compensation	0
Kc	p.u.	Reactive-current compensation gain	0,5
Tr1	s	Filter time constant for voltage measurements	0,001
vblkl	p.u.	Voltage below which the converter is blocked	0,1
vblkh	p.u.	Voltage above which the converter is blocked	1,2
Tblk delay	s	Time for which the converter will remain blocked	0,01
Thld	s	Reative current injection delay after voltage dip	0
iq frz	p.u.	Value at which injection is held after voltage dip	0
qvmin	p.u.	Reative power limit minimum	-1
Vmin	p.u.	Voltage control minimum	0,9
Iql1	p.u.	Minimum limit of reactive current injection	-2,5
dPmin	p.u./s	Ramp rate on power reference	-5
Pmin	p.u.	Minimum power reference	0
qvmax	p.u.	Reactive power limit maximum	1
Vmax	p.u.	Voltage control maximum	1,1

Iqh1	p.u.	Maximum limit of reactive current injection	2,5
dPmax	p.u./s	Ramp rate on power reference	2
Pmax	p.u.	Maximum power reference	1

C.3 - Protection model parameters

Parameter	Unit	Description	Value
T brk	s	Circuit breaker opening delay	0,05
Outage	-	Outage element trippping: 0 = no, 1 = yes	1
Prot u	-	Enable voltage protection: 0 = off, 1 = on	1
u max1	p.u.	Threshold slow overvoltage protection	1,1
Tumax1	s	Tripping delay slow overvoltage protection	60
u max2	p.u.	Threshold fast overvoltage protection	1,15
T umax2	s	Tripping delay fast overvoltage protection	0,1
u min1	p.u.	Threshold slow undervoltage protection	0,8
T umin1	s	Tripping delay slow undervoltage protection	1,5
u min2	p.u.	Threshold fast undervoltage protection	0,45
T umin2	s	Tripping delay fast undervoltage protection	0,8
Prot f	-	Enable frequency protection: 0 = off, 1 = on	1
f max	Hz	Threshold overfrequency protection	52,5
T fmax	s	Tripping delay overfrequency protection	0,1
f min	Hz	Threshold underfrequency protection	47,5
T fmin	s	Tripping delay underfrequency protection	0,1
u low	p.u.	Minimum voltage for frequency protection	0,8
T fblock	s	Frequency protection block time after UVRT	0,1
T fmeas	s	Frequency measurement filter time constant	0,1
Prot rocof	-	Enable ROCOF protetion: 0 = off, 1= on	1
df max	Hz/s	Maximum rate of change of frequency	2,5
df min	Hz/s	Minimum rate of change of frequency	-2,5
T rocof	s	Tripping delay ROCOF protection	0,1

C.4 – Protection model parameters

Parameter	Unit	Description	Value
Tfltr	s	Voltage measurement time constant	0,02
Vwgo	p.u.	Voltage threshold below which the WGO function is initiated	0,5
Pwgo1	p.u.	Power reference held during a fault when WGO function is initiated	0,5
rpw1	p.u./s	Ramp rate at which power is increased from Pwgo1 to Pwgo2	0,2
Pwgo2	p.u.	Power reference held for Thold seconds after the fault	0,7
rpw2	p.u./s	Ramp rate at which power is increased from Pwgo2 back to normal	0,2
Thold	s	Time for which the power reference is held at Pwgo2	1
eps	p.u.	Small hysteresis on voltage recovery to start the first ramp	0,01

Annex D

Grid-Forming Converters Dynamic Models Parameters

This annex provides the dynamic model parameters used for the grid-forming converters implemented in the IEEE 9-bus test system.

D.1 – Virtual Synchronous Machine model parameters

Parameter	Unit	Description	Value
Ta	s	Acceleration time constant	5
Dp	p.u.	Damping coefficient	100
w c	rad/s	Damping filter cut-off frequency	6
T LPF u	s	Voltage setpoint low-pass filter time constant	0,003
ured	p.u.	Voltage threshold, under-voltage Pset red.&lim.	0,8
ModeRed	-	Under-voltage Pset reduction: 0 = no, 1 = yes	1
ModeLim	-	Under-voltage Pset limitation: 0 = no, 1 = yes	1
mp ollim	-	Overload limiter gain	0,1
T ollim	s	Overload limiter LPF time constant	0,0025
f setpoint	p.u.	Initial speed setting	1
pmin	p.u.	Minimum power	0
pmax	p.u.	Maximum power	1

D.2 – Virtual Impedance model parameters

Parameter	Unit	Description	Value
r	p.u.	Basic virtual resistance	0,006
x	p.u.	Basic virtual reactance	0,006
Mode	-	Control mode: 0 = const. Z, 1 = Proportional over-current limitation	1
i lim	p.u.	Over-current threshold	0,01
kpr	p.u.	Proportional factor for additional resistance	8
kpx	p.u.	Proportional factor for additional reactance	8
T lpf	s	Time constant of low-pass filter	0,0001

D.3 – Output Voltage Calculation model parameters

Parameter	Unit	Description	Value
uconv	p.u.	Maximum internal converter voltage	1,4
Mode	-	Current limitation: 0 = disabled, 1 = enable	1
i max	p.u.	Maximum current	1,2
Rseries	%	Series resistance	0
Xseries	%	Series reactance	10
Tlpf mag	s	Time constant, low pass filter terminal voltage magnitude	5,00E-05
Tlpf angle	s	Time constant, low pass filter terminal voltage angle	5,00E-05

D.4 – Voltage Controller model parameters

Parameter	Unit	Description	Value
Tr	s	Measurement filter time constant	0,02
K	-	Controller gain	2
Ta	s	Controller time constant	0,025
Tq	s	Reactive power filter time constant	0,02
q min	p.u.	Minimum reactive power	-0,5
Kuel	-	UEL proportional gain	0,5
q max	p.u.	Maximum reactive power	0,5
Koel	-	OEL proportional gain	0,5
u set min	p.u.	Minimum AVR output voltage	-1,5
u set max	p.u.	Maximum AVR output voltage	1,5

D.5 – frequency Sensitive mode model parameters

Parameter	Unit	Description	Value
FSM on	-	Frequency Sensitive Mode (FSM): 0 = off, 1 = on	0
Mode Db	-	Frequency deadband FSM: 0 = without, 1 = with	1
f db1	mHz	Lowe frequency deadband FSM	-20
f db2	mHz	Upper frequency deadband FSM	20
delay init fsm	s	Initial response delay FSM	0
s1	%	Droop 1 (FSM upward regulation, for f < fn)	5
s2	%	Droop 2 (FSM downward regulation, for f > fn)	5
LFSMO on	-	Limited FSM-O (overfrequency): 0 = off, 1 = on	1
f1 lfsmo	Hz	Frequency threshold for LSFM_O (> fn)	50,2
delay init lfsmo	s	Initial response delay FSM-O	0
s3	%	Droop 3 (FSM-O downward regulation, for f > f1)	5
LFSMU on	-	Limited FSM-U (underfrequency): 0 = off, 1 = on	0
f2 lfsmu	Hz	Frequency threshold for LSFM_U (< fn)	49,8
delay init lfmsu	s	Initial response delay FSM-U	0
s4	%	Droop 4 (FSM-U upward regulation, for f < f2)	5
T smooth	s	Output smoothing time constant (PT1 filter)	0,02
dP fsm min	%	Minimum additional power FSM (dP<0)	-10
ddP fsm min	%/s	Min. Rate of change of dP FSM (neg.)	-4
dP lfsmo min	%	Max. Power reduction LFSM_O (dP<0)	-100
ddP lfsmo min	%/s	Min. Rate of change of dP LFSM-O	-100
ddP lfsmu min	%/s	Min. Rate of change of dP LFSM-U	-100
dP fsm max	%	Maximum additional power FSM (dP > 0)	10
ddP fsm max	%/s	Max. Rate of change of dP FSM (pos.)	4
ddP lfsmo max	%/s	Max. Rate of change of dP LFSM_O	100
dP lfsmu max	%	Max. Additional power LFSM-U (dP > 0)	100
ddP lfsmu max	%/s	Max. Rate of change of dP LFSM-U	100